SPIN INTERACTION IN SEMICONDUCTORS MEDIATED BY OPTICAL EXCITATIONS

By

Guillermo Federico Quinteiro Rosen

A DISSERTATION

Submitted to
Michigan State University
in partial fulfillment of the requirements
for the degree of

DOCTOR OF PHILOSOPHY

Department of Physics and Astronomy

2006

ABSTRACT

SPIN INTERACTION IN SEMICONDUCTORS MEDIATED BY ITINERANT EXCITATIONS

By

Guillermo Federico Quinteiro Rosen

Circumscribed to the field of condensed matter, this thesis aims to enhance our understanding of optically-induced indirect spin interactions in semiconductor structures, as well as to contribute to the development of solid state proposals for the emerging science of Quantum Information.

The theoretical formalism that is used throughout this thesis is discussed. This mathematical framework describes excitations of the semiconductor, light fields and localized spin states. It is shown how the Hamiltonian is derived from a microscopic model. This resulting Hamiltonian includes the: *i*) Interaction between laser light and excitations of the semiconductor; *ii*) Kinetic energies of excitations; *iii*) interaction of photons and excitons that yield exciton polaritons; *iv*) Spin interaction between localized centers and optical excitations in the semiconductor (excitons and/or exciton polaritons).

The formalism is first employed to analyze the spin indirect interaction mediated by excitons in semiconductors and extend the results of previous works in this subject. In contrast to previous works, a full analytical solution valid to all orders in the strength of the interaction between excitations and localized spins is found. New features arise from the non-perturbative solution. One important finding is that both ferromagnetic and anti-ferromagnetic indirect coupling can be achieved.

The indirect interaction for semiconductors embedded in a planar micro-cavity is then considered. This theory follows naturally as an extension of the one for bare

semiconductors. The focus is now on different features that are predicted using perturbation theory in the coupling between polaritons and localized spins. It is shown that the indirect interaction presents two distinct regimes, depending on the separation between the localized spins. In each regime, the dominant interaction is of a different type: Ising or Heisenberg. Moreover, the range of the interaction for a semiconductor in a micro-cavity is found to be of longer range when compared to that of a bare semiconductor.

The knowledge gained through the aforementioned investigations opens new possibilities for applications to quantum information. First, a detailed analysis of optical quantum control in a system consisting of quantum dots grown on top of a quantum well is presented. It is shown how this system is a possible candidate for quantum computers. Then a discussion follows, describing how the findings on bare semiconductor and micro-cavity indirect interactions are a rich ground for implementations of quantum computing and other quantum information technologies.

This dissertation ends with comments on the future developments of the research presented here.

ACKNOWLEDGMENTS

I would like to thank my advisor Prof. Carlo Piermarocchi for his full support in both the professional and personal aspects.

Contents

List of Figures

List of Tables

Introduction

Solid State Physics has experienced tremendous changes in the last century, and is currently one of the most active research fields. It gives us basic insight into our physical world, and enables us to control and modify the environment to improve our lives. Among its various areas of research, semiconductor physics and magnetism have had a central role. The research in semiconductors has made possible impressive technological developments, e.g. digital computers. Moreover, the past few decades have witnessed important technological advances that made possible the fabrication of semiconductor systems with novel properties. Research on materials that have both semiconductor and magnetic properties has also attracted much attention. These concurrent new investigations promise further technological developments in classical information technology as well as the new emerging field of quantum information.

Semiconductor engineered structures exhibit very interesting new features. [1] Perhaps, the best examples of novel systems are *quantum dots*(QD) [2, 3] and *planar micro-cavities* [4]. The former are usually regarded as *artificial atoms*. Although a QD can be a hundred times larger than its natural counterpart, they share some important characteristics. For instance, particles trapped in a QD are confined in all directions – like in a real atom; for this reason it is considered a zero dimensional structure. A planar micro-cavity consists of a very thin semiconductor structure – a quantum well (QW)[1] – enclosed by mirrors on both sides. When light is trapped between the mirrors, it couples to electronic excitations of the QW, giving rise to a

[1]Width of the order of tens of an atom size.

new quasi-particle named a *polariton* [5].

Magnetism has been the focus of extensive experimental and theoretical study. It is well accepted that this phenomenon is due to collective mechanisms where electron correlations play a crucial role. Other possible sources of magnetism, with no electronic correlation, do not account for experiments, and simple estimations show that they vanish at high temperatures; for example, the magnetic dipole-dipole interaction energy is about $10^{-4}\ eV$, which is approximately 1 Kelvin. Strong electronic correlations, that can persist at room temperatures, are the result of the Pauli exclusion principle and the Coulomb interaction, and are generally referred to as *exchange* interactions. This encompasses *itinerant-exchange*, *direct-exchange*, *super-exchange*, etc.

Semiconductors that exhibit magnetic properties can be obtained by doping or the implantation of impurities. [18,49] These embedded particles are then responsible for the magnetic features of the whole system. As explained above, various exchange mechanisms may account for the magnetic interaction. Depending on the system and conditions, the coupling among foreign particles may be assisted by excitations on the host material which, for example, may be produced coherently by optical excitation. [6–8] Thus we talk of *indirect-interaction* processes [9,10] that link localized states. The light-induced spin-spin interaction is a convenient way for a fast quantum control of spins. [6–8, 11]

The concept of *quantum computing* (QC) was originally proposed by Richard Feynman and others [12, 13]. They suggested that a new type of computer based entirely on the principles of quantum mechanics may outperform any conceivable *classical computer*. [14] A substantial effort is deployed now in the exploration of physical systems that may implement a QC. Within solid state physics, magnetic semiconductor nano-structures are very promising systems. The logical units (*qubits*) are realized by impurity spin states or electrons in quantum dots, and the logical operation performed using a variety of methods: electrical, optical, etc. [15–17]

In conclusion, engineered magnetic semiconductor systems exhibit new features that are worth studying from a fundamental perspective, and can have applications to QC or other branches derived from Feynman's original idea: *quantum cryptography*, *quantum teleportation*, etc.

The research in systems using the aforementioned principles has led to important results. A mechanism of indirect interaction between distant spins mediated by virtual excitons in semiconductors has been studied [6]. In addition, QC schemes using the indirect interaction were proposed, e.g. QD's inside a zero-dimensional cavity [15] and donors embedded in a 2D electron gas [78].

The work presented in this thesis is a theoretical contribution to the physics of the exchange interaction between spins assisted by excitations in semiconductor structures – a problem of a complex nature encompassing all fields mentioned above. The main results can be summarized as follow: *i*) In the case of bulk semiconductors, we find a non-perturbative solution to the spin-spin interaction. This allows us to predict that the corresponding coupling constant is either ferromagnetic or anti-ferromagnetic depending on the frequency of the optical excitation. *ii*) We study for the first time the spin-spin interaction in a planar micro-cavity mediated by polaritons. New features arise: The range of the coupling constant is dramatically increased and the interaction becomes anisotropic. *iii*) We analyze the optical quantum control and role of spontaneous emission on a model for QC. We demonstrate that this system, made out of excitons in QD's and impurity-qubits, is fault-tolerant and thus is a good candidate for QC.

Chapter 1 starts with an overview of the semiconductor physics necessary to build our theory. Next, I introduce the mathematical formalism that will be employed, with modifications and additions, throughout the whole dissertation.

Chapter 2 provides a theory of laser-induced interaction between spins localized by impurity centers in a semiconductor host. We solve non-perturbatively the problem of two localized spins interacting with one itinerant exciton, and we find an analytical

expression for the induced spin-spin interaction as a function of the spin separation, laser energy, and intensity. This non-perturbative approach is one of our main contributions to the existing theories on optically mediated spin coupling. The application of this theory to shallow neutral donors (Si) and deep rare-earth magnetic impurities (Yb) in III-V semiconductors yields the following main result not predicted in the previous perturbative treatments. When the photon energy approaches a resonance related to excitons bound to the impurities, the coupling between the localized spins increases, and may change from ferromagnetic to anti-ferromagnetic.

In chapter 3 we study the optically-induced spin interaction between two shallow donors mediated by polaritons in a planar micro-cavity. The spin coupling mediated by polaritons in a planar micro-cavity has been addressed for the first time in this thesis. Our findings are: *i*) The vacuum Rabi splitting makes the spin interaction anisotropic. *ii*) The spin interaction presents two distinct regimes, as a function of the inter-spin separation. *iii*) The existence of the cavity – or polaritons – extends the range of the spin interaction by several orders of magnitude compared to the case of a bare semiconductor.

I study the possible applications of the preceding theory in chapter 4. First, I show how the use of semiconductor excitation - localized state interaction can help tackling intractable and/or very difficult problems in QC. In particular, we analyze in detail the optical quantum control of impurity spins in the proximity of a quantum dot. A laser pulse creates an exciton in the dot and controls the spins by an indirect coupling. We show how to determine the control parameters to achieve maximal spin entanglement, the most important ingredient in quantum information. We consider errors in the quantum control due to the exciton radiative recombination. The control errors in the adiabatic and nonadiabatic case are compared to the threshold needed for scalable quantum computing. We find that the scheme we propose is fault-tolerant. Finally, I analyze the possible applications of the theories presented in chapter 2 and chapter 3 to quantum computing in semiconductors. The errors in the spin-

qubit operations due to the finite lifetime of the mediating particle represents one of the most important limitations in all the optically-induced indirect spin interaction schemes. The novel result we found for the quantum control – i.e. that by properly choosing the parameters the errors are below the correction threshold – suggests that this limitation can also be overcome in the systems of Chapter 2 and chapter 3.

This thesis ends with comments on future directions of research that may expand the investigation exposed here.

Chapter 1

The core mathematical model

Throughout this thesis, three physical systems will be analyzed. Though each one sheds light onto different questions and possible applications, they all share important features. These similarities stem from a common building block or core Hamiltonian, out of which the specific dynamics for each system is constructed. The following sections give a brief introduction to semiconductor physics, and show how the core Hamiltonian can be derived from first principles. We also discuss the approximations and their limitations.

1.1 Basic concepts in Semiconductor physics

Electron dynamics is of main importance to understand the transport and optical properties of metals and semiconductors. [5, 18, 20] Electrons in solids are subjected to the Coulomb potential due to lattice ions and other electrons. The theoretical study can be carried out in series of successive approximations. The first aproximation assumes that all sources of potential energy form an average single particle potential[1] that has the periodicity of the lattice. Therefore, Bloch's theorem applies. Bloch's theorem states that a possible description of the spatial wave function of particles in

[1] A common procedure to obtain such potential is through self consistent calculations.

a periodic potential is the product

$$\psi_k(\mathbf{r}) = \mathbf{e}^{\imath\mathbf{kr}}\mathbf{u}(\mathbf{r})$$

of a plane wave with wavevector $\mathbf{k}$ (*crystal momentum*[2] $\mathbf{p} = \hbar\mathbf{k}$) times an envelope function $u(\mathbf{r})$ with the periodicity of the potential. Alternatively, this can be expressed as

$$\psi_k(\mathbf{r} + \mathbf{R}) = \mathbf{e}^{\imath\mathbf{kR}}\psi_{\mathbf{k}}(\mathbf{r}),$$

where $\mathbf{R}$ is a lattice vector. A description of electrons in these so-called *Bloch* states can be given in terms of the momentum k restricted to the $1st$ Brillouin zone (BZ)[3] and a *band* index n.

Though rough, the use of average potentials proves useful, for the dynamics of the many electron system simplifies to the solution of a single-particle Schrödinger equation. Tight binding or nearly-free electron models can then be employed. The latter describes the loosely bound electrons in the outer orbitals. The starting point is the assumption of an unperturbed Bloch function with $u(\mathbf{r}) = \mathbf{1}$ that leads to a quadratic dispersion law. Degenerate states at the boundary of the BZ are solved by applying perturbation theory, and gaps between bands result. More accurate states and energy bands are determined with the use of self consistent theories with spin degrees of freedom, such as the original Hartree. Further refinements, e.g. Hartree-Fock [18, 19], introduce Pauli exclusion principle, symmetrization and spin dependent interactions as well. Metals, insulators and semiconductors, are studied within the formalism described above. The latter are binary compounds forming, in general, covalent bonds. They can be regarded as insulators with a smaller energy gap ($E_g <$ 5 eV) between the *valence* and *conduction* bands. A simplified band structure diagram

[2]This is not the linear momentum of the particle, for the problem does not have complete translational invariance.

[3]The Wigner-Seitz primitive cell in the reciprocal k space is known as Brillouin zone.

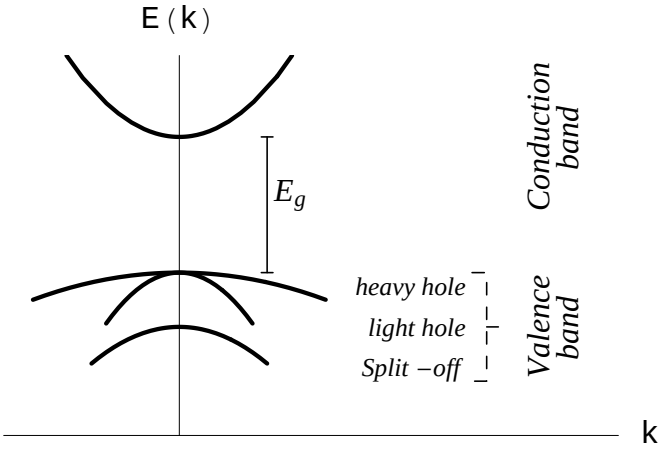

Figure 1.1: Band structure of direct band gap III-V semiconductors showing valence bands and the lowest conduction band close to the Γ point, with energy gap E_g. Spin-orbit coupling breaks the degeneracy of the p-like valence band, leaving the energy of the *split-off* $J = 1/2$ band lower than the *heavy hole* and *light hole* $J = 3/2$ bands.

of a direct band gap[4] semiconductor of the III-V[5] type is shown in Figure 1.1. The valence and conduction bands arise from p and s atomic-like states, respectively. Together with the spin degree of freedom, the total angular momentum is either $J = 1/2$ for the conduction band or $J = 3/2, 1/2$ for the valence band. This is completely degenerate at the Γ point ($k = 0$). Spin-orbit coupling lifts partially this degeneracy, leaving the energy of the *split-off* $J = 1/2$ band lower than the *heavy hole* and *light hole* $J = 3/2$ bands[6]. Other interactions, such as quantum confinement, lattice strain, etc. further break the degeneracy between *heavy hole* $m_j = \pm 3/2$ and *light hole* $m_j = \pm 1/2$. The ground state of a semiconductor consists of electrons filling completely the valence band; excited states are only occupied via the promotion of an electron from the valence to the conduction band. As the band gap energy is typically of the order of electron-Volts, optical excitations are possible: a photon with energy larger than E_g is absorbed and an electron changes state to one in the conduction band, leaving a *hole* in the valence band.

[4]Valence maximum and conduction minimum occur at the same wavevector k.

[5]Chemical composition: the semiconductor is formed with an element of the III and V groups of the periodic table.

[6]the splitting is of the order of magnitude of hundreds of meV.

1.1.1 Excitons

So far, the effect of electron-electron interaction on the optical excitation has not been described. In insulators and semiconductors, a well known consequence of Coulomb interactions is the occurrence of new states with energy lower than the band gap E_g[7]. A photo-excited electron in the conduction band binds to the hole left behind in the valence band in a state called *exciton*. [22] This particle is important to describe optical properties of bulk semiconductor and engineered structures, specially at low temperature.

The study of excitons was pioneered by Frenkel [24] and Wannier [23] in the 1930s. Consequently, this quasi-particle is nowadays classified according to whether the electron and hole are strongly (Frenkel exciton) or weakly (Wannier exciton) bound. The former occurs for example in ionic crystals, like $NaCl$ [25]. The latter is found in semiconductors that exhibit large dielectric constant (weaker screened Coulomb interaction), such as $GaAs$.

As already anticipated, the electron-electron interaction complicates the mathematical treatment, since a single-particle picture is no longer applicable [26]. The zero-order ground state of the crystal can be represented by an antisymmetrized product (Slater determinant) of atomic-like[8] single-particle wave functions of electrons each in its ground state a_0 and centered at R_i

$$\Phi_0 \doteq \mathcal{A} a_0(r_1 - R_1) a_0(r_2 - R_2) a_0(r_3 - R_3) \dots$$

Nevertheless, a similar representation:

$$\Phi_1(R_h, \beta) \doteq \mathcal{A} a_0(r_1 - R_1) \dots a_1(r_i - R_e) \dots \ ,$$

[7] The difference in energy between this new state and the bottom of the conduction band is of the few milielectron-Volts.

[8] Alternatively, Bloch wave functions can be used.

for the excited crystal state with one electron promoted from a single-particle state a_0 at R_h to an single-particle excited state a_1 at R_e ($\beta = R_e - R_h$) proves inadequate, for the energy of the functions $\Phi_1(R_h, \beta)$'s for different R_h are degenerate. However, a linear superposition of $\{\Phi_1(R_h, \beta)\}$ written as

$$\Phi_1(K, \beta) \doteq \frac{1}{\sqrt{N}} \sum_{R_h} e^{iKR_h} \Phi_1(R_h, \beta)$$

partially diagonalizes the full Hamiltonian. With the use of these *excitation waves*, originally introduced by Frenkel, and an equivalent representation Wannier showed that the full Hamiltonian can be resolved in two terms. One accounts for transitions with either electron or hole kept in its original site; this is a one-particle energy. The other term is related to the Coulomb attraction between the electron and hole. From this and the use of a new representation:

$$\Psi_\nu(K) \doteq \sum_\beta U_\nu(\beta) \Phi_1(K, \beta),$$

Wannier found that the equations for the coefficients $U_\nu(\beta)$, written in the form $U_\nu(\beta) = e^{i\alpha' K\beta} F_\nu(\beta)$, lead to an hydrogen-like equation for $F_\nu(\beta)$ in a medium of dielectric constant ϵ, with $\alpha' = m_e^*/(m_e^* + m_h^*)$. Thus, the problem resembles that of atomic systems with atomic energy spectrum and free center of mass motion. Notice that, in Frenkel's representation, the excitation is "free" to move with momentum K, but lacks relative motion; Wannier took into account the superposition of states with different separation β between electron and hole. In the language of creation/annihilation operators for electrons ($\alpha^\dagger/\alpha$) and holes ($\beta^\dagger/\beta$), the Wannier exciton creation operator is represented by

$$b_{\nu K}^\dagger = L^{-3/2} \sum_k \psi_\nu(k - K/2)\ \alpha_k^\dagger \beta_{K-k}^\dagger\ , \tag{1.1}$$

where ψ is the Fourier transform of the electron-hole relative motion hydrogen-like

wave function ν[9], and L is the linear size of the $3D$ system. Being a composite particle made up of two fermions, we can expect it to follow Bose statistics. Calculation of the commutator

$$[b_{\nu 0}, b_{\nu 0}^{\dagger}] = L^{-3} \sum_{k} |\psi_{\nu}(0)|^2 (1 - \alpha_k^{\dagger}\alpha_k - \beta_{-k}^{\dagger}\beta_{-k})$$

shows that excitons are approximately bosons, and their deviation is proportional to the density of electrons in the conduction and holes in the valence bands. [5]

In this thesis, we will consider an effective Hamiltonian for an electron and hole in a medium with dielectric constant ϵ that leads to Wannier excitons in the bosonic limit. Furthermore, we restrict the relative motion to the lowest $\nu = 1s$ state. [30]

1.1.2 Localized electrons in impurity centers and quantum dots

Doping or implantation of impurities in semiconductors has been a common method to alter both transport and optical properties of the host lattice. Nowadays, quantum dots also allow us to modify those properties in engineered systems, such as quantum wells.

The classification of impurities distinguishes two categories. These substitutional atoms may be *shallow* or *deep* impurities, and *donors*, *acceptors* or *iso-electronics*. The first division accounts for the effect introduced in the host lattice and the extension to which the hydrogen-like model for impurities can be used. The second distinction responds to the fact that impurities can donate to or accept from the lattice an electron.

Quantum dots embedded in quantum wells can be charged in a controlled way. An electron remains well localized within this structure and its dynamic follows closely that of a trapped particle in a parabolic potential, thus presenting discrete levels.

[9] In the language of Wannier: $F_{\nu}(\beta)$.

In analogy to our treatment of excitons, we assume that neither the electron in the impurity nor that in the quantum dot changes its orbital state, and remains always in the ground state. This is a sensible approximation, for – in the case of donors – the binding energy is around tens of meV, and thus much smaller than the energy of excitation of the laser field[10]. Ionization is also suppressed, for the dipole moment is very small for a transition connecting a localized state in the donor to a high energy state in the conduction band. Therefore, we focus on the spin degree of freedom of the electron in the impurity or quantum dot.

1.2 The core Hamiltonian

All three systems that are the subject of the following chapters share important physical properties that can be described using a unified formalism. The prototype system representing them, for which the core Hamiltonian is built, is a direct band gap semiconductor with valence and conduction bands arising from p and s atomic orbitals, respectively. Moreover, the valence band is split due to spin-orbit coupling and other particular effects (described in each chapter); thus, only heavy-hole valence and conduction bands are taken into account. As a result, excitons are linear combination of states belonging to these two bands. The optical excitation of the system is always achieved by monochromatic light with energy slightly below the excitonic absorption line. This ensures that only virtual transverse excitons appear. Moreover, their density is controlled by the detuning and the intensity of the light field. Localized electrons are included in the model; they come either from impurities or quantum dots. They interact via Coulomb forces with the electron or hole belonging to the exciton. Exchange is usually the dominant interaction and the most interesting effect. In almost all cases the hole spin interacts weakly with the electron spin, and therefore it remains in its state through the evolution of the system.

[10]The laser is tuned slightly off-resonance with the exciton line, that lies hundreds of meV to eV above the bottom of the valence band.

For Wannier excitons in the effective mass approximation, the resulting effective core Hamiltonian in first quantization form reads

$$\begin{aligned} H &= H_0 + H_L + H_I \\ H_0 &= -\sum_i \frac{\hbar^2}{2m_i}\nabla_i^2 + \sum_l V(r_l) \\ H_L &= \sum_e E(r_e)\, d_e\, e^{-i(kr_e-\omega t)} \\ H_I &= \sum_{e,l} \frac{q^2}{\epsilon|r_e - r_l|} \quad , \end{aligned} \tag{1.2}$$

where subindexes $\{e, l, i\}$ refer to the electron in the exciton, the electron localized in the impurity/QD, and the exciton center-of-mass, respectively; d the dipole moment. The first term is the kinetic energy of excitons plus the energy of localized electrons in impurities/QDs. The second term is the coupling of the electron in the exciton to the laser light. The last term is the Coulomb potential energy between the electron in the exciton and the electron in the impurity/QD in a medium of dielectric constant ϵ. Terms that give rise to energy shift, such as exciton-ion interaction, are not considered. The binding of the exciton to the impurity/QD will be addressed in Chapter 2.

1.2.1 Kinetic energy

The exciton spatial wave functions is the product of relative and center of mass motion wave functions. The former is of the $1s$ type, while the latter is a plane wave. As such, when transforming to creation/annihilation operators in $2nd.$ quantization form, the matrix element of the Laplacian gives a quadratic dispersion law. The energy of different projections of spin are degenerate and symbolized by greek subindexes. Therefore,

$$H_0 = \varepsilon_\lambda^0 + \sum_{k\alpha}\left(\epsilon_0 + \frac{\hbar^2\, k^2}{2\, m}\right)\ \hat{b}_{k\alpha}^\dagger \hat{b}_{k_\alpha}\ ,$$

where the constant ϵ_0 is the energy of the $k = 0$ exciton. $\{b^\dagger, b\}$ are the creation and annihilation operators for excitons with momentum k and spin projection α. The energy ε_λ^0 of the localized states is degenerate.

1.2.2 Light - exciton interaction

The Hamiltonian for the interaction between light and matter is obtained with the use of the canonical momentum [27, 28], and reads

$$h = \frac{1}{2\,m}\left[p - eA(\mathbf{r}, t)\right]^2 + e\phi \ , \tag{1.3}$$

where A and ϕ are the vector and scalar potentials, respectively; and the particle has mass m and charge e. In the Coulomb gauge $[A, p] = 0$ holds, since $\nabla \cdot A = 0$. Thus, expanding the square in Eq. 1.3 we obtain

$$h = \frac{p^2}{2\,m} + e\phi - \frac{e}{m}p \cdot A + \frac{e^2}{2m}A^2 \ , \tag{1.4}$$

where A accounts for a plane electromagnetic wave, and ϕ may represent a confining potential for the particle. In the case of an atom, all terms that contain the vector potential result in a small perturbation to the rest of the interaction; in addition, a numerical estimate for the rate of the linear to the quadratic term in A gives 10^4. This allows us to retain only the term $e/m(p \cdot A)$, which is a good approximation if the photon density is low. An important additional simplification, possible in the atomic case, is also good for excitations of semiconductors: Consider a monochromatic plane wave, with $A = A_0 e^{i(k\mathbf{r}-\omega\mathbf{t})} + c.c.$ in the visible region of the spectrum, $\lambda \simeq 600\,nm$, in resonance with the $1s$ exciton state. Assuming a very large, though realistic, value for the spatial extension of the exciton wave function $a_0 \simeq 10\,nm$, there is no appreciable variation of A in this scale. Therefore, in the evaluation of matrix elements for the optical transition one can take $e^{i(k\mathbf{r})} \simeq 1$, procedure known as dipole-moment

approximation. In the following we restrict to the case of a semiconductor, where the light couples to electrons and the aforementioned approximations are valid. The Hamiltonian is

$$h = \frac{p^2}{2\,m} + e\phi - \frac{e}{m} p \cdot (A_0 e^{-i\omega t} + A_0^* e^{i\omega t}) \ . \tag{1.5}$$

We first focus on the dynamics of one electron with momentum p in the presence of the total average potential ϕ. This unperturbed part, which we call h_0, leads to electrons, holes, bands, excitons[11], etc. as explained before, and is a function of p^2 and its $\mathbf{r}$ operator. The operator p can be written as

$$p = -i\frac{m}{\hbar}[r, h_0].$$

We would like to keep a classical description of the light while using a creation / annihilation operator language for electrons and holes. The optical transition is calculated by evaluating the matrix elements between initial and final states. Due to the symmetry of the wave functions and the operator $\mathbf{r}$, the only non-vanishing matrix elements are those connecting states of different parity, such as the valence (p-like) and conducting (s-like) bands,

$$\langle c| \, [r, h_0] \, |v\rangle = -(E_g - \Delta)\langle c| \, \mathbf{r} \, |v\rangle = -\hbar\omega_X \langle c| \, \mathbf{r} \, |v\rangle \ , \tag{1.6}$$

where the Coulomb binding energy Δ for the electron and the hole lowers the energy of the exciton state with respect to a free electron-hole pair. Thus, the perturbation becomes

$$\begin{aligned} H_L \ &= \ -i\omega_X (A_0 e^{-i\omega t} + A_0^* e^{i\omega t}) \langle c| \, e\mathbf{r} \, |v\rangle \alpha^\dagger \beta^\dagger + \\ &\quad i\omega_X (A_0 e^{-i\omega t} + A_0^* e^{i\omega t}) \langle v| \, e\mathbf{r} \, |c\rangle \alpha\beta \ . \end{aligned} \tag{1.7}$$

[11] To introduce excitons we need to include the electron-electron interaction. However, this new energy term does not affect the analysis that follows, since still $p = -im/\hbar \ [r, h_0]$.

The terms containing $e^{i\omega t}$ and $e^{-i\omega t}$ represent emission and absorption of a photon, respectively. We apply the *rotating wave approximation* and consider only terms that create a photon when annihilating an exciton, and vice versa. Taking into account all possible direct transitions with wavevector k [12], we obtain

$$\begin{aligned} H_L &= -\sum_k i\omega_X A_0 e^{-i\omega t}\langle c|\, e\mathbf{r}\,|v\rangle \alpha_k^\dagger \beta_{-k}^\dagger + \sum_k i\omega_X A_0^* e^{i\omega t}\langle v|\, e\mathbf{r}\,|c\rangle \alpha_k \beta_{-k} \\ &= -\sum_k E_0\, d_{vc}\, e^{-i\omega t}\alpha_k^\dagger \beta_{-k}^\dagger + h.c.\ , \end{aligned} \tag{1.8}$$

where the dipole moment d_{vc} is the matrix element of $e\mathbf{r}$, the vector potential is related to the electric field by $A_0 = -iE_0/\omega$, and we have matched $\omega_X = \omega$ giving $\omega_X/\omega = 1$ [13]; the quantities d_{vc} and E_0 are k dependent. The next step consists of writing H_L in terms of exciton operators. This is accomplished using the inverse of Eq. 1.1: $L^{-3/2}\sum_\nu \psi_\nu(q)^* b_{\nu,K}^\dagger = \alpha_{K/2+q}^\dagger \beta_{K/2-q}^\dagger$. The wavevector K represents the momentum of the light that contributes to the center-of-mass motion of the electron-hole system; this contribution can be safely neglected, for the photon momentum at energies close to E_g is much smaller than the typical exciton momentum. In addition, the spin of the photon introduces optical selection rules. Circular polarizations $\sigma+$ and $\sigma-$ correspond to spin projections of light equal to $s_z = -1$ and $s_z = 1$ respectively[14]. The sum of total angular momentum of the electron plus the hole must equal σ; we include both polarizations and the spin index to the exciton operators. Then,

$$H_L = -L^{-d/2}\sum_{\sigma\nu,k} \hbar\, \wp_\sigma \psi_\nu(k)^* e^{-i\omega t} b_{\nu,0,\sigma}^\dagger + h.c.\ ,$$

where we have defined the *Rabi Energy* $\hbar\wp \doteq E_0 d_{vc}$. The sum on ν is eliminated, for we restrict to $1s$ exciton states $\psi_\nu \to \psi_{1s}$ (with ψ_{1s} real). An extra simplification is

[12] The frequency ω_X depends on k.

[13] In the off-resonance case, where $\omega_X \neq \omega$, the deviation of ω_X/ω from one is usually smaller than 1% and can be neglected.

[14] The z-axis is normal to the QW, and coincides with the propagation direction of the light.

possible thanks to $\sum_k \psi_{1s}(k)$,

$$\begin{aligned}
\sum_k \psi_{1s}(k) &= \left(\frac{L}{2\pi}\right)^3 \int d\mathbf{k}\ \psi_{1s}(k) \\
&= \left(\frac{L}{2\pi}\right)^3 \int d\mathbf{k} \int d\mathbf{r}\ \phi_{1s}(\mathbf{r})\, e^{-i\mathbf{k}\,\mathbf{r}} \\
&= \left(\frac{L}{2\pi}\right)^3 \int d\mathbf{r}\ \phi_{1s}(\mathbf{r}) \int d\mathbf{k}\, e^{-i\mathbf{k}\,\mathbf{r}} \\
&= \left(\frac{L}{2\pi}\right)^3 \int d\mathbf{r}\ \phi_{1s}(\mathbf{r})\, [(2\pi)^3 \delta(\mathbf{r})] = L^3 \phi_{1s}(0)\ ,
\end{aligned}$$

where ψ_{1s} and ϕ_{1s} are conjugate functions for the Fourier transform. Finally, we arrive at the expression that will be used hereafter,

$$H_L = L^{3/2} \sum_\sigma \hbar\, \wp_\sigma \phi_{1s}(0)\, e^{-i\omega t} b^\dagger_{0,\sigma} + h.c.\ . \tag{1.9}$$

1.2.3 Exciton - localized spin interaction

The interaction of excitons with localized electrons can be described using a basis set of delocalized functions for excitons and atomic-like wave functions for the localized states, with the inclusion of the spin degrees of freedom. It is not necessary to specify the form of the basis used, which depends on the particular system (quantum well, bulk, quantum dot, etc.). We only need to know that the wave function has a spatial (ψ or ϕ) and spin (χ for electrons or η for holes) components. The complete wave function for the system is composed by products of the itinerant $\psi_k \eta \chi$ and localized $\varphi\chi$ wave functions. This product must be anti-symmetrized with respect to the two electrons, one belonging to the exciton (e) and the other to the localized state (l). The total wave function is then written as

$$\begin{aligned}
\Psi_k \doteq \frac{\eta}{\sqrt{2}} \cdot \Big[&+ \psi_k(r_e, r_h)\varphi(r_l)\chi(s_e)\chi(s_l) \mp \psi_k(r_e, r_h)\varphi(r_l)\chi(s_l)\chi(s_e) \\
&\pm \psi_k(r_l, r_h)\varphi(r_e)\chi(s_e)\chi(s_l) - \psi_k(r_l, r_h)\varphi(r_e)\chi(s_l)\chi(s_e) \Big]\ ,
\end{aligned} \tag{1.10}$$

where the $\mp$ and $\pm$ signs comes from the anti-symmetrization either of the spatial or the spin part.

This function can also be written in an equivalent form that stresses its permutation symmetries and facilitates the derivation of the Heisenberg Hamiltonian. I make use of the coupled representation and separate the *spin* triplet and singlet wave functions,

$$\begin{aligned}
S &= \frac{\eta}{\sqrt{2}}[\psi_k(r_e,r_h)\varphi(r_l)+\psi_k(r_l,r_h)\varphi(r_e)]\times\frac{1}{\sqrt{2}}[u(s_e)d(s_l)-u(s_l)d(s_e)]\\
T_0 &= \frac{\eta}{\sqrt{2}}[\psi_k(r_e,r_h)\varphi(r_l)-\psi_k(r_l,r_h)\varphi(r_e)]\times\frac{1}{\sqrt{2}}[u(s_e)d(s_l)+u(s_l)d(s_e)]\\
T_+ &= \frac{\eta}{\sqrt{2}}[\psi_k(r_e,r_h)\varphi(r_l)-\psi_k(r_l,r_h)\varphi(r_e)]\times u(s_e)u(s_l)\\
T_- &= \frac{\eta}{\sqrt{2}}[\psi_k(r_e,r_h)\varphi(r_l)-\psi_k(r_l,r_h)\varphi(r_e)]\times d(s_e)d(s_l)\ , \qquad (1.11)
\end{aligned}$$

where $u(x)$ and $d(x)$ stands for spin up and down of particle x respectively; the complete basis is resolved into singlet S and triplet T_i states. The spin-orbital of the decoupled representation Eq. 1.10 are linear combinations of Eq. 1.11.

The next step is to evaluate matrix elements of the Hamiltonian Eq. 1.2 between complete wave functions, either of the form Eq. 1.10 or Eq. 1.11. First the coupled representation is used to illustrate the procedure. Eq. 1.10 has the following structure,

$$\begin{aligned}
S &= \frac{\eta}{\sqrt{2}}[A+B]\times ...\\
T &= \frac{\eta}{\sqrt{2}}[A-B]\times ...\ ,
\end{aligned}$$

where $A \doteq \psi_k(r_e,r_h)\varphi(r_l)$ and $B \doteq \psi_k(r_l,r_h)\varphi(r_e)$ are the spatial part of the wave function. The spin part is given in matrix form. Every term in the Hamiltonian operates only on the spatial part of the state.

The direct and exchange Coulomb integrals read,

$$\begin{aligned} V^{AA} &= V^{BB} = \int A_k^* \, H_I \, A_{k'} \, dr_e dr_h dr_l \\ V^{AB} &= \int A_k^* \, H_I \, B_{k'} \, dr_e dr_h dr_l \ . \end{aligned}$$

The dependence of V on (k, k') is implicit and omitted to simplify the notation. A detailed evaluation of the integrals V is found in Appendix A.

$$H_{I,\,kk'} = \frac{\hbar^2}{2}\Big\{ (V^{AA} + V^{BB})\, \mathbb{I}_e - 2Re\,[V^{BA}]\, \mathbb{M} \Big\}\, \mathbb{I}_h \ , \tag{1.12}$$

where $\mathbb{I}_i$ is the identity matrix in the subspace of the i-particle and,

$$\mathbb{M} \doteq \begin{pmatrix} -1 & 0 & 0 & 0 \\ 0 & 1 & 0 & 0 \\ 0 & 0 & 1 & 0 \\ 0 & 0 & 0 & 1 \end{pmatrix} = \left(\frac{\hat{s}}{\hbar}\right)^2 - 1 \tag{1.13}$$

and $\hat{s} \doteq \hat{s}_e + \hat{s}_l$.

Alternatively, in the decoupled spin basis (Eq. 1.10), the Hamiltonian can be expressed in terms of $s = 1/2$ spin operators as

$$H_{I,\,kk'} = \frac{\hbar^2}{2}\left\{ (V^{AA} + V^{BB})\, \delta_{s_e s_l} - 2\, Re[V^{BA}] \left(\frac{\delta_{s_e s_l}}{2} + 2\, \hat{s}_e \cdot \hat{s}_l \right) \right\} \delta_{hh'} \ . \tag{1.14}$$

This representation makes clear the Heisenberg form of the Hamiltonian, and shows that it is linked to the exchange integral V^{AB}. The first term is unimportant, for it only leads to a shift or renormalization of the energy. Hereafter, we focus on the spin dependent part.

The many body interaction hamiltonian for excitons and N localized spins follows

from Eq. 1.14 using $2nd.$ quantization, and reads

$$\hat{H}_I = L^{-3}\delta_{hh'} \sum_{l=1}^{N} \sum_{kk'} J_{k,k'}\, e^{-i\,(\mathbf{k}-\mathbf{k'})\cdot\mathbf{R}_l}\, \hat{s}_e \cdot \hat{s}_l \;\; \hat{b}_k^{\dagger}\hat{b}_{k'} \;, \tag{1.15}$$

where the sum over the wave vector extends over the entire band of excitons with creation ($\hat{b}_k^{\dagger}$) and annihilation ($\hat{b}_{k'}$) operators, and the index l identifies a particular localized spin. We have resolved the factor $-2\,Re[V^{BA}]$ into a phase $exp(-i(k-k')R)$, the normalization L^{-3} and the remaining J. The operator $\hat{s}_e$ must be understood as acting on the particular set of bins $\{k, k'\}$: it transforms the spin of an exciton that undergoes scattering from states k' to k. We find that a more intuitive and suitable representation of the many body problem is to write the spin part of the interaction in matrix form. Thus, we replace $\hat{b}_k^{\dagger}$ and $\hat{b}_{k'}$ by separate bosonic operators for each projections of the electronic spin in the exciton (remember the spin of the hole is fixed), and we replace the operator s_e by a tensor $\hat{s}_{\alpha\alpha'}$, which in matrix form reads

$$s = \frac{\hbar}{2} \begin{pmatrix} \hat{z} & \hat{x} - i\hat{y} \\ \hat{x} + i\hat{y} & -\hat{z} \end{pmatrix} \;. \tag{1.16}$$

This takes into account the selection rules for transitions between different exciton states, represented by different operators $\hat{b}_{k\alpha}^{\dagger}/\hat{b}_{k\alpha}$, with α being $1 \equiv\uparrow$ (up) or $2 \equiv\downarrow$ (down): for instance, $s_{12} \equiv s_{\uparrow\downarrow}$. The final form of the Hamiltonian is

$$\hat{H}_I = L^{-3}\delta_{hh'} \sum_{l=1}^{N} \sum_{\substack{k\,k'\\ \alpha\,\alpha'}} J_{k,k'}\, e^{-i\,(\mathbf{k}-\mathbf{k'})\cdot\mathbf{R}_l}\, s_{\alpha\alpha'} \cdot \hat{s}_l \;\; \hat{b}_{k\alpha}^{\dagger}\hat{b}_{k'\alpha'} \;. \tag{1.17}$$

1.2.4 The complete core Hamiltonian

The preceding sections have shown the different parts of the Hamiltonian, their derivation and approximations. The final form of the complete core Hamiltonian is

$$\begin{aligned} H &= \varepsilon_\lambda^0 + \sum_{k\alpha}\left(\epsilon_0 + \frac{\hbar^2\,k^2}{2\,m}\right)\ \hat{b}^\dagger_{k\alpha}\hat{b}_{k_\alpha} + \\ & L^{-3}\delta_{hh'}\sum_{l=1}^{N}\sum_{\substack{k\ k'\\ \alpha\ \alpha'}} J_{k,k'}\,e^{-i\,(\mathbf{k}-\mathbf{k'})\cdot\mathbf{R}_l}\,s_{\alpha\alpha'}\cdot\hat{s}_l\ \ \hat{b}^\dagger_{k\alpha}\hat{b}_{k'\alpha'} + \\ & L^{3/2}\sum_\sigma \hbar\,\wp_\sigma\phi_{1s}(0)\,e^{-i\omega_L t}b^\dagger_{0,\alpha+\beta=\sigma} + h.c.\ , \end{aligned} \tag{1.18}$$

and describes Wannier excitons in the $1s$ state with electron spin α, hole spin β and wavevector k generated by monochromatic light of frequency ω_L of circular polarization σ. In addition, there are N localized spins with degenerate energy ε_λ^0 in the lattice that interact through exchange with the photo-generated excitons.

1.3 The effective spin - spin interaction

For each particular system, the results and conclusions will be drawn using an effective Hamiltonian that describes the dynamics of two localized spins without the explicit inclusion of excitons nor light. To achieve this, a transformation to a rotating frame[15] with frequency ω_L is performed so as to apply time-independent second order perturbation theory in the light - exciton interaction (Sec. 1.2.2). The resulting expression is then used to solve for the exciton - localized spin interaction (Sec. 1.2.3) in the framework of single particle Green's functions, with the final elimination of the

[15]The transition to a rotating frame is implemented with the unitary transformation $U = exp(-i\nu t\hat{R})$, which maps, respectively, the state and Hamiltonian to $|\psi\rangle \rightarrow U\,|\psi\rangle$ and $H \rightarrow (UHU^\dagger - \nu R)$, in such a way that the Schrödinger equation holds and part of the time dependency is eliminated from the Hamiltonian. The simplest case that resembles our problem clarifies this procedure: Consider a system made of three levels $\{\,|a\rangle,\,|b\rangle,\,|c\rangle\}$, and $H = H_0 + H_L + H_I$. $H_0 = E_c\,|c\rangle\langle c| + E_b\,|b\rangle\langle b|$ is diagonal, $H_L = g\,exp(i\nu t)\,|a\rangle\langle b| + h.c.$ and $H_I = \Delta\,S\,|c\rangle\langle b| + h.c.$, where S is an operator commuting with all others. It can be shown that, for $U = exp[-i\nu t(\,|c\rangle\langle c| + |b\rangle\langle b|\,)]$, $UH_LU^\dagger \rightarrow g\ |a\rangle\langle b| + h.c.$ and H_I is invariant; in addition, there appears a new term $\nu(\,|c\rangle\langle c| + |b\rangle\langle b|\,)$ contributing a shift to the energy.

exciton degree of freedom.

Perturbation theory may be developed using projection operator techniques [29]. The light - exciton interaction couples states belonging to subspaces of different number of excitons. We single out the zero-exciton subspace $\Im_0$ using the projector operator P and the remaining part of the Hilbert space with the operator $Q = 1 - P$. The resolvent $G(z) = (z - H)^{-1}$ in the subspace of interest is

$$PGP = \frac{P}{z - P(H_0 + H_I)P - PRP} \ ,$$

which shows that the *level-shift* operator R can be regarded as a Hamiltonian in the $\Im_0$ subspace that corrects the unperturbed energy $(H_0 + H_I)$. The expansion of PRP reads

$$PRP = PH_LP + PH_LQ\frac{1}{z - (H_0 + H_I)}QH_LP + \dots \ .$$

The first term vanishes, since H_L is non-diagonal in the subspace of fixed number of photons. By defining $|\lambda\rangle$ as any of four vectors $\{|\uparrow\uparrow\rangle, |\uparrow\downarrow\rangle, |\downarrow\uparrow\rangle, |\downarrow\downarrow\rangle\}$ of $\Im_0$, the Hamiltonian is transformed to its effective form[16]

$$H_{eff,\lambda\lambda'} = \langle\lambda| H_LQ\frac{1}{z - (H_0 + H_I)}QH_L |\lambda'\rangle \ ,$$

with no explicit exciton dependence[17]. H_L transforms a vector $|\lambda\rangle$ in $\Im_0$ to one of same localized spin state and one exciton of wavevector $k = 0$ and angular momentum σ, named $|\lambda 0\sigma\rangle$. This vector belongs to the complement of $\Im_0$; therefore, in the last

[16]With no light and restricting to the subspace of zero exciton, the unperturbed Hamiltonian is trivial and uninteresting with all four states degenerate.

[17]This expression accounts for completely coherent processes of stimulated absorption and emission.

expression, the operator Q is redundant and can be omitted,

$$\begin{aligned} H_{eff,\lambda\lambda'} &= L^3\hbar^2 \sum_\sigma |\wp_\sigma|^2 |\phi_{1s}|^2 \langle \lambda 0\sigma | \frac{1}{(z - H_0) - H_I} | \lambda' 0\sigma \rangle \\ &= L^3\hbar^2 \sum_\sigma |\wp_\sigma|^2 |\phi_{1s}|^2 G_{\lambda\lambda' 0\sigma} \ , \end{aligned}$$

where H_0 was grouped with z to show that $(z - H_0)^{-1}$ can be regarded as the bare Green's function, and the whole operator as the full resolvent of the system. The value of z can be approximated by the value of the unperturbed energy ε^0_λ of the state $|\lambda\rangle$ in $\Im_0$. G is

$$\begin{aligned} G_{\lambda\lambda' 0\sigma}(\omega_L) &= \langle \lambda 0\sigma | \frac{1}{[G^0(\omega_L)]^{-1} - H_I} | \lambda' 0\sigma \rangle \\ G^0_k(\omega_L) &= \frac{\delta_{\lambda\lambda'}\delta_{kk'}}{\hbar\omega_L - \left(\epsilon_0 + \frac{\hbar^2 k^2}{2\,m}\right) + i\eta} \ , \end{aligned}$$

where ε^0_λ is finally chosen to be equal to zero, without lost of generality. Note that, while G depends on spin, G^0 does not. We remark that we work in the off-resonance regime for which $\omega_L < \epsilon_0$, thus making the real part of G^0 always negative.

This will be the starting point for Chapters 2 and 3, where it will be solved either exactly or expanding in power series of H_I.

Chapter 2

A non-perturbative solution for the indirect interaction mediated by excitons

It was pointed out by Piermarocchi *et al.* [6] that itinerant excitons, i.e. optical excitations free to move in the host material that embeds the localized spins, can induce an effective spin-spin interaction between localized spins. This mechanism has been dubbed *Optical RKKY* (ORKKY), in analogy to the mechanism in the theory of magnetism [32], where electrons are involved. In the coherent optical case virtual excitons are created, and the ORKKY coupling is obtained from a second order perturbation theory in the exchange coupling between the itinerant exciton and the localized spin. The ORKKY result predicts that the coupling between the localized spins is always ferromagnetic, independently of the sign of the coupling with the excitons. In this chapter we show that higher order terms in the exciton-impurity coupling can modify the strength and sign of the interaction, and affect its dependence as a function of the spin separation. The calculation of the spin-spin interaction can be reduced to a spin dependent scattering problem that can be solved including exactly all the multiple scattering terms between the two localized spins. We follow here an

approach similar to that used to calculate multiple scattering effects of $\pi^{\pm}$ mesons by deuterons [31]. The higher order terms in the exciton-impurity coupling describe bound states which affect strongly the optically induced spin-spin interaction. In particular, a controlled anti-ferromagnetic (AF) coupling can be realized when the laser energy is tuned in the bonding-antibonding gap for the exciton localized by two impurities. This laser controlled switching of sign of the spin-spin interaction opens new directions in the investigation of competing interactions in spin systems.

The exchange between nuclear spins through excited electronic states has been discussed in the past in the case of molecules [33] and insulators [34]. In particular, Bloembergen and Rowland predicted in Ref. [34] an exponential decay of the spin-spin interaction with a characteristic length $\kappa = \hbar/\sqrt{2mE_g}$. This length depends on the energy gap E_g of the insulator and on the mass of the virtual electron hole pairs across the gap. In the optically induced RKKY, the energy gap is effectively reduced by the laser field which increases the effective length to $\kappa = \hbar/\sqrt{2m(E_g - \hbar\omega_P)}$, with $\hbar\omega_P$ being the energy of the laser. Also, the density of electrons in the occupied bands in the insulator is replaced in the optical case by the density of photons in the field. The innovative strength of the optically induced case resides in the control potentialities since both the intensity and the frequency of the laser can be controlled in an experiment. Going beyond second order perturbation theory presents intrinsic

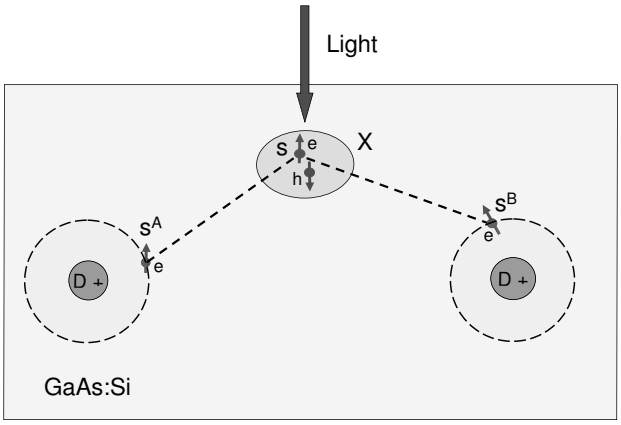

Figure 2.1: Scheme of the light induced spin-spin interaction in the case of two shallow donors.

difficulties in the case of metals [35]. These difficulties are not present in the optical coherent case since there is no Fermi sea of electrons. The presence of a Fermi sea simultaneously with the laser would produce light-induced Kondo effects [51], which we do not consider here.

The chapter is organized as follows: In section 2.1 we recall the expression for the effective Hamiltonian of two localized spins in the presence of a light field, relating it to the spin-dependent T matrix operator of a two-center scattering problem. We study first in Sec. 2.2 the scattering of one exciton with one center. By generalizing a result from scattering theory [36] to the spin dependent case, we show in section 2.3 how the T matrix operator for the exciton scattering on two centers can be expressed in terms of the T operator for the one center scattering. We also study in this section the effects of the polarization of the light and we show that a circularly polarized field will induce an additional term representing a magnetic field. The theory is applied in section 2.4 to two systems: shallow donors, and deep rare earth magnetic impurities. We discuss implications for quantum computing implementations and for the optical control of macroscopic magnetic properties in Chapter 4, Sec.4.3.

2.1 The effective Hamiltonian for localized spins coupled by the light

A scheme showing the realization of a light induced spin-coupling in the case of two shallow donors is given in Figure 2.1. We are not interested in calculating the optical properties of the whole system, but we want to consider the effect of a coherent field on the dynamics of the two initially non-interacting localized spins s^A and s^B. The light creates virtual/real excitons in the semiconductor host and couples the localized spins. We want to study the behavior of the two localized spins in the coherent optical regime. This implies that the laser is always off resonance with respect to the free exciton band to avoid strong energy absorption. We therefore consider

only single exciton processes in the presence of a monochromatic laser field. The system of two localized spins coupled to one itinerant exciton is described by the sum of two Hamiltonian terms. H_0 describes a free exciton of mass m with dispersion $\epsilon_k = \epsilon_0 + \hbar^2 k^2/2m$,

$$\begin{aligned} H_0 &= \epsilon_0 + \sum_{k\sigma} \frac{\hbar^2\, k^2}{2m}\ \hat{b}^\dagger_{k\sigma}\hat{b}_{k_\sigma} \\ H_I &= \frac{1}{V}\sum_{kk'\alpha\alpha'\beta} J_{k,k'}(s^A\cdot s_{\alpha'\alpha} + e^{-i(k'-k)R}\ s^B\cdot s_{\alpha'\alpha})\ b^\dagger_{k'\alpha'\beta}b_{k\alpha\beta} \end{aligned} \tag{2.1}$$

and H_I describes the spin dynamics, where the two localized spins 1/2 are described by s^A and s^B. V is the volume, and s is the electronic spin of the itinerant exciton. $b^\dagger_{k\alpha\beta}$ creates an exciton with center of mass momentum k, electron spin α, and hole spin β. R is the separation between the two impurities. $J_{k,k'}$ is the exciton-spin exchange interaction. The strength and the sign of this term depend strongly on the nature of the localized spin. The sign, for instance, is determined by the competition between the ferromagnetic potential exchange and the anti-ferromagnetic kinetic exchange which is due to the hybridization of the itinerant exciton state with the localized state [37]. We will keep for the moment a general approach independent of the nature of the $J_{k,k'}$, and we will discuss two specific examples in section 2.4. A spin-independent term corresponding to a direct Coulomb interaction between the exciton and the impurity is also present. This term is small for shallow impurities, where kinetic exchange effects dominate, but becomes important for deep impurities. We will include this term in the case of rare earth impurities discussed in Sec. 2.4.2, and we disregard it in the general discussion since it only introduces spin-independent energy shifts. We assume that the $1s$ excitons dominate the light induced effect, as discussed in Ref. [6]. Moreover, we focus on systems where the localized states interact only with the electron in the exciton: the full Hamiltonian in Eq. (2.1) is diagonal in the hole spin index β. This is a good approximation for electrons in neutral donors, since it is equivalent to neglecting the electron-hole exchange interaction which in

most semiconductors is much smaller than the electron-electron exchange. Concerning the second example we will consider, i.e. the case of the Yb^{3+} ions in III-V, it is known that these ions act as strong isoelectronic traps for electrons and the s-f exchange in the conduction band dominates.

The interaction of the excitons with an external time dependent optical field provides the mechanism for the control of the two localized spins and is described by the Hamiltonian

$$H_L = \sqrt{V} \sum_{\sigma} \wp_{\sigma} e^{i\omega_L t} \phi_{1s} b_{k=0,\alpha+\beta=\sigma} + h.c. \ , \tag{2.2}$$

where $\wp_{\sigma}$[1] is the Rabi energy of the interband optical transition and $\hbar\omega_L$ is the energy of the laser, σ is the polarization of the light. We have used the rotating wave approximation in Eq. (2.2). ϕ_{1s} is the envelope function of the electron hole pair taken at $\rho = r_e - r_h = 0$. In the case of a cw laser field, the time dependence can be eliminated by moving to the rotating frame with frequency ω_L, thus replacing ϵ_k by $\epsilon_k - \hbar\omega_L$ in H_0.

We are deriving an effective Hamiltonian for the two localized spins in the presence of the laser field, as shown in Chapter 1.

$$H_{eff,\lambda\lambda'} = V \sum_{\sigma} \mid \wp_{\sigma} \mid^2 \mid \phi_{1s} \mid^2 G_{\lambda 0\sigma,\lambda' 0\sigma}(\omega_L) \tag{2.3}$$

where

$$G_{\lambda 0\sigma,\lambda' 0\sigma}(\omega_L) = \langle \lambda 0\sigma | \frac{1}{[G^0(\omega_L)]^{-1} - H_I} | \lambda' 0\sigma \rangle \tag{2.4}$$

is the Green's function for the system composed by the exciton and two spins, with

$$G^0(\omega_L) = \frac{\delta_{kk'}}{\hbar\omega_L - (\epsilon_0 + \frac{\hbar^2 k^2}{2m}) + i\eta} \ . \tag{2.5}$$

Since we are dealing with only single-exciton processes, the Lippman-Schwinger equation for G can be rewritten in terms of an equation for the T-matrix defined by the

[1] In Chapter 1 the Rabi energy is designated by $\hbar\wp$.

relation $G = G_0 + G_0 T G_0$. We solve the problem in two steps: (i) the T^A and T^B operators representing the scattering of the exciton with only one impurity (identified by the index A or B) is solved. (ii) The T-matrix for the exciton interacting with two impurities is explicitly rewritten in terms of T^A and T^B using [36]

$$T = \frac{1}{1 - T^A G^0 T^B G^0} T^A [1 + G^0 T^B] + (A \rightleftharpoons B) \tag{2.6}$$

where $(A \rightleftharpoons B)$ stands for repeating the previous term with interchange of superscripts A and B. Eq. (2.6) takes into account exactly all the multiple scattering processes between the exciton and the two localized spins. We will focus in the next section on the interaction of the exciton with a single localized spin. Multiple scattering effects in the two spins case are addressed in section 2.3.

2.2 Exciton - single impurity scattering

This section focuses on the solution of the T-matrix equation for one scattering center (named A). Due to the short range nature of the exchange interaction, the exchange integral $J_{k,k'}$ in H_I is often reduced to a constant, corresponding to a delta-like interaction in space. Here we consider a more realistic form of the interaction using the separable potential approximation [38, 39] where $J_{k,k'} = J v_k v_{k'}$, with v_k being a dimensionless form factor that depends only on $k = |\vec{k}|$. v_k describes the effect of the finite size of the non-local exchange interaction (see Appendix E). The separable form of $J_{k,k'}$ will allow us to obtain analytical expressions for the T-matrix, and provide a flexible theoretical framework with parameters that can be taken from the experiments. On the other hand, this potential can support at most one s-like bound state. The integral equation for the T-matrix, $T = H_I + H_I G_0 T$, can then be written

explicitly as

$$T^A_{kk'\alpha\alpha'} = \frac{J}{V} v_k v_{k'} s^A \cdot s_{\alpha\alpha'} + \frac{J}{V} \sum_{k''\alpha''} v_k v_{k''} s^A \cdot s_{\alpha\alpha''} G^0_{k''} T^A_{k''k'\alpha''\alpha'} \tag{2.7}$$

We can write the T-matrix as a sum of a scalar and vector part

$$T^A_{kk'\alpha\alpha'} = \frac{v_k v_{k'}}{V} [T_0 \delta_{\alpha\alpha'} + T_1 s^A \cdot s_{\alpha\alpha'}] \tag{2.8}$$

and, using the identity

$$(s^A \cdot s)^2 = \frac{3}{16} - \frac{s^A \cdot s}{2} \tag{2.9}$$

we rewrite Eq. (2.7) in the form of two coupled equations

$$T_1 = J + JF_0(T_0 - T_1/2) \tag{2.10a}$$

$$T_0 = \frac{3}{16} JF_0 T_1 \tag{2.10b}$$

where

$$F_0(\omega_L) = \frac{1}{V} \sum_{k''} v^2_{k''} G^0_{k''} \tag{2.11}$$

The reduction of the integral equation to two algebraic equations is a consequence of the form of the interaction and the fact that the all spins follow SU(2) algebra[2]. The two coupled equations in Eq. (2.10) are solved and give

$$T_0 = \frac{3J}{16} \frac{JF_0}{1 + \frac{JF_0}{2} - \frac{3(JF_0)^2}{16}} \tag{2.12a}$$

$$T_1 = \frac{J}{1 + \frac{JF_0}{2} - \frac{3(JF_0)^2}{16}} \tag{2.12b}$$

This analytical solution allows us to investigate the strong coupling regime in which the quantity JF_0 is not small. The most interesting feature of the strong coupling

[2]In the general case of spin $s > 1/2$ the integral equation requires the inclusion of other powers of the spin operators.

regime is the formation of bound states of the exciton with the impurities, identified by the poles in the T-matrix. Varying the frequency of the laser ω_L, which will modify the F_0, we can scan the spectrum to obtain the energies of those bound states. We remark that under the condition $\omega_L < \epsilon_0$, and assuming that the potential $v(k)$ is an analytic function of k, no singularities or branch cuts exist for the function F_0. Therefore, the only source of poles is given by the zeros of the function $1+\frac{JF_0}{2}-\frac{3(JF_0)^2}{16}$, appearing in T_1 and T_0. Considering separately the singlet and triplet channels we find

$$T^S \doteq \langle S|\, T\, |S\rangle = -\frac{3/4J}{1+3/4JF_0} \tag{2.13a}$$

$$T^T \doteq \langle T|\, T\, |T\rangle = \frac{J/4}{1-1/4JF_0}\,. \tag{2.13b}$$

Where $|S\rangle = 1/\sqrt{2}(\,|\uparrow\downarrow\rangle - |\downarrow\uparrow\rangle)$ and $|T\rangle$ is any of the triplet states. In the singlet and triplet channels only one of the two poles in Eq. (2.12) is present. Due to the fact that $F_0(\omega_L)$ is negative for all allowed values of ω_L, we also remark that, as expected, the exciton binds in a singlet spin state if $J > 0$ (antiferromagnetic coupling), while the bound state is a triplet if the exciton-electron exchange is ferromagnetic (i.e. $J < 0$).

2.3 Exciton - two impurities scattering

Starting from the results obtained in the previous sections, we construct in this section the solution for the exciton-two impurities T-matrix and the corresponding H_{eff} for the localized spins. Eq. (2.6) can be expanded in terms of T operators as

$$T = T^A + T^A G^0 T^B + T^A G^0 T^B G^0 T^A + ... \tag{2.14}$$

The matrix for T^B can be obtained from a simple phase shift: if $T^A_{kk'}$ is the T-matrix for a scattering center with potential $V(r)$ then $e^{-i(k'-k)\cdot R}T^A_{kk'}$ is the corresponding one

for a potential $V(r-R)$, i.e. $T^B_{kk'}$ [36]. We can take the matrix elements of Eq. (2.14) in the k representation. To illustrate how this series can be summed let us consider as an example the third term in Eq. (2.14)

$$\begin{aligned}\langle k \mid T^A G^0 T^B G^0 T^A \mid k' \rangle &= \frac{1}{V^3} \sum_{k'',k'''} v_k v_{k''} \Upsilon^A G^0_{k''} e^{-i(k'''-k'')\cdot R} v_{k''} v_{k'''} \\ &\quad \times \Upsilon^B G^0_{k'''} v_{k'''} v_{k'} \Upsilon^A \end{aligned} \tag{2.15}$$

where we have defined

$$\Upsilon^{A(B)} = T_0 + T_1 s^{A(B)} \cdot s \ . \tag{2.16}$$

Reordering factors and defining the function

$$F_R(\omega_L) = \frac{1}{V} \sum_k e^{ik\cdot R} v_k^2 G^0_k \ , \tag{2.17}$$

this term takes the form,

$$\frac{v_k v_{k'}}{V} F_R^2(\omega_L) \Upsilon^A \Upsilon^B \Upsilon^A \ . \tag{2.18}$$

Following the same procedure, the full series can be summed to

$$T_{k,k'} = \frac{v_k v_{k'}/V}{1 - F_R^2 \Upsilon^A \Upsilon^B} \Upsilon^A [1 + F_R \Upsilon^B] + (A \rightleftharpoons B) \ . \tag{2.19}$$

The T-matrix is now expressed as an operator in a 8-dimensional space generated by three spins 1/2: one electron in the exciton and two localized electron states. By direct inversion and products of 8 by 8 matrices, Eq. (2.19) can be rewritten in terms of a combination of spin products (see Appendix B), and using $G = G_0 + G_0 T G_0$ we obtain the spin dependent effective Hamiltonian

$$H_{eff} = B_{eff} \cdot (s^A + s^B) + J_{eff} s^A \cdot s^B \ . \tag{2.20}$$

B_{eff} represents an effective magnetic field acting on both spins and J_{eff} is an effective isotropic Heisenberg exchange. The effective magnetic field and exchange constant can be written as

$$B_{eff} = \frac{|\wp_{\sigma+}|^2 - |\wp_{\sigma-}|^2}{\delta^2} \frac{|\phi_{1s}|^2 v_0^2 J(1 - JF_R^-)}{(1 - JF_R^+)[1 - JF_R^+(3JF_R^- - 2)]} \frac{\hat{z}}{2} \tag{2.21}$$

and

$$J_{eff} = \frac{|\wp_{\sigma+}|^2 + |\wp_{\sigma-}|^2}{\delta^2} \frac{|\phi_{1s}|^2 v_0^2 J^2 F_R/2(1 - JF_R^-)}{(1 - JF_R^+)[1 - JF_R^+(3JF_R^- - 2)][1 - JF_R^-(3JF_R^+ - 2)]} \ , \tag{2.22}$$

where we have defined

$$F_R^{\pm}(\omega_L) = \frac{1}{4V} \sum_k (1 \pm e^{ik \cdot R}) v_k^2 G_k^0 \ . \tag{2.23}$$

$\hat{z}$ identifies the direction of propagation of the light, $\delta = \epsilon_0 - \hbar\omega_L$ is the optical detuning, and $\wp_{\sigma\pm}$ correspond to the contributions to the Rabi energy from the two circularly polarized components of the light. From Eq. (2.19) a spin-independent term is also derived which is not shown in Eq. (2.20) since it is irrelevant for our purposes. If we want to include the effect of the degenerate light hole band the two expressions in Eqs. (2.21) and (2.22) should be multiplied by 2/3 and 4/3, respectively. By keeping the lowest order in J in Eqs. (2.21) and (2.22) we obtain

$$B_{eff} = \frac{|\wp_{\sigma+}|^2 - |\wp_{\sigma-}|^2}{\delta^2} |\phi_{1s}|^2 v_0^2 J \frac{\hat{z}}{2} + O(J^2) \ , \tag{2.24}$$

and

$$J_{eff} = \frac{|\wp_{\sigma+}|^2 + |\wp_{\sigma-}|^2}{\delta^2} |\phi_{1s}|^2 v_0^2 J^2 F_R/2 + O(J^3) \tag{2.25}$$

which recovers the Optical RKKY result of Ref. [6]. The magnetic field induced by virtual excitons has recently been analyzed using a more fundamental approach in the case of a single impurity by Combescot and Betbeder-Matibet in Ref. [40]. In this

reference the spin independent term that provides a correction to the optical Stark shift is also discussed.

2.4 The spin - spin coupling

In this section we apply the results obtained above to (i) excitons mediating the interaction between two electronic spins localized in shallow donors (e.g. GaAs:Si) and (ii) excitons mediating the interaction between two magnetic ions with spin 1/2 (two rare earth ion Yb^{3+} in InP). Yb in InP is one of the most investigated rare earth doped III-V material. In principle Yb^{3+} in GaAs could be used but it is technically more challenging to obtain samples where only substitutional Yb is present. [41] We will focus on the effect of the binding of excitons on the spin-spin coupling. The parameters J and the range of the potential v_k can be fixed in such a way that the single-spin exciton T-matrix reproduces the binding energy and the spin configuration of the bound exciton obtained from the experiment.

2.4.1 Shallow donors

For a scheme of the system we can refer again to Figure 2.1. For excitons interacting with a shallow neutral donor the effective mass approximation can be used. The problem of excitons bound to neutral donors and acceptors has been heavily investigated both experimentally and theoretically [42]. In the case of GaAs it is known that the exciton binds to a neutral donor with a binding energy of about 1 meV. It is also clear from the magnetic field dependence of the bound exciton resonance that the two electrons are paired in a singlet around the donor ion and the hole is bound by Coulomb interaction. The picture is very similar to the one of a positive charge bound to an H^- ion. As in the H^- ion case, the dominant term responsible for the binding of the two electrons is a kinetic exchange term and we can therefore disregard the effect of a spin independent term in the Hamiltonian. The range of the kinetic exchange is

determined by the hybridization between the localized electron state in the neutral donor and the electron state in the free exciton. We therefore assume that the v_k is of the form

$$v_k^2 = \frac{1}{1+(\Lambda k)^2} \ , \tag{2.26}$$

where the parameter Λ determines the range of the potential. In the following we will use the excitonic atomic units, see Appendix C. We can calculate the functions F_0 and F_R in Eq. (2.11) and Eq. (2.17) as

$$F_0 = -\frac{1}{4\pi\Lambda}\frac{1}{(\Lambda\sqrt{\delta\nu}+\nu)} \tag{2.27}$$

$$F_R = -\frac{1}{4\pi R}\frac{e^{-R/\Lambda}-e^{-R\sqrt{\delta/\nu}}}{\Lambda^2\delta-\nu} \ , \tag{2.28}$$

where $\nu = \mu/m$ is the reduced total mass ratio of the excitonic system which is about $1/5$ in GaAs taking $m_e = 0.08$ and $m_h = 0.17$. Notice that F_R can be rewritten as

$$F_R = F_0 \ \Lambda\nu\frac{e^{-R/\Lambda}-e^{-R\sqrt{\delta/\nu}}}{R(\Lambda\sqrt{\delta\nu}-\nu)} \tag{2.29}$$

and has no poles for positive detuning δ; for $R \gg \lambda$, F_R has a Yukawa form with a detuning-related decay length $a_B^*\sqrt{\nu/\delta}$ as found in Ref. [6], while at short R the finite range of the potential regularizes the $1/R$ divergence. In v_k we take Λ =0.25. Using the fact that the exciton binds to the donor only in the singlet channel, we can determine the value of J in the T^S in Eq. (2.13a) in such a way to have a pole at the experimental binding energy. The J is positive, as expected from the fact that the kinetic exchange is antiferromagnetic, and we take its value to be $J = 1\ Ry^*(a_B^*)^3$ which gives a binding energy for the singlet of 0.23 Ry^*, in accordance with the experimental value of 1 meV. The triplet is unbound.

We plot in Figure 2.2 the coupling constant J_{eff} obtained from Eq. (2.22) as a function of the energy of the laser measured from the bottom of the free exciton

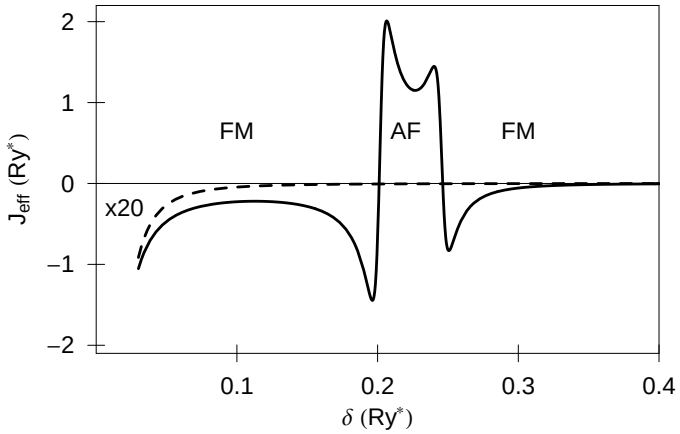

Figure 2.2: Coupling constant J_{eff} between the two electronic spins localized in a shallow neutral donor embedded in GaAs as a function of the laser energy, measured from the bottom of the free exciton band. The intensity of the laser corresponds to a Rabi energy of $\wp_{\sigma+} = 0.05$ meV. The dashed line gives the result predicted with the same parameters using second order perturbation theory in the coupling constant J.

band, $\delta = \epsilon_0 - \hbar\omega_L$. A small imaginary contribution to the energy, $\eta = 0.0001 Ry^*$, has been added in all the plots. The Rabi energy is $\wp_{\sigma+}$ =0.05 meV. The $\sigma-$ component of the Rabi energy is zero. The separation between the two neutral donors R is 2 a_B^*. In the region of large detuning we have a ferromagnetic coupling in agreement with the results obtained in the ORKKY limit. When we approach the energy corresponding to the binding of the exciton to the impurity, at $\delta = 0.23$, we observe that the interaction is strongly enhanced and there is a region with an antiferromagnetic (AF) coupling. Multiple scattering between the two impurities results in the formation of bonding-antibonding states for the exciton. When the light has a frequency in the bonding-antibonding gap the effective interaction changes sign. This is analogous to the antiferromagnetic coupling generated by superexchange in magnetic materials. [37] When the laser is tuned above the resonances we recover again the ferromagnetic coupling. In the same plot we also show the effective coupling that would result by keeping the lowest order in J (ORKKY). In this case no resonances due to the binding of the excitons are present and, in order to obtain a sizeable coupling, the laser has to be tuned close the bottom of the excitonic band. In Figure 2.3 we show a contour plot of the effective spin-spin coupling as a function of the detuning

and impurity separation. Dark gray corresponds to either strong negative or strong positive coupling depending on the region, the light gray tone in the upper-right corner corresponds to zero. At large R the coupling is mostly ferromagnetic and there is only a small region close to the exciton binding energy where the coupling can be AF. When the distance between the two impurities decreases, the bonding-antibonding gap and the region corresponding to the antiferromagnetic coupling is wider. The thick dashed line indicates a change of sign of J_{eff}. Notice also the different decay of the interaction as a function of R for different values of the detuning. At δ =0.4 the maximum strength is at $R = 0.8$ and decays quickly within a quarter of a_B^* to the minimum value in the plot. At δ =0.1 the same minimum is reached within a much larger interval of about 2 a_B^*. This is consistent with the fact that at a small detuning there is a contribution from the free exciton band which can give a longer range for the effective interaction.

2.4.2 Rare earth impurities

The magnetic properties of the Yb^{3+} ion in III-V [43] arise from its partially filled $4f$ shell, possessing 13 electrons. In III-V materials, for a substitutional impurity, the crystal fields split the ground manifold of the ion into two doublets (spin=$\frac{1}{2}$), Γ_6 and Γ_7, and a quadruplet (spin=$\frac{3}{2}$), Γ_8. The lowest lying state is the Kramers doublet Γ_6, which behaves like a spin $\frac{1}{2}$ with an effective isotropic $g = 24/7$. [44] Yb in InP replaces Indium and acts as an isoelectronic trap. From electrical [45] and optical [46] measurements it is known that the exciton binds to this isoelectronic impurity with a binding energy of 30 meV. The binding is due to a short range potential that arises from the difference in the core pseudopotential between the impurity and the host ion it replaces. [47] It is reasonable to assume that this short range potential is spin-independent and we take it into account by adding to the exciton-impurity

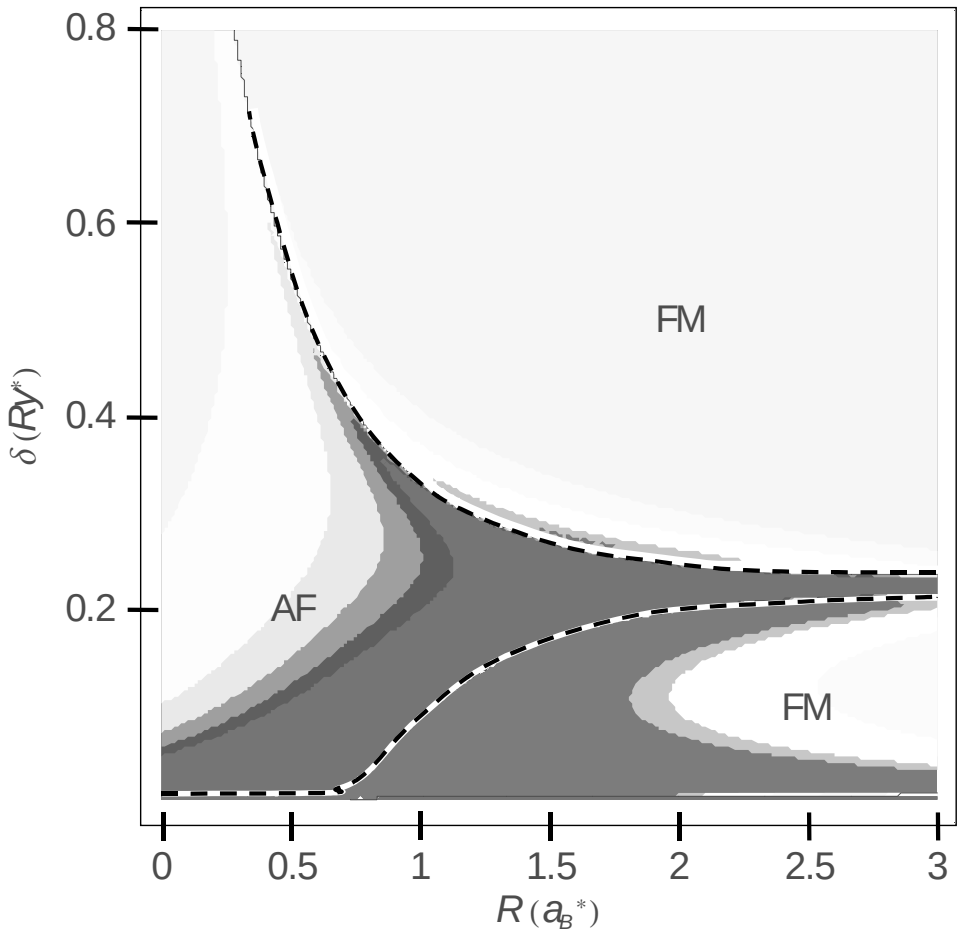

Figure 2.3: J_{eff} as a function of the donors separation R and detuning δ . The contour plot identifies the regions where the coupling is Ferromagnetic (FM) or antiferromagnetic (AF). The thick dashed lines indicate a change of sign of J_{eff}. The intensity of the laser corresponds to a Rabi energy of $\Omega = 0.1$ meV. The intensity of gray represents the value of J_{eff}.

Hamiltonian of Eq. (2.1) the term

$$H_2 = \frac{1}{V}\sum_{k,k'} \Delta_{k,k'}(1 + e^{-i(k'-k)R}) b^\dagger_{k'\alpha\beta} b_{k\alpha\beta} \ . \tag{2.30}$$

We use the separable potential approximation also for the spin-independent short-range potential and we parametrize it in the form $\Delta_{k,k'} = \Delta v_k v_{k'}$, i.e. it has the same k dependence of $J_{k,k'}$. A more general analytical result can be obtained using a separable form for $\Delta_{k,k'}$ with different coefficients, but we expect the range of the s-f exchange and that of the impurity potential to be very similar. The value of Δ is determined by imposing that the exciton-single impurity T-matrix has a pole for both singlet and triplet channels at 30 meV. Following the same procedure used in Sec. 2.2 we obtain for the T operators in the singlet and triplet channels

$$T^S = \frac{-3/4J + \Delta}{1 + 3/4JF_0 - \Delta F_0} \tag{2.31a}$$

$$T^T = \frac{J/4 + \Delta}{1 - 1/4JF_0 - \Delta F_0} \ . \tag{2.31b}$$

The expressions for the J_{eff} and B_{eff} modified by the presence of Δ can be obtained by plugging the Eqs. (2.31) in the general expressions of Eqs. (B.5) in Appendix B. The quantity J is the s-f exchange interaction between the impurity and the electron in the exciton. In typical rare earth ferromagnetic semiconductors the s-f exchange is ferromagnetic and is of the order of few eV Å^3 [48], comparable to the s-d exchange in Mn based diluted magnetic semiconductors. [49] We are using $J = -10^{-4}$ in our units which corresponds to a conservative estimate of 0.7 eV Å^3 in InP. In InP the value of the Ry^* is about the same as that of GaAs (5 meV), while the Bohr radius is about 120 Å. For Λ in v_k we take $\Lambda = 0.01$ which is of the order of the ionic radius of Yb^{3+}.

We show in Figure 2.4 the contour plot of J_{eff} as a function of the laser detuning $\delta = \epsilon_0 - \hbar\omega_L$ and of the separation between the impurities R. At large distances we

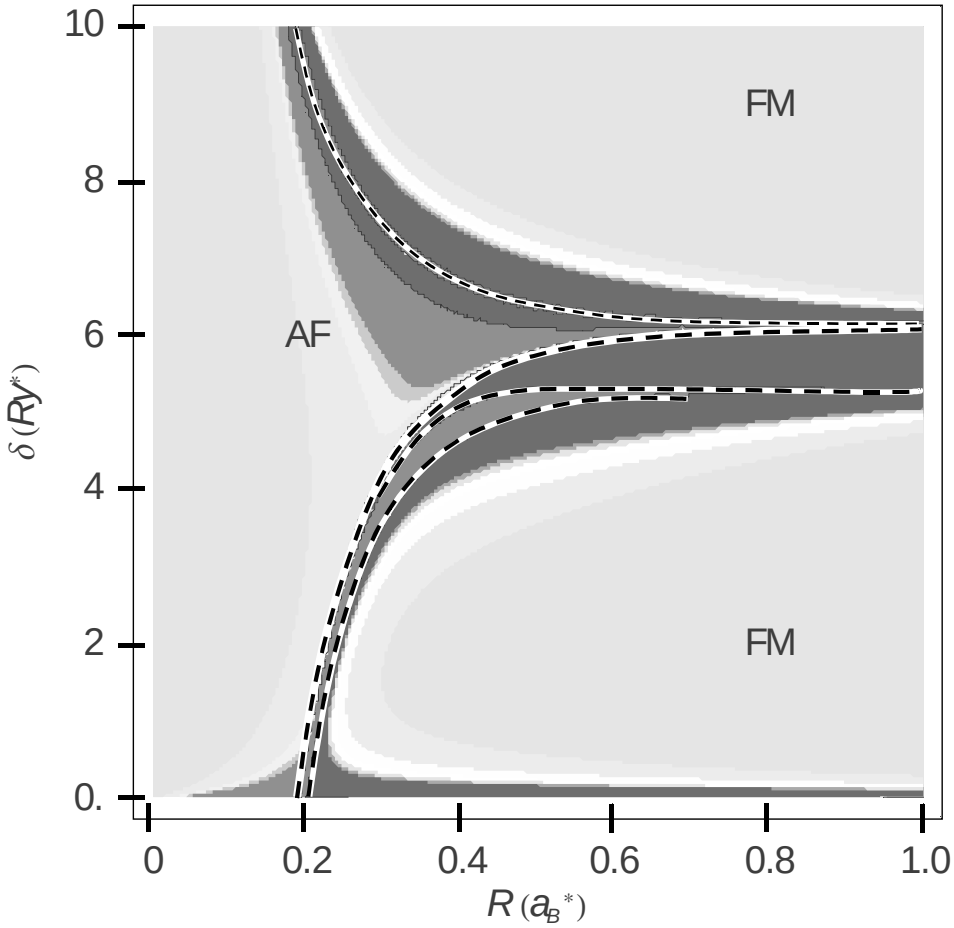

Figure 2.4: Coupling constant J_{eff} between two magnetic Yb^{3+} localized in InP as a function of the laser detuning $\delta = \epsilon - \hbar\omega_L$ and separation between the ions. The thick dashed lines indicate J_{eff}=0 and a change form ferromagnetic to antiferromagnetic coupling. The intensity of the laser corresponds to a Rabi energy of $\Omega = 0.1$ meV. The intensity of gray represents the value of J_{eff}.

observe two resonances related to the binding of the exciton in the singlet and triplet channels. Figure 2.5 (a) shows in detail the J_{eff} for a distance $R = 1\ a_B^*$. The two peaks in Figure 2.5 (a) correspond to the exciton bound to the impurity in the triplet and singlet channel. The peak at larger detuning corresponds to the triplet since the s-f exchange is ferromagnetic. For shorter distances we see from Figure 2.4 that each of the two peaks starts to split. The singlet (at smaller detuning) follows a behavior similar to the one of the shallow donors described above: the bonding and antibondig states identify a region where the coupling becomes antiferromagnetic. The triplet state splits in many different peaks as can be seen from Figure 2.5 (b). The sign of the interaction can change many times as a function of the detuning in this short distance region. This is indicated by the sign of J_{eff} plotted in the lower part of Figure 2.5 (b). Overall the antiferromagnetic coupling dominates at short distances while the interaction is ferromagnetic at large R.

2.5 Discussion

In conclusion, we have studied the problem of two 1/2 spins localized by impurities in semiconductor in the presence of an intense light field. The light induces a frequency dependent spin-spin coupling and a magnetic field that can be controlled by the polarization of the light. The effects are enhanced by the presence of impurity bound excitons which may split into bonding and antibonding states in the case of two impurities. The sign of the spin-spin coupling is generally ferromagnetic, but it can switch to antiferromagnetic when the laser is tuned to the bonding-antibondig gap. We have developed a flexible theoretical approach based on scattering theory where the parameters from the experiment can be used to estimate the size of the effect. We have discussed explicitly the case of two neutral donors in GaAs and two rare earth magnetic ions (Yb^{3+}) in InP.

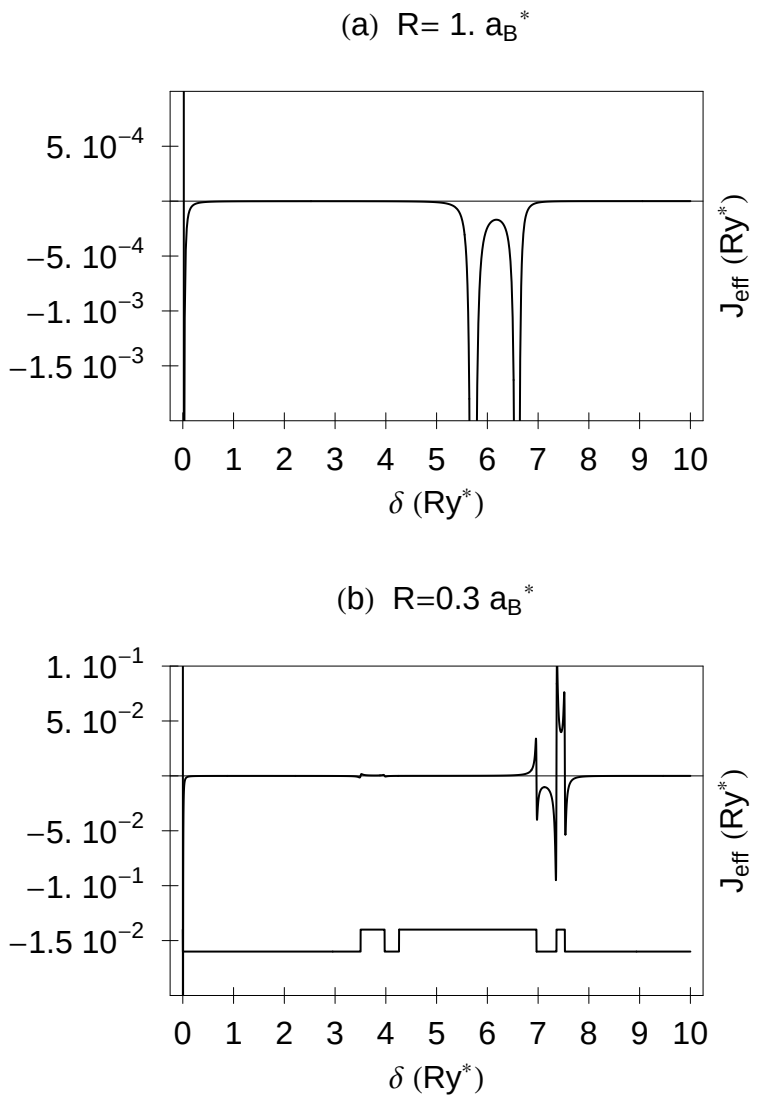

Figure 2.5: Coupling constant J_{eff} between two Yb^{+3} ions in InP as a function of the detuning δ. (a) Large distance. The coupling is ferromagnetic and the resonances in the interaction are close to the energy of the exciton bound to the Yb. (b) Short distance. The triplet channel splits in many different peaks producing many changes of the spin-spin coupling sign. The lower curve shows the sign of the coupling constant.

Chapter 3

Indirect interaction in micro-cavities

Planar micro-cavities are semiconductor devices that confine the electromagnetic field by means of two parallel semiconductor mirrors. When a quantum well is placed inside a micro-cavity the optical excitations (excitons) in the well couple to the electromagnetic modes of the dielectric structure. In the so-called strong-coupling regime, excitons and cavity photons give rise to new states, *exciton polaritons* [5], which appear in two branches separated by a vacuum Rabi splitting. Due to their hybrid light-matter nature, cavity polaritons have an effective mass that can be four to five orders of magnitude smaller than the exciton mass, and this is known to affect their interaction with phonons [52] and with interface disorder [53, 54]. In this chapter, we show that the small polariton mass also has a strong effect on the optically induced spin coupling between localized spins.

The physical system that we consider is a set of shallow donors embedded in a Quantum Well (QW) enclosed in a planar micro-cavity. A possible candidate is Si in a GaAs QW. However, the same idea can be applied to other spin-based implementations, e.g. charged quantum dots. Under strong coupling conditions, optically active excitons and cavity photons combine into polaritons, while dark excitons remain un-

affected. If the system is excited by an extra-cavity cw light source with a frequency below the polariton resonance, virtual polaritons appear in the system. These virtual particles mediate an indirect interaction between pairs of impurities. We seek to understand the indirect interaction of two spins when polaritons and dark excitons mediate the interaction, and the consequence this has on the optically-induced paramagnetic to ferromagnetic transition of an array of such impurities. The form of the effective Hamiltonian that contains only spin operators for the impurities is derived using perturbation theory to second order, similar to the optical indirect interaction $ORKKY$ [6,7]. For the sake of clarity, when solving for numerical data we will assume our system consists of Si donors in $GaAs$ micro-cavity QW.

3.1 Polaritons

A simplified picture of a planar micro-cavity is that of a Fabry-Pérot interferometer, where light incident normal to the surface only propagates for discrete frequencies. If a semiconductor QW is placed within the mirrors[1], excitons are generated by the interaction with light (see Figure 3.1). If the combined decay rates for cavity photons and excitons is smaller than the strength of the interaction[2] between these two particles a strong coupling develops. In this regime, the stationary states of the system are no longer the excitons and/or photons, but an admixture of them, the polaritons. An intuitive picture of the process is that of a photon that creates an exciton, which in turn by coupling to the cavity mode, produces a photon, and the process continues back and forth. The study of polaritons is done in the context of either classical or quantum electrodynamics. [5, 54, 55, 57] We employ the latter.

[1] Instead of metallic mirrors, a series of semiconductor layers, the *Distributed Bragg reflectors*, are used.

[2] This is strictly true when the energy of the exciton equals that of the cavity photons at $k = 0$, that is in resonance condition.

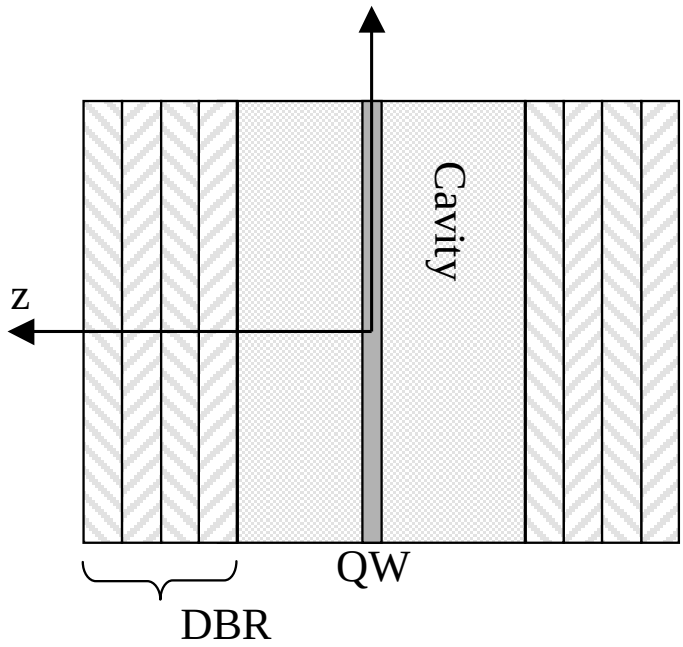

Figure 3.1: Micro-cavity with DBR mirrors (not to scale). Typical values for the size of the system are: width of each DBR period $\lambda/4$, cavity width $\lambda/2$, QW width $100\mathring{A}$, with λ the wavelength of the light.

The Hamiltonian describing cavity photons and excitons is

$$\begin{aligned} H &= \hbar \sum_{dark} \omega_{X,k}\, b_k^\dagger b_k + \hbar \sum \omega_{ph,k}\, c_k^\dagger c_k + \hbar \sum_{o.a.} \omega_{X,k}\, b_k^\dagger b_k \\ &\quad -i\hbar \sum g_k\, c_k^\dagger b_k + \text{h.c.}\ , \end{aligned} \tag{3.1}$$

where $b/b^\dagger$ and $c/c^\dagger$ are operators for excitons and cavity photons[3]; *o.a.* and *dark* stand for optical active and dark excitons. Photons only couple to *o.a.* states. In Equation 3.1

$$\begin{aligned} \omega_{X,k} &= \epsilon_0 + \frac{\hbar k^2}{2\,m} \\ \omega_{ph,k} &= \frac{c}{n}\sqrt{k^2+q^2} \\ \hbar g_k &= L^{-1/2} d_{cv} \phi_{1s}(0) \sqrt{2\pi\hbar\,\omega_{ph,k}}\ , \end{aligned}$$

[3]Following the quasimode approximation, we treat the electromagnetic field inside (*cavity* photons) and outside (*extra-cavity* photons) the micro-cavity as different entities. [54] This in addition to the fact that we deal with the off-resonance case, allows us to apply perturbation theory to the Hamiltonian that describes the extra-cavity or laser field H_L.

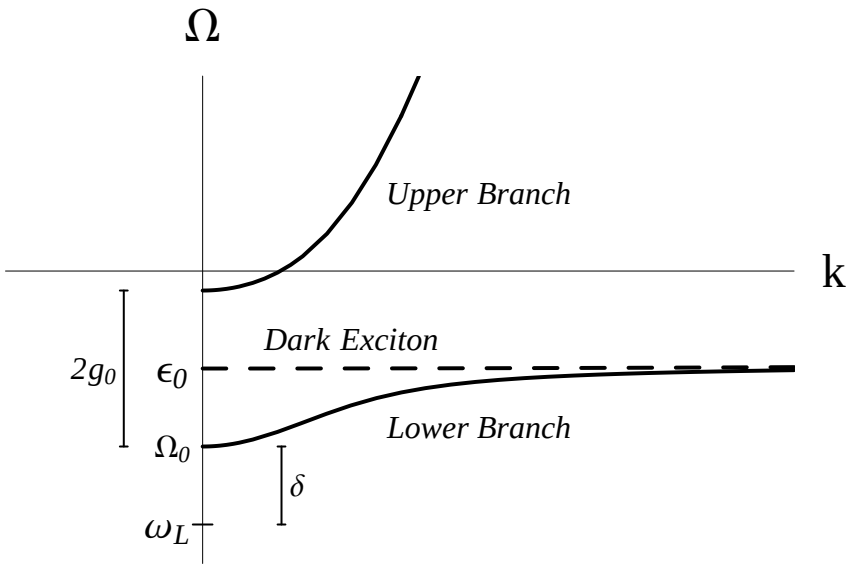

Figure 3.2: Polariton dispersion law for a QW (solid line) and dark exciton band (dashed line), for resonant conditions $\Delta = 0$.

where k is the in-plane momentum, q is the momentum in the growth direction (z-axis), c/n is the speed of light in the medium of index of refraction n, and L is the quantization length of the electromagnetic field in the growth direction.[4] A complete quantum mechanical treatment is possible using the Hopfield transformation that brings the photon and exciton operators to polariton ones, and diagonalizes the Hamiltonian. These polariton operators p_i, $i = 1, 2$ represent the so-called upper and lower polariton branches respectively, as shown in figure 3.2. The transformation reads

$$\hat{p}_{i,k} \;=\; u_{i,k}\,\hat{b}_k + v_{i,k}\,\hat{c}_k \;, \tag{3.2}$$

where,

$$u_{i,k} \;=\; \sqrt{\frac{\Omega_{i,k} - \omega_{phk}}{2\,\Omega_{i,k} - \omega_{phk} - \omega_{Xk}}}$$

$$v_{i,k} \;=\; \pm i\sqrt{\frac{\Omega_{i,k} - \omega_{Xk}}{2\,\Omega_{i,k} - \omega_{phk} - \omega_{Xk}}} \tag{3.3}$$

$$\Omega_{k,\,i} \;=\; \frac{1}{2}(\omega_{Xk} + \omega_{phk}) \pm \frac{1}{2}\sqrt{(\omega_{Xk} - \omega_{phk})^2 + 4g_k^2}\;. \tag{3.4}$$

[4] In Chapter 1 the quantity ϵ_0 is an energy, in contrast here it is taken as a frequency.

	$\Delta < 0$	$\Delta > 0$
Lower: Ω_2	ω_X	ω_{ph}
u_2	1	0
v_2	0	$-i$
Upper: Ω_1	ω_{ph}	ω_X
u_1	0	1
v_1	i	0

Table 3.1: Limits of the energy dispersion law and Hopfield's coefficients for coupling $g \to 0$, where $\Delta \doteq \omega_{X0} - \omega_{ph0} = \epsilon_0 - \frac{c}{n}q$ $(k = 0)$.

In the last equations, $-$ and $+$ correspond to lower $(i = 2)$ and upper $(i = 1)$ branches respectively. The Hamiltonian 3.1 is thus replaced by

$$H = \hbar \sum_{dark} \omega_{X,k}\, b_k^\dagger b_k + \hbar \sum_{k,\,i} \Omega_{ik}\, p_{ik}^\dagger p_{ik} \ . \tag{3.5}$$

Table 3.1 shows that in limit $g \to 0$ the excitonic or photonic physics is recovered on one or the other branch depending on the sign of exciton-cavity detuning $\Delta \doteq \omega_{X0} - \omega_{ph0} = \epsilon_0 - \frac{c}{n}q\,(k = 0)$.

3.2 The Hamiltonian of the system

As starting point, we use the total Hamiltonian for the system, as described in Chapter 1, and the cavity Hamiltonian 3.5. In addition, the interaction between holes and localized spins will be included, since it is important in the case of deep impurities. The light-exciton interaction H_L and the localized spin-exciton interaction H_I must be rewritten in terms of the new polariton operators. The calculation can be simplified by restricting the analysis to the lower polariton branch. In a digression at the end of Section 3.3, with more tools at hand, we show why this approximation is meaningful.

An important feature that we would like to capture is the difference between the indirect interaction mediated by excitons and the one mediated by polaritons. For this reason we want to be able to take the limit $g \to 0$ to recover the only-exciton scenario.

From now on, we will restrict to the lower polariton branch, with the requirement $\Delta < 0$, which ensures the correct limit for $g \to 0$ – the branch index i will be dropped. At low intensity and high detuning, only processes involving one virtual particle are present. We further restrict the discussion to circular polarization σ_+. Hereafter, we refer to the particle type, either polariton or dark exciton, as the *channel*. Therefore, the system consists of two localized spins plus one virtual excitation, either polariton or dark exciton.

The extra-cavity light generates virtual optical active excitons and thus polaritons. The interaction H_I connects different channels, since a flip of the electronic spin will cause (*o.a.* $\Leftrightarrow$ *dark*). The terms H_L and H_I are obtained by inverting the Hopfield coefficients $\{u, v\}$: $\hat{b}_k = r_k \hat{p}_k$ (Eq. 3.2), and replacing in the 2D versions of Eq. 1.9 and Eq. 1.17. They read

$$\begin{aligned} H_L &= \hbar\sqrt{A}\sum_{\sigma} \wp_\sigma r_0 e^{i\omega_L t}\phi_{1s} p_{k=0,\alpha+\beta=\sigma} + h.c. \\ H_I &= \frac{\hbar J}{A}\sum_{j\,kk'\alpha\alpha'\beta} e^{-i(k'-k)R_j} v_k v_{k'} \left(H^j_{PX} + H^j_{XP} + H^j_{PP} + H^j_{XX}\right) \ , \end{aligned} \tag{3.6}$$

where for the case of an arbitrary impurity j located at R_j

$$\begin{aligned} H^j_{PP} &= r^*_{k'}\, r_k\ \mathcal{S}^j_{PP}\ p^\dagger_{k'\alpha'} p_{k\alpha} \\ H^j_{XX} &= \qquad\ \mathcal{S}^j_{XX}\ b^\dagger_{k'\alpha'} b_{k\alpha} \\ H^j_{PX} &= r^*_{k'}\quad \mathcal{S}^j_{PX}\ p^\dagger_{k'\alpha'} b_{k\alpha} \\ H^j_{XP} &= r_k\quad\ \mathcal{S}^j_{XP}\ b^\dagger_{k'\alpha'} p_{k\alpha}\ , \end{aligned} \tag{3.7}$$

and the exciton-impurity exchange interaction is chosen separable (see Appendix E) $J\, v(k)v(k')$ with $v(k) = [1+(\Lambda\, k)^2]^{-1}$ [38]; indexes $\{X, P\}$ refer to the particle type or *channel*: either dark exciton or polariton. The time dependency in H_L is eliminated by transforming to the rotating frame at frequency ω_L. $\mathcal{S}$ contains the spin part, which as stated before, has the interaction electron - localized state, and hole - localized state.

The former consists of an Heisenberg interaction. The latter is of the Ising form, for the existence of transverse spin operators acting on the hole would cause its spin to undergo transitions to states of $s_z = \pm 1/2$ which belong to the light hole band[5]:

$$\begin{aligned} \mathcal{S}^A_{XX} &= \mathcal{S}^A_{PP} = s^A_z(s_{1/2z} + \zeta\, s_{3/2z}) \\ \mathcal{S}^A_{PX} &= \mathcal{S}^A_{XP} = \frac{1}{2}s^A_x(s_{1/2+} + s_{1/2-}) + \frac{1}{2i}s^A_y(s_{1/2+} - s_{1/2-}) \ , \end{aligned}$$

where s and $s_{1/2}$ are spin operators for the localized spin and for the electron in the polariton/exciton respectively.[6] We also include a constant ζ to account for the difference in strength between these two contributions to H_I. [49] The interaction that connects an initial state of polaritons with a final state of dark excitons (or vice versa) must be one that flips the spin of the state; this is accomplished with operators s_- and s_+. No spin flip occurs for the case of the interaction that conserves the particle type (either polariton or dark exciton)[7].

The new physics we would like to describe is indeed evident already in second order in J, the coupling between localized states and excitons[8]; thus, we restrict to this order to keep the mathematical treatment simple and easy to grasp. Again, an effective Hamiltonian for the interaction between two localized states will be derived for the off-resonance excitation of polaritons.

[5]We remind that the quantum confinement splits the heavy-hole and light-hole bands, and thus, transitions to the light-hole are suppressed. In other words, quantum confinement [56] forces the hole to lie in the z-direction, thus contributing an Ising interaction.

[6]Note that $H^\dagger_{XP} = H_{PX}$.

[7]H_I as described in this chapter is the expanded version of $S_{\alpha'\alpha}$ given in matrix form in Chapter 1, with the addition of the hole interaction. For example, $\mathcal{S}_{PP}$ is either S_{11} or S_{22}, and $\mathcal{S}_{XP}$ is either S_{12} or S_{21}.

[8]Notice also, that the hole can not flip between the states $|S_z = 3/2\rangle$ and $|S_z = -3/2\rangle$, because this will imply the use of three operators $s_{3/2+/-}$, which is third order in J.

3.3 The effective Hamiltonian

Using the formalism of effective Hamiltonian described in Section 1.3, modifying Eq. 3.1 and Eq. 3.6 according to a rotating frame with frequency ω_L and defining the Green's function we write

$$H_{eff} = \hbar^2 A |r_0|^2 |\wp_\sigma|^2 |\phi_{1s}|^2 \langle p_0 | G(\omega_L) | p_0 \rangle \ ,$$

where p_0 is a polariton with an in-plane wavevector $k = 0$ generated with circular polarization $\sigma+$ such that $(\alpha + \beta) = \sigma+$.

The problem is better analyzed if the state space $\Im_1$ of one quasi-particle (polariton or dark-exciton) is resolved into subspaces that are invariant under the action of G^0:

$$\begin{aligned} \Im_{1X} &: \{|k, 0, \alpha, 0\rangle\} \\ \Im_{1P} &: \{|0, k, 0, \alpha\rangle\} \ , \end{aligned}$$

leaving the bare Green's function G^0 completely diagonal, depending only on channel and wavevector. The bare polariton/dark exciton Green's function reads

$$\begin{aligned} G^0_{P,k} &\doteq \langle k, 0, \alpha, 0 | \, G^0 \, | k', 0, \alpha', 0 \rangle = \frac{\delta_{kk'}\delta_{\alpha\alpha'}}{\hbar} \frac{1}{\omega_L - \Omega_k} \\ G^0_{X,k} &\doteq \langle 0, k, 0, \alpha | \, G^0 \, | 0, k', 0, \alpha' \rangle = \frac{\delta_{kk'}\delta_{\alpha\alpha'}}{\hbar} \frac{1}{\omega_L - \omega_{X,k}} \\ G^0_{PX,k} &\doteq \langle 0, k, 0, \alpha | \, G^0 \, | k', 0, \alpha', 0 \rangle = 0 \\ G^0_{XP,k} &\doteq \langle k, 0, \alpha, 0 | \, G^0 \, | 0, k', 0, \alpha' \rangle = 0 \ . \end{aligned}$$

However, the Green's function G depends on wavevector, spin and channel, and has non-zero off-diagonal matrix elements in all these indexes.

The expansion of $\hat{G}$ reads

$$G = G^0 + G^0 H_I G^0 + G^0 H_I G^0 H_I G^0 + O(J^3) \ . \tag{3.8}$$

The zero order term contributes a shift to the energy. The first order term is an effective magnetic field. The second order term is the lowest contribution to the indirect interaction, and contains cross terms formed out of H_I belonging to different sites, as well as single site terms. Our concern is with two site scattering and so, we focus on the cross terms. Moreover, we consider only two localized states[9] A and B at positions $\mathbf{r} = 0$ and $\mathbf{r} = \mathbf{R}$, respectively. In matrix representation

$$\begin{aligned}\langle \Gamma' p_0 | \, G^{(2)} \, | \Gamma p_0 \rangle &= G^0_{P,0\sigma+} \langle \Gamma' p_0 | \, H_I^A G^0 e^{i\phi} H_I^B \, | \Gamma p_0 \rangle G^0_{P,0\sigma+} \\ &= \frac{1}{\hbar^2} \left(\frac{1}{\omega_L - \Omega_k} \right)^2 \langle \Gamma' p_0 | \, H_I^A G^0 e^{i\phi} H_I^B \, | \Gamma p_0 \rangle \ ,\end{aligned}$$

plus a term with site indexes interchanged. The phase ϕ is related to the separation between impurities, see Eq. 3.6. We are studying the coherent stimulation of the system, so $|\Gamma p_0\rangle = |\Gamma\rangle \otimes |0, k = 0, 0, \sigma+\rangle$, where $|\Gamma\rangle$ stands for the spin degrees of freedom of the two localized states. In matrix representation

$$\begin{aligned} H_I^A G^0 e^{i\phi} H_I^B &= \begin{pmatrix} \widetilde{H}^A_{XX} & \widetilde{H}^A_{XP} \\ \widetilde{H}^A_{PX} & \widetilde{H}^A_{PP} \end{pmatrix} \begin{pmatrix} G^0_X & 0 \\ 0 & G^0_P \end{pmatrix} e^{i\phi} \begin{pmatrix} \widetilde{H}^B_{XX} & \widetilde{H}^B_{XP} \\ \widetilde{H}^B_{PX} & \widetilde{H}^B_{PP} \end{pmatrix} \\ &= \begin{pmatrix} - & - \\ - & \widetilde{H}^A_{PX} G^0_X e^{i\phi} \widetilde{H}^B_{XP} + \widetilde{H}^A_{PP} G^0_P e^{i\phi} \widetilde{H}^B_{PP} \end{pmatrix} , \end{aligned}$$

where, in the final matrix, we focus only in the element that is relevant for us. $\widetilde{H}^j_{MN} = (\hbar J/A) \sum_{kk'\alpha\alpha'\beta} e^{-i(k'-k)R_j} v_k v_{k'} H^j_{MN}$ where the dependence on the other quantum numbers is omitted for clarity. The apparent asymmetry of the result is a consequence of analyzing the coherent process that has the same initial and final (polariton) state. From the definition 3.7, it is clear that the element H_{XX} does not enter the process

[9] G^0 does not depend in this new quantum number.

because $b^\dagger b\,|p\rangle = 0$. The resulting second order term is

$$\begin{aligned}\langle \Gamma' p_0|\, G^{(2)}\,|\Gamma p_0\rangle &= \frac{1}{\hbar^2}\left(\frac{1}{\omega_L-\Omega_k}\right)^2 \times \\ &\langle \Gamma' p_0|\, \widetilde{H}^A_{PX} G^0_X e^{i\phi}\widetilde{H}^B_{XP} + \widetilde{H}^A_{PP} G^0_P e^{i\phi}\widetilde{H}^B_{PP}\,|\Gamma p_0\rangle\ . \end{aligned} \tag{3.9}$$

As an example, the first term – intermediate scattering of a dark exciton – for arbitrary initial and final states of polaritons (without projecting the spins) is

$$\begin{aligned}\left[\widetilde{H}^A_{PX} G^0_X e^{\phi}\widetilde{H}^B_{XP}\right]_{k\,k'} &= \sum_{k''} \widetilde{H}^A_{PX,k\,k''} G^0_{X,k''} e^{i(k''-k')\cdot R}\widetilde{H}^B_{XP,k''k'} \\ &= \frac{(\hbar\, J)^2}{A} v_k v_{k'} r^*_k r_{k'} \mathcal{S}^A_{PX}\mathcal{S}^B_{XP}\frac{e^{-ik'\cdot R}}{A}\sum_{k''} v^2_{k''} e^{ik''\cdot R} G^0_{X,k''}\ . \end{aligned}$$

For both terms, the intermediate scattering mediated either by a polariton or a dark exciton gives rise, respectively, to the series

$$\begin{aligned} F_{R_X} &= \frac{1}{A}\sum_{k''} v^2_{k''} e^{ik''\cdot R} G^0_{Xk''} \\ F_{R_P} &= \frac{1}{A}\sum_{k''} v^2_{k''} |r_{k''}|^2 e^{ik''\cdot R} G^0_{Pk''}\ , \end{aligned} \tag{3.10}$$

both depending on R and ω_L, as well as other parameters.

A similar analysis of other terms in the expansion of G in Eq. 3.8 shows that the expansion is in powers of JF. In the spinless case it reads

$$\langle \Gamma' p_0|\, G\,|\Gamma p_0\rangle = G^0\left\{1+\left(G^0 v_0^2\frac{\hbar J}{A}\right)\left[1+JF+(JF)^2+\ldots\right]\right\}\ ,$$

where F is any of the functions defined in Eq. 3.10.

Our interest is in the second order term. After some algebra on Eq. 3.9, evaluating it at $k = k' = 0$, and choosing the functions $\{r, \wp_+, \phi_{1s}\}$ real, we obtain

$$H^{eff} = 2\left(\frac{\hbar\, J\, v_0\, {r_0}^2\, \wp_+\, \phi_{1s}}{\omega_L-\Omega_0}\right)^2 \left[F_{Rx}\,\mathcal{S}^A_{px}\,\mathcal{S}^B_{xp} + F_{Rp}\,\mathcal{S}^A_{pp}\,\mathcal{S}^B_{pp} + A \rightleftharpoons B\right]\ ,$$

where the only operators that appear are the ones for the spin of localized states A and B. The spin dependent term reads

$$\begin{aligned}
\mathcal{S}^A_{PP}\mathcal{S}^B_{PP} &= s^A_z s^B_z (s_{1/2z} + \zeta\, s_{3/2z})^2 = s^A_z s^B_z \left[\frac{\hbar^2}{4} + \zeta^2 \left(s_{3/2z}\right)^2 + 2\zeta\, s_{1/2z} s_{3/2z}\right] \\
\mathcal{S}^A_{PX}\mathcal{S}^B_{XP} &= \frac{1}{4}[s^A_x(s_{1/2+} + s_{1/2-}) - i s^A_y (s_{1/2+} - s_{1/2-})] \times \\
&\quad [s^B_x(s_{1/2+} + s_{1/2-}) - i s^B_y (s_{1/2+} - s_{1/2-})] \\
&= \frac{1}{4}[s^A_x s^B_x (s_{1/2+} + s_{1/2-})^2 - i s^A_x s^B_y (s_{1/2+} + s_{1/2-})(s_{1/2+} - s_{1/2-}) - \\
&\quad i s^A_y s^B_x (s_{1/2+} - s_{1/2-})(s_{1/2+} + s_{1/2-}) - \\
&\quad s^A_y s^B_y (s_{1/2+} - s_{1/2-})^2] \,. \qquad (3.11)
\end{aligned}$$

For the circular polarization $\sigma+$ considered here, the polariton generated in the cavity has electron spin $s_z = -1/2$ and hole spin $s_z = 3/2$. Projecting expressions 3.11 onto this state we obtain

$$\begin{aligned}
\langle p_0|\, \mathcal{S}^A_{pp}\mathcal{S}^B_{pp}\, |p_0\rangle &= \frac{\hbar^2}{4}\left(1 - 6\zeta + 9\,\zeta^2\right) s^A_z s^B_z = \frac{\hbar^2}{4} 9 \left(\zeta - \frac{1}{3}\right)^2 s^A_z s^B_z \\
\langle p_0|\, \mathcal{S}^A_{px}\mathcal{S}^B_{xp}\, |p_0\rangle &= \frac{\hbar^2}{4}[s^A_x s^B_x + s^A_y s^B_y + i\,(s^A_y s^B_x - s^A_x s^B_y)] \,,
\end{aligned}$$

$$H^{eff} = C_1\, C_2(g) \left[F_{Rp}\, 9 \left(\zeta - \frac{1}{3}\right)^2 s^A_z s^B_z + F_{Rx}(s^A_x s^B_x + s^A_y s^B_y)\right] \,, \qquad (3.12)$$

with $C_1 \doteq \left(\hbar\, v_0\, J\, \wp_+\, \phi_{1s}\right)^2$ and $C_2(g_0) \doteq \left({r_0}^2/\delta\right)^2$, with detuning $\delta \doteq \omega_L - \Omega_0$.[10] Eq. 3.12 presents some important features. The coupling between light and matter breaks the degeneracy of dark and optical active excitons, making the indirect interaction mediated by a polariton and a dark exciton different in strength and form; the interaction is anisotropic. In addition, the different nature of electron and hole interactions introduces an extra source of anisotropy.

[10] We make explicit the dependence on g_0 of C_2 since this parameter controls the transition from the exciton to the polariton picture, and is of crucial important for this work. Likewise, we prefer to talk about δ instead of ω_L because that is the parameter that makes possible to compare both cases, excitons and polaritons. As a consequence of the change in g_0 the bands drift and, if not corrected, this contributes to a change in detuning $\delta = \omega_L - \Omega_0$.

3.4 The neglect of the upper branch polaritons

The following considerations support the neglect of the upper branch polaritons. *i*) Consider the transformation that links the exciton operators with the polariton operators for both branches: $b_k = r_k\, p_{2,k} + t_k\, p_{1,k}$. Figure 3.3 presents the numerical evaluation of the coefficients as a function of wave-vector for different coupling g_0. Note that, for the sign of Δ chosen, the limit of the coefficients for $g_0 \to 0$ are 1 and 0 for lower and upper branches respectively. Moreover, t_k is smaller than r_k for all k. *ii*) The extra-cavity light frequency is tuned below the lower branch. To second order,

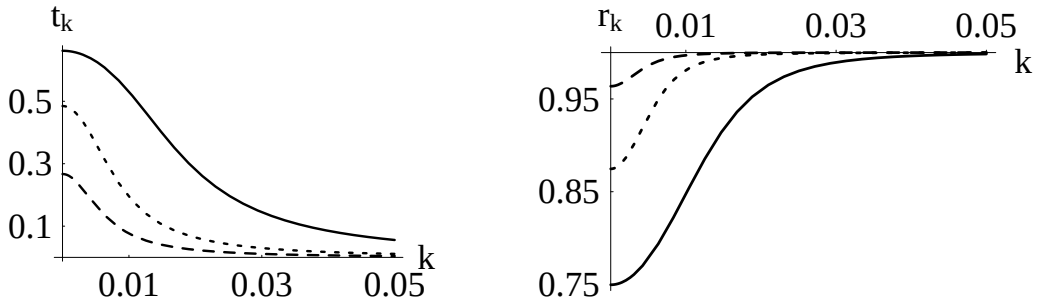

Figure 3.3: Transformation coefficients as a function of wave-vector for different coupling: $g_0 = 0.4$ solid, $g_0 = 0.08$ dotted and $g_0 = 0.03$ dashed lines.

the probability of exciting a state is inversely proportional to the difference between the laser energy and the state energy, power $4th$. Then, it is much more likely to excite lower than upper branch polaritons, since the detuning of the former is much smaller than that of the latter. Therefore, the only process considered must be one that has the same initial and final states, namely a lower branch polariton with wavevector $k = 0$ and spin ($\alpha + \beta = \sigma+$): $|\Gamma p_{0\sigma+}\rangle$. *iii*) Given the last argument, we are in a position to understand that a scattering process with spin flip and intermediate upper branch polariton is forbidden to second order in J: We must start with an initial state $|\Gamma\, p_{0\sigma+}\rangle$, if scattered with spin flip, the result is necessarily a dark state (there is no such thing as a dark polariton), so the resulting state must belong to the dark exciton band; given that we only consider second order in J the next scattering of this dark state must lead inevitably to the channel that is coupled to the extra-cavity. Said in

a different way, the second scattering process must return the state to $|\Gamma\, p_{0\sigma+}\rangle$. If the second scattering led to an upper branch polariton, a third interaction would be required to comply with our stimulated emission process; the whole scattering would be $3rd$ order. We still need to rule out the scattering that has no spin flip: iv) Assume that upper branch polaritons are included in the model. New operators H^j_{UI}, that account for the interaction between them and the other channels I (any of U, X, P) will appear in Expression 3.7. As already explained, we know that $H^j_{UU} = H^j_{UX} = H^j_{XU} = 0$. A new term in $H_I G^0 H_I$ will appear, of the form $H_{PU} G^0_U H_{UP}$ leading to

$$\begin{aligned} F_{R_U} &= \frac{1}{A}\sum_{k''} v^2_{k''} |t_{k''}|^2 e^{ik''\cdot R} G^0_{Pk''} \\ &= \frac{1}{A}\sum_{k''} v^2_{k''} |t_{k''}|^2 e^{ik''\cdot R} \frac{1}{\omega_L - \Omega_U} \ ; \end{aligned}$$

clearly, $F_{R_U} << F_{R_P}$ for all k (the actual interval of k for which the integral is meaningful is finite and "small"; this effective cut-off restricts the integrals to k such that there is no overlap of lower and upper polariton branches.). The reason is twofold: $t_k < r_k$ and $\omega_L - \Omega_U > \omega_L - \Omega_P$. Therefore, the scattering from lower to upper branch polaritons gives a negligible contribution to the effective Hamiltonian, and can be eliminated.

3.5 Results

Due to the quasi-continuum character of the bands, we can replace sums by integrals in the expressions for the functions F_{R_X} and F_{R_P}. The former can be solved analytically to

$$\begin{aligned} F_{R_X} &= \frac{1}{(2\pi)^2 \hbar} \int_0^\infty \frac{e^{ikR\cos(\theta)}}{[1+(\Lambda k)^2]^2(\omega_L - \omega_x)} k \ dk\, d\theta \\ &= \frac{m\left(2\,R\,\hbar\,K_0 - 2\,\Lambda\,R\,\sqrt{2\,\hbar\,m\,\delta_x}\,K_0 + \frac{R^2}{\Lambda}\,(\hbar - 2\,m\,\delta_x\,\Lambda^2)\,K_1\right)}{2\,\pi\,\Lambda\,\hbar\,(\hbar - 2\,m\,\delta_x\,\Lambda^2)^2} \ , \end{aligned} \tag{3.13}$$

where the K's are modified Bessel functions. For large R, behaves as Yukawa 2D potential:

$$F_{R_X} \cong \frac{-\left(\frac{m^3}{\delta_x}\right)^{\frac{1}{4}}}{2^{\frac{3}{4}}\sqrt{\pi}\,(1-2\,m\,\delta_x\,\Lambda^2)^2}\frac{e^{-\sqrt{2m\,\delta_x}R}}{\sqrt{R}}\ , \tag{3.14}$$

with $\delta_x = \omega_L - \omega_x$. For F_{Rp} we have,

$$F_{R_P} \;=\; \frac{1}{(2\pi)^2\hbar}\int_0^\infty\int_0^{2\pi}\frac{r^2\ e^{ikR\cos(\theta)}}{[1+(\Lambda k)^2]^2(\omega_L-\Omega_p)}k\ dk\,d\theta\ , \tag{3.15}$$

for which no analytical expression can be obtained.

3.5.1 A diagrammatic representation of the interaction

The relevant diagrams associated to the effective interaction for $\zeta = 0$

$$H^{eff} = C_1\,C_2(g)\left[F_{Rp}s_z^As_z^B + F_{Rx}(s_x^As_x^B + s_y^As_y^B)\right] \tag{3.16}$$

are depicted in figure 3.4. They describe processes by which the laser excites a $k = 0$ lower polariton that, after exchange interaction with one impurity becomes either a dark exciton or a lower polariton with momentum k. After a second exchange interaction with another impurity the quasiparticle becomes a $k = 0$ lower polariton that closes the diagram. Interestingly, the spin properties of the intermediate states are very different. If spin exchange occurs, the intermediate particle is a dark exciton whereas spin conserving exchange yields a lower polariton as an intermediate particle. The different dispersion of dark excitons and lower polaritons results in anisotropic interactions with different dependence on the inter-spin separation, R. The diagram with dark excitons as intermediate particles yields a transverse coupling whose intensity $F_{R_X}(R)$ is very similar to Optical RKKY interaction [6]. The polariton mediated coupling $F_{R_P}(R)$ is spin conserving or Ising. Its strength differs from ORKKY due to

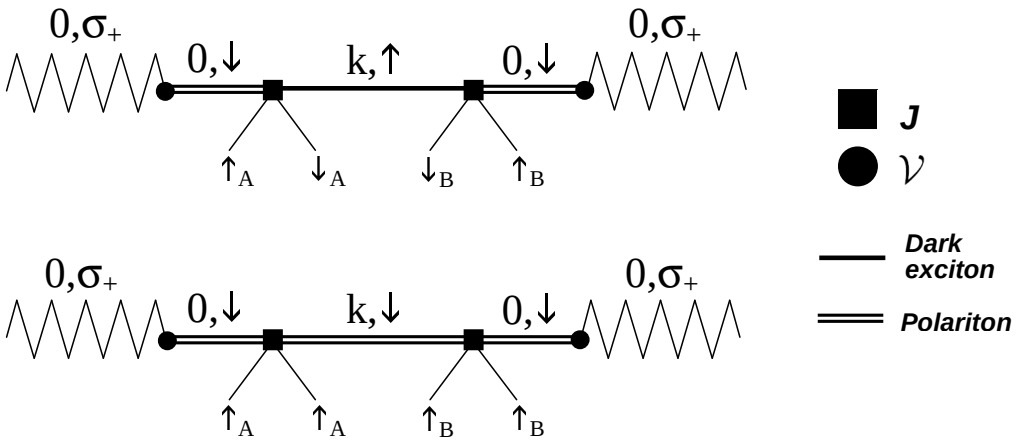

Figure 3.4: Diagrams for the dark-exciton mediated (upper) and lower polariton mediated (lower) interactions between local spins A and B. Zig-zag lines represent the external laser, with 0 in-plane momentum.

the different dispersion and form factor for small momenta.

3.5.2 The enhancement of the cavity

The effective Hamiltonian Eq. 3.12 can be rewritten in a way that makes clear the enhancement of the interaction due to the cavity.

We see in figure 3.5 that we can assign to the functions r and Ω_p two characteristic wave vectors k_r and k_Ω, and use $k_c \doteq Max[k_r, k_\Omega]$ to separate the integral in two regions. For $k > k_c$ both integrands of F_{R_P} and F_{R_X} coincide because $r = 1$ and the effective mass of the polariton, $\hbar(\frac{d^2\Omega_p}{dk^2})^{-1}$, is the same of that of the exciton. The $k < k_c$ part represents the deviation of F_{Rp} from F_{Rx}. Thus, we write

$$F_{R_P} \simeq F_{R_X} + \int_0^{k_c} dk\ k \int_0^{2\pi} d\theta (I_P - I_X) \doteq F_{R_X} + \mathcal{D}_{P_X}\ , \tag{3.17}$$

where I_i is the integrand of either F_{Rp} or F_{Rx}:

$$\begin{aligned} I_P(k,R) &\doteq \frac{1}{(2\pi)^2\hbar}\frac{r^2\ e^{i\mathbf{k}\cdot\mathbf{R}}}{[1+(\Lambda k)^2]^2(\omega_L - \Omega_p)} \\ I_X(k,R) &\doteq \frac{1}{(2\pi)^2\hbar}\frac{e^{i\mathbf{k}\cdot\mathbf{R}}}{[1+(\Lambda k)^2]^2(\omega_L - \omega_x)}\ , \end{aligned} \tag{3.18}$$

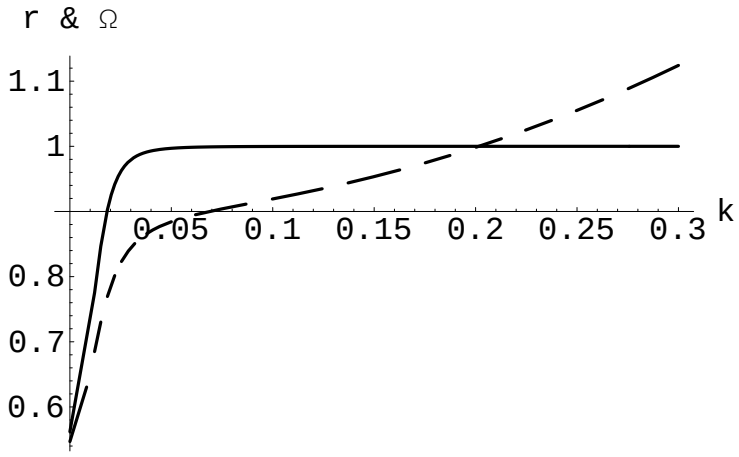

Figure 3.5: k dependence of the two functions r (solid) and Ω (dashed) in the integrand of F_{Rp}. The cut-off $k_r = 0.037$ was chosen at 10^{-2} the asymptotic value of $r = 1$; for $k_\Omega = 0.27$ the cut-off is at 10^{-2} the deviation of the polariton mass from the exciton mass.

where $\mathcal{D}_{PX}$ represents the scattering that has no exciton nature (*only-polariton effect*), while all the excitonic effects (dark-excitons plus polaritons at large k) are gathered in F_{R_X}. Related to k_c there is a crossover length R_c that depends on the detuning δ, Rabi frequency $\wp$ and is inversely proportional to k_c. This decomposition allows us to make clear the transition from exciton to polariton effective Hamiltonians.[11] For the value of parameters and their range of variation in $Si : GaAs$ we have, $k_\Omega \gg k_r$. Therefore, k_c is determined by k_Ω. The determination of the analytical dependency of this function on the parameters (Δ, ϵ, g_0) is hindered by the complexity of the function Ω. Nevertheless, it is possible to describe qualitatively some relevant features. The only parameter that substantially affects Ω is g_0, the others (Δ, ϵ) only produce a small effect; we point out that g_0 depends on the dipole moment and the exciton relative motion wave function at $k = 0$, $\hbar g_0 = L^{-1/2} d_{cv} \phi_{1s}(0) \sqrt{2\pi\hbar\,(\epsilon_0 - \Delta)}$. Taking this into account, it is possible to get a numerical solution for $k_c(g_0)$, and it turns out to be a positive monotonic function. As $k_c \to 0$, we have $\mathcal{D}_{PX} \to 0$, and so it can be seen how the effective Hamiltonian tends to the one representing the problem of excitons alone.

[11] Alternatively, a simplified analysis in terms of two regions with different masses is possible.

With the decomposition Eq. 3.17 the effective Hamiltonian reads

$$H^{eff} = C_1\, C_2(g_0) \times \left\{ F_{Rx} \left[9 \left(\zeta - \frac{1}{3} \right)^2 s_z^A s_z^B + s_x^A s_x^B + s_y^A s_y^B \right] + \mathcal{D}_{px}\, 9 \left(\zeta - \frac{1}{3} \right)^2 s_z^A s_z^B \right\} . \tag{3.19}$$

Notice that $9\left(\zeta - \frac{1}{3}\right)^2 \geq 0$, and thus, there is no change in sign no matter the value of ζ. In addition, $F_{R_X} < 0$; however, for certain values of the parameters D_{PX} may change sign. Therefore, the interaction may be either ferro- or anti-ferromagnetic.

Although both the first and second terms in Eq. 3.19 have contributions from the two diagrams of Fig. 3.4, their physical interpretation is clear: the first term is the standard optical exchange interaction and the second term represents the enhancement of the optical exchange interaction due to the presence of the cavity.

3.6 Shallow donors

In what follows, the case of shallow donors is analyzed, for which the electron-hole interaction can be neglected ($\zeta = 0$). For the sake of clarity, a particular system (Si in $GaAs$ QW) will be used to extract numerical results. The calculation can be easily extended to other donors, and with some modifications, to the case of deep impurities in which the hole interaction must be taken into account. The truncation of the series of G to second order is justified by the numerical data used, where $(JF) < 1$ for $R > 2a_B^*$. This only imposes a limitation to the distance between impurity, that is not relevant for our results.

The form of the effective Hamiltonian

$$H^{eff} = C_1\, C_2(g) \left(F_{R_X} s^A \cdot s^B + \mathcal{D}_{PX}\, s_z^A s_z^B \right) \tag{3.20}$$

makes evident the transition from a regime where excitons and photons are indepen-

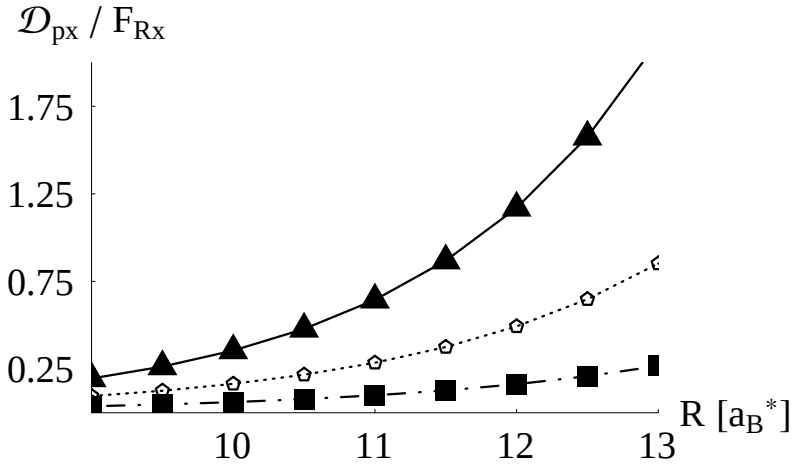

Figure 3.6: Transition from weak to strong coupling regime. The relative weight of only-polariton to exciton contributions is shown as a function of the separation between impurities: $g_0 = 0.4$ (triangle), $g_0 = 0.3$ (pentagon), $g_0 = 0.2$ (square).

dent entities to the strong-coupling of polaritons: As the coupling is turned on (g_0 increases) the value of $\mathcal{D}_{PX}$ increases, as shown in Figure 3.6 [12]. The analytic and numerical values for F_{R_X}, F_{R_P} and $\mathcal{D}_{PX}$ are presented in Figure 3.7. The striking feature is the existence of two distinct regions separated by the crossover distance R_c. For $R < R_c$, the dominant interaction is of the isotropic Heisenberg form, while it changes to an Ising like interaction for $R > R_c$. The former is mediated by exciton-like particles and the second by polariton. This validates intuition: due to their small mass, polaritons are well delocalized compared to excitons.[13] Fig. 3.8 shows that, in the scale of few a_B^*, the interaction decays exponentially for excitons while it is clearly of longer range for polaritons. For sufficiently large R, both F_{R_X} and F_{R_P} can be fitted to a Yukawa law: $J_\alpha(R) \simeq R^{-1/2} e^{-R/R_{0\alpha}}$ where $\alpha = P$ or X and $R_{0\alpha}$ is the range of the corresponding interaction. As expected from fig. 3.8, $R_{0P} >> R_{0X}$. In both cases the range of the interactions is related to the effective mass and the detuning of

[12]The calculation leading to Figures 3.6/3.7/3.8 is taken for fixed δ, achieved by adjusting the laser frequency ω_L.

[13]This can also be understood noticing that for large R, the integrand of the function F_{R_X} oscillates and the integral of it in the interval $[k_c, \infty)$ tends to zero, which is what we expect to get a Yukawa potential. On the other hand, the integrand of $\mathcal{D}_{PX}$ behaves as a monotonic function for small R and develops only few oscillations that are strongly damped for R close to its maximum value, so the integral is almost constant in the interval $[0, k_c]$.

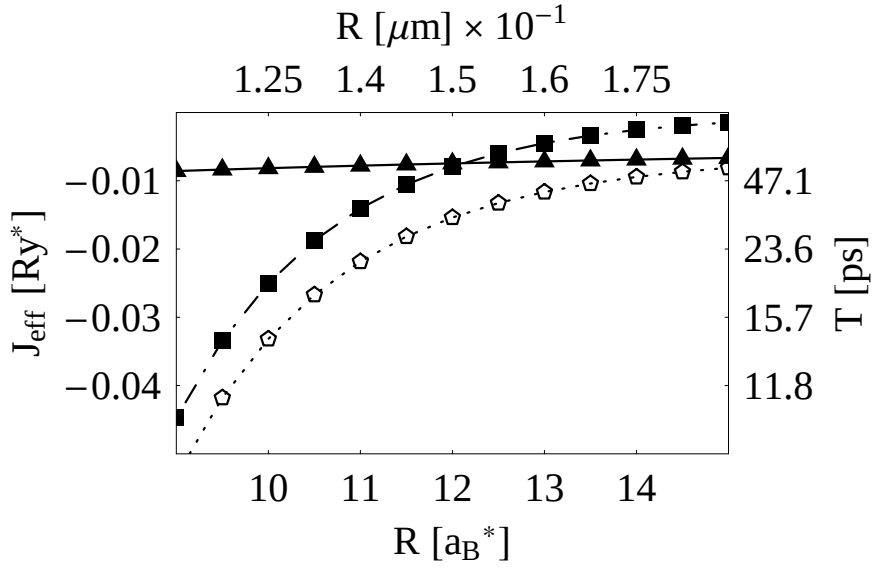

Figure 3.7: The existence of two regimes separated by the crossover length $R_c \simeq 12\, a_b^*$ ($\delta = -0.15 Ry^*$, $\wp = 0.16 Ry^*$) is evident from the crossing of the effective coupling constants $J_{eff} \doteq C_1 C_2 \mathcal{D}_{PX}$ (triangle) and $J_{eff} \doteq C_1 C_2 F_{R_X}$ (square). For completeness, the plot shows the function $J_{eff} \doteq C_1 C_2 F_{R_P}$ (pentagon). The two regimes are: isotropic Heisenberg and Ising Hamiltonians, typical for excitons and polaritons respectively.

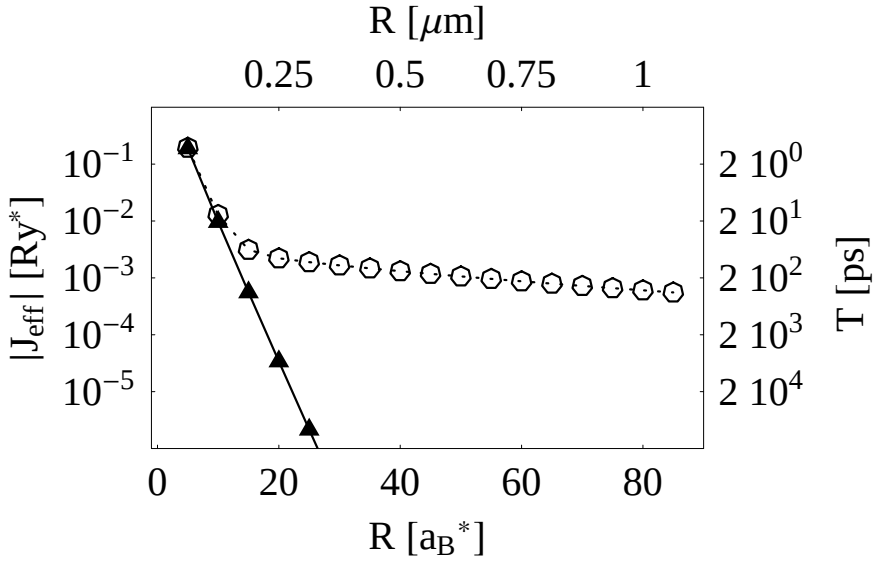

Figure 3.8: Logarithmic plot of F_{R_X} (triangle) and F_{R_P} (circle), that shows the exponential decay and non-exponential behavior respectively ($\delta = -0.2 Ry^*$ and $\wp = 0.11 Ry^*$)

the corresponding quasiparticle, $R_{0\alpha}^{-1} = \sqrt{2 M_\alpha \delta_\alpha}$. In the polaritonic case the fitting is consistent with $\delta_P = \delta$ and M_P equal to the lower polariton effective mass, defined as

the value that fits the lower polariton dispersion for small k to $\Omega_k^P \simeq \Omega_0^{LP} + \frac{k^2}{2M_P}$. For the values of figure 3.8 we have $M_P = 10^{-5} m_0$, where m_0 is the free electron mass. On the other side, for the excitonic case it can be analytically shown that $M_{\alpha=X} = M_X$ and $\delta_X = \delta + g_0$, which is the detuning of the dark exciton and the laser. Therefore, the long-range interaction of the cavity-enhanced optical exchange interaction is related to the low effective mass of the lower polariton.

3.6.1 The critical temperature of an array of spins

As demostrated by Fernández-Rossier *et al.* [58], an array of localized spins can undergo a ferromagnetic phase transition induced by light. This ordering is mediated by photo-generated excitations of the host material. In this section, the Curie or critical temperature of an array of impurities in the presence of polaritons is determined and compared to the case where only excitons exist. We assume the array in thermal equilibrium and use the standard mean field approximation (MFA) – See Appendix D for an overview of the procedure.

As seen in the previous section, there is a characteristic distance between impurities R_c that separates the exciton and polariton regimes. Let us assume that the array of impurities form a square lattice with lattice constant d, embedded in a host lattice (e.g. $GaAs$) of unit cell area a and N sites per unit cell; the concentration χ of impurities is related to those quantities by $d^2 = a/(N\chi)$.

For $d > R_c$ (low impurity concentration) the largest term in Equation 3.20 is the polariton Ising interaction with coupling $\mathcal{D}_{PX}$. In this limit it is valid to neglect the Heisenberg term and write for the critical temperature

$$kT_c = \frac{\hbar^2}{4} C_1 \, C_2(g_0) \left| \sum_j \mathcal{D}_{px}(R^j) \right| .$$

The presence of the cavity prevents the T_c to decrease rapidly, as it will happen at this concentration in a bare semiconductor. To obtain the T_c, we notice that

$| d \cdot \mathcal{D}_{px}^{-1}\, d\mathcal{D}_{px}/dR | \ll 1$; thus, we can transform the sum into an integral, as

$$\sum_j \mathcal{D}_{px}(R^j) \;\; \rightarrow \;\; \frac{1}{d^2}\int_0^\infty d^2R\,\mathcal{D}_{px}(R) - \frac{1}{d^2}\int_0^d d^2R\,\mathcal{D}_{px}(R)\ .$$

The calculation is carried out by adding and subtracting the integral in $(0,d)$ and using expression 3.18, for inverting in the first term the integration in R and k yields a $\delta(k)$ and thus an analytical result:

$$\begin{aligned}
\frac{1}{d^2}\int_0^\infty d^2R\,\mathcal{D}_{px}(R) &= \frac{1}{d^2}\int_0^\infty d^2R \int d^2k\,(I_P - I_X) \\
&= \frac{1}{d^2}\int_0^\infty d^2R \int d^2k\, e^{i\mathbf{k}\cdot\mathbf{R}}[I_P(k,0) - I_X(k,0)] \\
&= \frac{1}{d^2}\int d^2k \left(\int_0^\infty d^2R\, e^{i\mathbf{k}\cdot\mathbf{R}}\right)[I_P(k,0) - I_X(k,0)] \\
&= \frac{1}{d^2}\int d^2k\,\delta(\mathbf{k})[I_P(k,0) - I_X(k,0)] \\
&= \frac{1}{d^2}[I_P(0,0) - I_X(0,0)] = \frac{1}{d^2}\frac{1}{(2\pi)^2\hbar}\left(\frac{r_0^2}{\omega_L - \Omega_0} - \frac{1}{\omega_L - \epsilon}\right)\ ,
\end{aligned}$$

where the integration in k is over a disc of radius k_c. Due to the long range nature of $\mathcal{D}_{PX}$, the numerical evaluation of the integral of $\mathcal{D}_{PX}$ in $(0,d)$ is easier than an integral in $(0,\infty)$. The final expression for the critical temperature is

$$k\,T_c \;=\; \frac{C_1}{d^2}\left(\frac{r_0^2}{\delta}\right)^2\left[\frac{1}{(2\pi)^2\hbar}\left(\frac{r_0^2}{\delta} - \frac{1}{\delta + \Omega_0 - \epsilon}\right) + \int_0^d d^2R\,\mathcal{D}_{px}(R)\right]\ . \quad (3.21)$$

The numerical result is shown in Figure 3.9.

For $d < R_c$ (high impurity concentration) the leading term in the Hamiltonian Equation 3.20 is the Heisenberg interaction with constant F_{R_X}. Therefore, any direction of magnetization is equivalent, in contrast to the previous case where only magnetization in the z-axis leads to ordering. We assume that a direction has been singled out. The condition $| d \cdot F_{Rp}^{-1} dF_{Rp}/dR | \ll 1$ is also satisfied, and a procedure similar to that used for the case $d > R_c$ is used. Here, a complete analytical solution

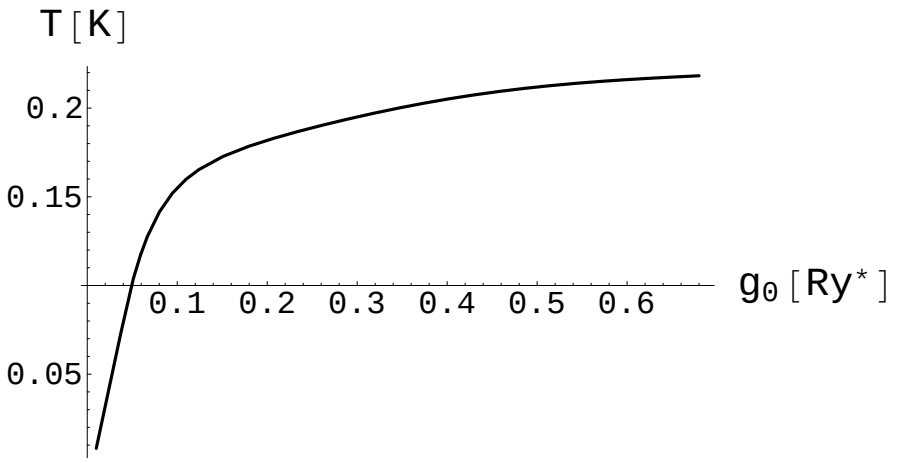

Figure 3.9: Critical temperature as a function of the coupling g_0 for $d > R_c$. Parameters: $R_c \simeq 12\, a_b^*$, $\delta = -0.15 Ry^*$, $\wp = 0.16 Ry^*$ and $d = 30 a_B^*$.

is attainable:

$$\begin{aligned} kT_c &= \frac{\hbar^2}{4} C_1\, C_2(g_0) \frac{1}{d^2} \int_0^\infty d^2 R\, F_{R_X}(R) \\ &= \frac{\hbar^2}{4} C_1 \left(\frac{r_0^2}{\delta}\right)^2 \frac{1}{d^2} \frac{1}{(2\pi)^2 \hbar} \left(\frac{1}{\omega_L - \epsilon_0}\right) \\ &= \frac{\hbar\, (\hbar\, v_0\, J\, \wp_+\, \phi_{1s})^2}{(4\,\pi\, d)^2} \left(\frac{r_0^2}{\delta}\right)^2 \left(\frac{1}{\delta + \Omega_0 - \epsilon_0}\right) \ . \end{aligned} \tag{3.22}$$

Figure 3.10 shows that coupling photons to excitons actually reduces T_c, for constant δ. Notice that the increase of g_0 leads to an increase of δ_x.

We can compare our approach to the one by Fernández-Rossier *et. al.* [58] for the critical temperature mediated by excitons, noting that both models are derived in quite a different way. In ref. [58], the critical temperature reads

$$k_B T_C \propto (J_e - J_h)^2\, c_{Mn} \frac{|\psi_{1s}(0)|^2 \Omega^2}{4\delta^3} \ , \tag{3.23}$$

where J_i is the coupling between electrons or holes with the localized Mn whose concentration is c_{Mn}; δ is the detuning; Ω is the Rabi energy; and ψ_{1s} is the exciton

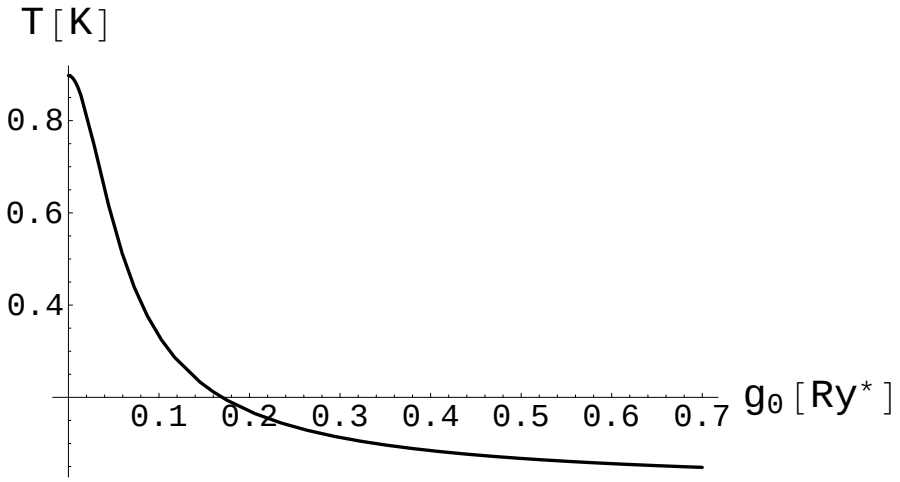

Figure 3.10: Critical temperature as a function of the coupling g_0 for $d < R_c$. Parameters: $R_c \simeq 12\, a_b^*$, $\delta = -0.15 Ry^*$, $\wp = 0.16 Ry^*$ and $d = 30 a_B^*$.

wave function for relative motion. Comparing Eq. 3.23 with Eq. 3.21 and Eq. 3.22 we observe a complete analogy.

In conclusion, we have shown that the existence of the crossover length R_c introduces a strong dependence of the critical temperature on the impurity concentration. In addition, the direction of preferred magnetization changes from isotropic in-plane to an easy-axis in the z-direction.

If the case of deep impurities were treated, another source of anisotropy would be found, arising from the Ising interaction that holes introduce.

Chapter 4

Applications

The preceding chapters presented our theoretical formalism together with the study of two particular systems: excitons in bulk and polaritons in micro-cavities. The goal was to gain a better understanding of the physics of indirect interaction. Nevertheless, the technological implications of our findings has not yet been discussed. This is the subject of the current chapter. As anticipated in the Introduction we are particularly interested in applications to quantum information; in Section 4.1 we give a very short introduction of quantum computing (QC). In Section 4.2 we undertake the study of a system where the indirect interaction is controlled with a light pulse that creates excitons in a quantum dot. We demonstrate that it is possible to prepare an arbitrary two-qubit state of the localized impurities near the QD. This is the building block of QC algorithms. Furthermore, we show that the system is robust with respect to errors. Section 4.3 and Section 4.4 give an account of the applications that may result from our findings in the study of excitons in bulk semiconductor (Chapter 2) and polaritons in micro-cavities (Chapter 3), respectively.

4.1 Quantum computing

Quantum information brings together the main fields of physics, computer science, and mathematics. [60] It encompasses quantum cryptography, quantum teleportation, and quantum computing (QC); the latter being possibly the most promising for applications, and at the same time the most difficult to implement. As its name suggests, quantum information relies on some peculiar features of quantum mechanics. The most important one became clear after the EPR paradox: the entanglement. In QC, the use of operations using entanglement and interference can lead to algorithms that outperform by far those of classical computers (CC). So far, the number of algorithms of this kind found is rather small. In spite of this, it shows that some hard problems (computational complexity) for CC are tractable with a QC, for example the factorization problem.

A quantum computer should include the following: *i*) *qubits* which are the logical units for storing and performing operations; qubits are realized using two level systems, such as nuclear or electronic spin 1/2, atomic levels, etc. The two possible states are designated by $|0\rangle$, $|1\rangle$. *ii*) A procedure to prepare the set of qubits to a given initial state, e.g. $|0000....\rangle$. *iii*) Control on the dynamics, using unitary transformations, of both individual and groups of qubits. This control works as logical operations or gates that are part of algorithms. *iv*) A procedure to measure the state of a set of qubits after the set of operations – reading the output. It can be shown that only four gates are required to construct any possible operation; this set of universal gates consists of three one-qubit and one two-qubit operations. A possible set of universal operations are the Hadamard, σ_x, $R_z(\pi/4)$ and CNOT. These are

$$H = \frac{1}{\sqrt{2}} \begin{pmatrix} 1 & 1 \\ 1 & -1 \end{pmatrix} \quad \sigma_x = \begin{pmatrix} 0 & 1 \\ 1 & 0 \end{pmatrix} \quad R_z(\pi/4) = \begin{pmatrix} 1 & 0 \\ 0 & e^{i\pi/4} \end{pmatrix}$$

$$CNOT = \begin{pmatrix} 1 & 0 & 0 & 0 \\ 0 & 1 & 0 & 0 \\ 0 & 0 & 0 & 1 \\ 0 & 0 & 1 & 0 \end{pmatrix} .$$

We are concerned with the physical realization of two-qubit operations in semiconductors. It is instructive to see how a CNOT gate can be implemented [59]: $CNOT = R_y^{(a)}(-\pi/2)R_z^{(b)}(-\pi/2)R_z^{(a)}(-\pi/2)e^{i\pi/4\sigma_z^{(b)}\sigma_z^{(a)}}R_y^{(a)}(\pi/2)$, where the super indeces a, b stand for two distinct qubit. Therefore, we see that besides rotations of single qubits, an operation involving two qubits is necessary. This operation is governed by an Ising interaction. It is worth noting that there are other schemes that make use of the Heisenberg interaction between two spins to realize two-qubit operations. This is the connection between the previous chapters and QC.

The prescription given above does not acknowledge the existence of decoherence, which affects any real system. Decoherence causes the system to evolve non-unitarily [1], away from the evolution of the desired operation. In QC, the errors introduced by decoherence destroy the operations. Fortunately, error correction codes (ECC) has been developed, much alike those in CC. They allow to reconstruct the state of the system in each step of the operation, making feasible the realization of QC. Therefore, any realistic scheme should take into account the errors and the possibility of correcting them via ECC. We deal with this issue in Section 4.2.

[1] Decoherence can be seen as the environment performing measurements on the system. Measurements project the state of the system, and are represented by operators of the form $|a\rangle\langle a|$, which are not unitary.

4.2 Entanglement and errors in the control of spins by optical coupling

Impurity spins embedded in semiconductors are currently under investigation for quantum computing implementations. Recently, optical techniques have been proposed to control the spin-spin coupling and realize two-qubit quantum gates. [6, 7, 61–65] The optical method suggests the possibility of an ultrafast control of the qubits. The flexibility in the control that can be obtained by pulse shaping [66] and the absence of noisy contacts represent additional advantages. On the experimental side, ensemble optical measurements have demonstrated the production of spin entanglement for impurities embedded in a semiconductor host. [67] More recently, the measurement of the quantum state of a single impurity spin obtained by coupling it to a single exciton in a QD has been experimentally carried out. [68] Here we study theoretically the control of impurity spin states when the interaction among them is controlled by optically-generated excitons in a QD. We analyze the control errors due to the radiative recombination of the exciton that mediates the interaction between the spins. Moreover, we illustrate how the control parameters can be obtained directly from simple analytical expressions. The method is applied to design the control parameters in the production of maximal spin entanglement.

4.2.1 The system

The physical system consists of two impurity spins placed close or inside a QD in such a way that there is not a direct interaction between them. A schematic picture is given in Figure 4.1. By coding the qubit in more than one spin efficient schemes for fault-tolerant [69] and exchange-only [70] quantum computation can be naturally applied to this setup. Dots of different size provide the frequency selectivity to address specific spin pairs and realize two-qubit readouts. The model we use contains few parameters describing the exciton-light and exciton-impurity coupling and can be

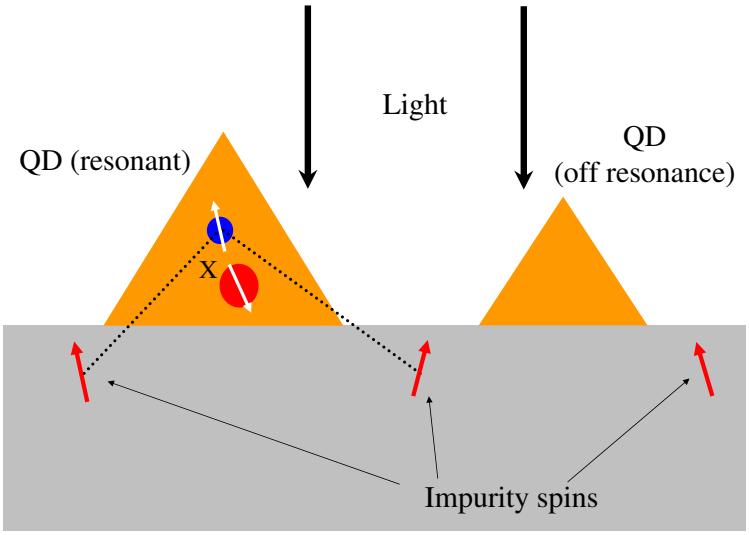

Figure 4.1: Scheme of the system: localized spins located near self assembled QDs are coupled by an exciton created by a laser pulse. Dots of different size provide selective control and readout.

applied to different physical systems. For instance, it can be used for excitons localized by monolayer fluctuation in III-V and II-VI quantum wells and interacting with a finite number of localized impurities as in Ref. [67]. III-V or Si/Ge self-assembled QDs can also be used as shown in Figure 4.1. For typical semiconductor systems we can restrict the analysis to heavy-hole excitons due to the splitting between heavy-hole and light-hole bands in the dot. The heavy-hole exciton spans a four dimensional space consisting of two optically-active and two dark states. We treat the interaction between the electromagnetic field and the excitons semiclassically, and we consider spin states that interact only with the photoexcited electron in the dot. This is the case for instance of donor impurity spins in typical semiconductors because the electron-hole exchange is much smaller than the electron-electron exchange. Notice that by using circularly polarized light the exciton induces, besides the spin-spin coupling, also a local effective magnetic field on the spins as found in Chapter 2. [71] This effective magnetic field can be controlled by the laser polarization and disappears for linearly polarized light. We will consider below the case of circularly polarized light. The exciton-spin part of the Hamiltonian ($\hbar = 1$) is

$$H_0 = \epsilon \sum_{\alpha} b_{\alpha}^{\dagger} b_{\alpha} - 2V \sum_{n=1}^{2} \sum_{\alpha\alpha'} (s_{\alpha\alpha'} \cdot s_n) b_{\alpha}^{\dagger} b_{\alpha'} \ , \tag{4.1}$$

where ϵ is the energy of a single exciton in the dot, and b_α is the creation operator of an exciton with electron spin α. The spin-spin interaction of the impurity n with the exciton is given by $s_{\alpha\alpha'} \cdot s_n$. $\alpha =\downarrow$ represents an optically active exciton with electron spin $-1/2$ and hole spin $+3/2$, while $\alpha =\uparrow$ is a dark state exciton with electron spin $+1/2$ and hole spin $+3/2$ (due to splitting of the degenerate valence band, we are able to restrict our analysis to the heavy hole band with $s_z = \pm 3/2$ [1]). For each impurity, the operator s_n represents its spin degree of freedom. V is the exchange interaction between the impurity spins and the photoexcited electron in the dot. The strength and the sign of V depend on the system. For instance, this coupling is expected to be ferromagnetic for electrons in the dot interacting with localized rare-earth magnetic impuritites, while it is antiferromagnetic for a dot mediating the interaction between shallow donors, see Chapter 2 and Ref. [63]. Without loss of generality, we will assume $V > 0$ below. Note that, since the exciton is well localized inside the QD, there is no phase $exp(-ikR)$ arising from the position of the impurity. Alternatively, this can be understood recalling that the exciton in a QD is an 0D excitation with no center-of-mass motion, and so $k = 0$. This fact allows us to use the formalism of Schwinger bosons [76] to diagonalize the Hamiltonian Expression 4.1 in a basis of coupled angular momentum, as follows. The transformation

$$\begin{aligned} N &= b_{\uparrow}^{\dagger} b_{\uparrow} + b_{\downarrow}^{\dagger} b_{\downarrow} \\ L_x &= \frac{1}{2}(b_{\downarrow}^{\dagger} b_{\uparrow} + b_{\uparrow}^{\dagger} b_{\downarrow}) \\ L_y &= \frac{i}{2}(b_{\downarrow}^{\dagger} b_{\uparrow} - b_{\uparrow}^{\dagger} b_{\downarrow}) \\ L_z &= \frac{1}{2}(b_{\downarrow}^{\dagger} b_{\downarrow} - b_{\uparrow}^{\dagger} b_{\uparrow}) \end{aligned}$$

maps a set of two decoupled harmonic oscillators (in our case the optically active $b_\downarrow$ and dark $b_\uparrow$ excitons) onto a rotator with angular momentum L. The Hamiltonian

can be rewritten as

$$H_0 = \epsilon N - 2V(J^2 - S^2 - L^2) \ , \tag{4.2}$$

where S is the total spin of the two impurities. The total angular momentum $J_i = L_i + S_i$.

The coupling of the excitons in the QD and the external laser field is given by

$$H_L = \frac{\Omega(t)}{2} e^{-i\omega t} b_\downarrow^\dagger + h.c. \ , \tag{4.3}$$

where $\Omega(t)$ is the time-dependent Rabi energy associated with the optical pulses, and ω is the energy of the laser. We consider only anti-clockwise polarization (σ_+) which generates excitons with electron and hole spin states $-1/2$ and $+3/2$, respectively. Excitons with hole spin $-3/2$ are not included in the model since they are not excited by σ_+ light and the impurity spins can only flip the spin of the photoexcited electron.

A scheme of the relevant energy levels is given in Figure 4.2. In the ground state $n = 0$ (where n is the quantum number associated with the operator N) we have the singlet and the triplet states corresponding to the two non-interacting impurities. In the excited state $n = 1$, the electron in the dot splits the triplet states in a quadruplet $J = 3/2$ and a doublet $J = 1/2$. The total Hilbert space is thus spanned by a total of 12 states. The arrows in the scheme identify the selection rules for σ_+ optical transitions. The transitions have different oscillator strengths, which are calculated using the Clebsch-Gordan coefficients. Notice that the light does not connect directly states with different spin S. The structure of the energy levels provides a natural readout scheme for the coded logical qubit $|0_L\rangle$, $|1_L\rangle$ in the exchange-only scheme. [70] An optical setup similar to the one for single spin readout [68] could be used: a single peak at ϵ corresponds to $|0_L\rangle$ while two peaks separated by $6V$ correspond to the logical state $|1_L\rangle$.

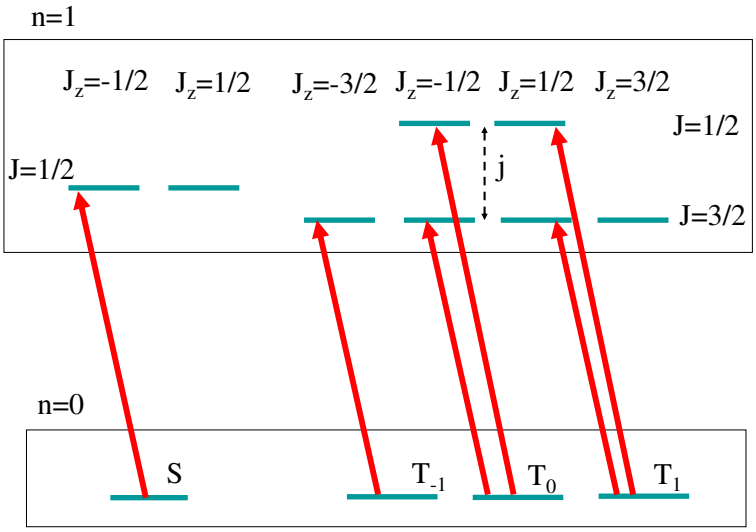

Figure 4.2: Energy level diagram and optical selection rules for σ_+ polarized light. In $n = 1$, the total splitting is $j = 6V$.

4.2.2 Quantum control

In order to illustrate how to design the optical control we consider the production of maximal spin entanglement. We choose the initial state $|\uparrow\downarrow\rangle \otimes |0\rangle$ as the tensor product of a linear superposition of impurity states $\{|S\rangle, |T_0\rangle\}$, and the exciton $|0\rangle$ representing an empty QD. We consider separately the case of infinite and finite γ^{-1}, i.e. spontaneous radiative recombination lifetime for the exciton in the dot. Other decoherence processes, such as pure dephasing due to elastic scattering with phonons, are suppress in large QDs as experimentally shown by Bonadeo *et. al.* [72]. In the first case we determine analitically the control parameters that provide maximal spin entanglement. In the second case, we solve numerically the master equation for the full system in Figure 4.2. This will allow us to analyze errors due both to the radiative recombination and to the finite probability of remaining with an exciton in the dot at the end of a pulse. The latter is an error similar to a double occupancy error in the case of spins controlled by gate voltages [73]. Ideally, the QD must be empty at the end of each optical pulse, and this can be achieved by an adiabatic evolution, or by a nonadiabatic evolution plus additional conditions in the pulse area [74].

Infinite radiative lifetime

In the following, we make extensive use of the concept of adiabatic evolution of the system. We clarify this in the context of our model, which can be analyzed, in the simplest situations, in terms of decoupled two or three level systems. Let us take the situation, where only the singlet is excited. In the rotating frame (the perturbation still retains the time dependency of the pulse envelope function), the energy of the levels is renormalized by the frequency of the laser, giving rise to the detuning. If the perturbation evolves slowly enough with respect to the energy difference between unperturbed states (the detuning), i.e. $dH/dt << \delta^2$, the state will evolve adiabatically. This means that if the initial state is an instantaneous eigenvector of the unperturbed H – say u_n – the evolution will only introduce a phase: $\psi(x,t) = u_n(x,t)\, exp(-i\int_0^t E_n dt')$.

We first study the ideal case of a nonadiabatic evolution at $\gamma = 0$. We call nonadiabatic the evolution that follows from a laser resonant with at least one transition between the $n = 0$ and $n = 1$ subspaces in Figure 4.2. This implies that there is a substantial exchange of energy between the electromagnetic field and the dot, which in turn results in a significant population inversion during the pulse. Using a numerical simulation we illustrate in Figure 4.3 the evolution of the $|S\rangle$ and $|T_0\rangle$ populations under a Gaussian pulse giving a Rabi energy of the form,

$$\Omega(t) = \frac{\Omega}{\sqrt{\pi}}\, e^{-(t/\tau)^2} \ . \tag{4.4}$$

The pulse is resonant with the bare exciton energy, which in the scheme of Figure 4.2 corresponds to a resonant transition for the singlet state. In order to have no excitonic population at the end of the pulse, we need the pulse area for the resonant excitation to be multiple of 2π, therefore Ω and τ are chosen so that the pulse area is $\Omega\tau = 8\pi$.[2] Notice that the population of the ground state singlet $|S\rangle$ is completely

[2]This is readily seen in the case of a two level system $\{|0\rangle, |1\rangle\}$ with a square shape pulse Hamiltonian connecting both states: $H_I = \Omega(t)\vartheta$ with $\vartheta = (\,|0\rangle\langle 1| + |1\rangle\langle 0|\,)$. As $[H_I(t_1), H_I(t_2)] = 0$ the evolution operator is $U = exp(-i\int_0^t H_I(t')dt') = exp(-i\Omega\tau\vartheta) = \cos(\Omega\tau) + \vartheta\sin(\Omega\tau)$. If the

depleted during the pulse but at the end comes back to the original population (0.5). In contrast, the triplet ($|T_0\rangle$) population follows an adiabatic evolution due to the exchange interaction affecting the optical resonance. In Figure 4.3 (inset) we show the real and imaginary part of the coherence $\langle S|\rho|T_0\rangle$. In order to create the maximally entangled state we need a $\pm\pi/2$ phase in this matrix element and the chosen optical pulse achieves this goal. This relative phase transforms, for example, the state $|\uparrow\downarrow\rangle$ into $2^{-1/2}(|S\rangle + i|T_0\rangle) \propto |\uparrow\downarrow\rangle + i|\downarrow\uparrow\rangle$. For a given value of the exchange coupling V and pulse width τ, the maximum intensity of the field Ω in Eq. (4.4) is found from the roots of the equation

$$\phi_T(\Omega, V, \tau) \pm \pi/2 = 0 \ , \tag{4.5}$$

where $\phi_T = \int_{-\infty}^{\infty} \lambda_T^0(t)\ dt$ is the dynamic phase that the state $|T_0\rangle$ picks up following the adiabatic evolution. Notice that since the pulse is a multiple of 2π the singlet will only pick up a trivial phase (± 1). λ_T^0 is the eigenvalue satisfying $\lambda_T^0(\pm\infty) = 0$ for a 3-level Hamiltonian representing the triplet states,

$$H_T(t) = \frac{1}{2}\begin{bmatrix} 0 & \sqrt{\frac{2}{3}}\Omega(t) & \sqrt{\frac{1}{3}}\Omega(t) \\ \sqrt{\frac{2}{3}}\Omega(t) & 2\delta - \frac{2}{3}j & 0 \\ \sqrt{\frac{1}{3}}\Omega(t) & 0 & 2\delta + \frac{4}{3}j \end{bmatrix} . \tag{4.6}$$

The optical detuning $\delta = \epsilon - \omega$, and $j = 6V$ is the splitting in the excited state between $J = 3/2$ and $J = 1/2$ states. If we assume that the three eigenvalues of the matrix in Eq. 4.6 do not cross during the pulse evolution, the expression for $\lambda_T^0(t)$ can be written as

$$\lambda_T^0(t) = \frac{j}{9} + \frac{2}{3}\delta + \frac{q(t)}{3}\cos\left(\frac{\theta(t)}{3}\right) \ , \tag{4.7}$$

where

$$\theta(t) = 2k\pi + \arccos\left(\frac{r(t)}{q^3(t)}\right) \tag{4.8}$$

initial state is $|0\rangle$, then the only choice for the final state to return to $|0\rangle$ is $\Omega\tau = 2\pi n$. This also can be shown to apply for pulses of arbitrary shape.

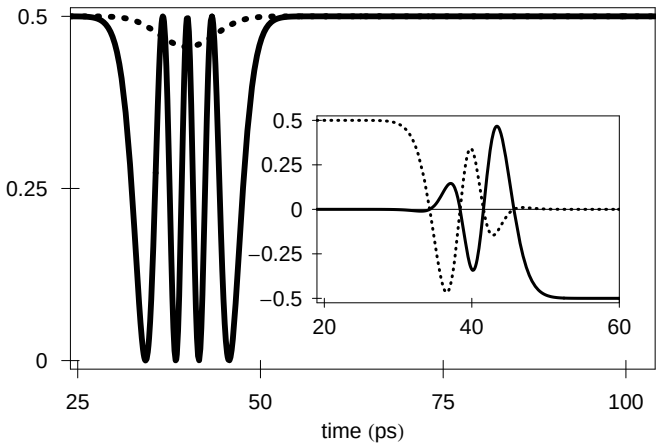

Figure 4.3: Nonadiabatic control, $\gamma = 0$. Evolution of the $|S\rangle$ (solid line) and $|T_0\rangle$ (dotted line) populations under a Gaussian pulse of area 8π. The temporal width of the pulse τ is 7.02 ps and the ratio Ω/V is 0.6697. (Inset) Real (dotted line) and imaginary (solid line) part of the coherence $\langle S|\rho|T_0\rangle$.

with

$$\begin{aligned} q(t) &= \sqrt{28j^2 + 12j\delta + 36\delta^2 + 27\Omega^2(t)} \\ r(t) &= 4(4j - 3\delta)(5j + 3\delta)(j + 6\delta) - 81(2j + 3\delta)\Omega^2(t) \ . \end{aligned}$$

If the exciton impurity coupling is ferromagnetic ($j > 0$), we have to take in Eq. (4.8) $k = 1$ for $\delta > j/3$, $k = 2$ for $-2j/3 < \delta < j/3$, and $k = 3$ for $\delta < -2j/3$. In contrast, for $j < 0$, we have to take in Eq. (4.8) $k = 1$ for $\delta > -2j/3$, $k = 2$ for $1/3j < \delta < -2j/3$, and $k = 3$ for $\delta < j/3$. The analytical expression in Eq. (4.7) allows us to determine exactly the control parameters from the roots of Eq. (4.5) . In the $\gamma = 0$ adiabatic regime the laser pulse is tuned away from the optical resonances between the $n = 0$ and $n = 1$ levels. An example of a simulation of an adiabatic control is shown in Figure 4.4. The laser is tuned 2 meV below the bare excitonic energy and 1 meV below the triplet resonances corresponding to $J = 3/2$ in Figure 4.2. We plot in Figure 4.4 the same quantities of Figure 4.3. Notice that in this case the pulse area can be arbitrary, provided the adiabaticity is preserved. The change of phase in the coherence $\langle S|\rho|T_0\rangle$ is now obtained with a smooth transition. The control parameters

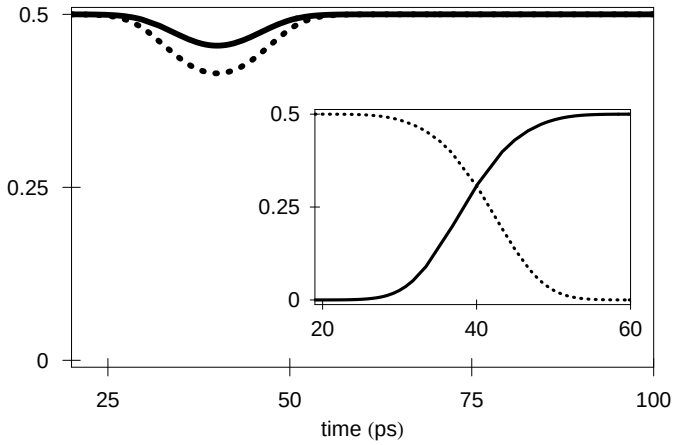

Figure 4.4: Adiabatic control, $\gamma = 0$. The laser is tuned in 2 meV below the bare excitonic energy. Evolution of the $|S\rangle$ (solid line) and $|T_0\rangle$ (dotted line) populations under a Gaussian pulse. The temporal width of the pulse τ is 10.2 ps and the ratio Ω/V is 1.24. (Inset) Real (dotted line) and imaginary (solid line) part of the coherence $\langle S|\rho|T_0\rangle$.

in this adiabatic case are determined by the roots of

$$\phi_T(\Omega, V, \tau) - \phi_S(\Omega, V, \tau) \pm \pi/2 = 0 \ . \tag{4.9}$$

In contrast to the case of Figure 4.3, the singlet now picks up a nontrivial dynamic phase $\phi_S = \int_{-\infty}^{\infty} \lambda_S^0(t)\ dt$ where λ_S^0 is the eigenvalue of the singlet Hamiltonian

$$H_S(t) = \frac{1}{2} \begin{bmatrix} 0 & \Omega(t) \\ \Omega(t) & 2\delta \end{bmatrix} \tag{4.10}$$

with the property $\lambda_S^0(\pm\infty) = 0$. As for H_T this has a simple analytical form $\lambda_S^0(t) = \frac{\delta}{2} \pm \frac{1}{2}\sqrt{\delta^2 + \Omega^2(t)}$, (+ for $\delta < 0$ and $-$ for $\delta > 0$) which can be used to determine the control parameters from the roots of Eq. (4.9).

Finite radiative lifetime

In order to determine how this control scheme is affected by the finite lifetime of the exciton in the dot we introduce a finite value for γ, and solve the master equation

$\dot{\rho} = -i[H, \rho] + \mathcal{L}[\rho]$ using the values of the control parameters corresponding to the evolution of Figs. 4.3 and 4.4. $\mathcal{L}[\rho]$ is the Liouvillian superoperator that can be written as $\mathcal{L}[\rho] = L^\dagger \rho L + \frac{1}{2}\{L^\dagger L, \rho\}$ where $L^\dagger = \sqrt{\gamma}\, b_\downarrow$ [3] accounts for the spontaneous radiative recombination of the exciton in the dot. Once ρ is obtained, a 4×4 reduced density matrix for the impurity spins ρ_S is computed by tracing out the exciton degrees of freedom. The entanglement in the Bell state is mostly sensitive to decoherence processes and its analysis provides a good test for the scheme. We quantify the error on the reduced density matrix ρ_S using two different methods, the Purity and the Peres criterion of separability. [75] According to the Peres criterion a state is entangled iff $E_{min} < 0$, where E_{min} is the minimum eigenvalue of a matrix constructed by transposing the non-diagonal 2×2 blocks of ρ_S. A maximally entangled state has a $E_{min} = -1/2$. The deviation from that value gives a measure of the effect of the radiative recombination on the entanglement and we quantify the entanglement error as $\Delta E = E_{min} + 1/2$. The purity of ρ_S is a different parameter that characterizes the error in the spins states due to their entanglement with the exciton in the dot. We quantify this error as $\Delta P = Tr\rho_S^2 - 1$. In principle there are errors that can disentangle the spin states without a change in the purity, for instance by affecting the phase picked up in Eq. (4.9). Therefore, in principle the errors induced by γ affect independently ΔE and ΔP. Next, we study the dependence of the errors in the Entanglement ΔE (upper) and in the Purity ΔP on γ alone. We remind that both Ω and γ depend on the dipole moment of the exciton in the dot. Therefore, a change in γ at constant Ω may be realized by compensating with a change in the intensity of the external laser field. This allows us to study how γ affects the errors with all the other parameters kept constant. Figure 4.5 shows the results for the adiabatic and nonadiabatic evolution. Both errors increase linearly at small γ. However, the errors in the adiabatic case are always smaller than in the nonadiabatic case in the range of

[3] There are two harmonic oscillators for the excitation in the QD, i.e. $b_\uparrow$ and $b_\downarrow$, but only the latter can couple to the continuum of electromagnetic radiation. Also, the assumption is that the temperature equals zero.

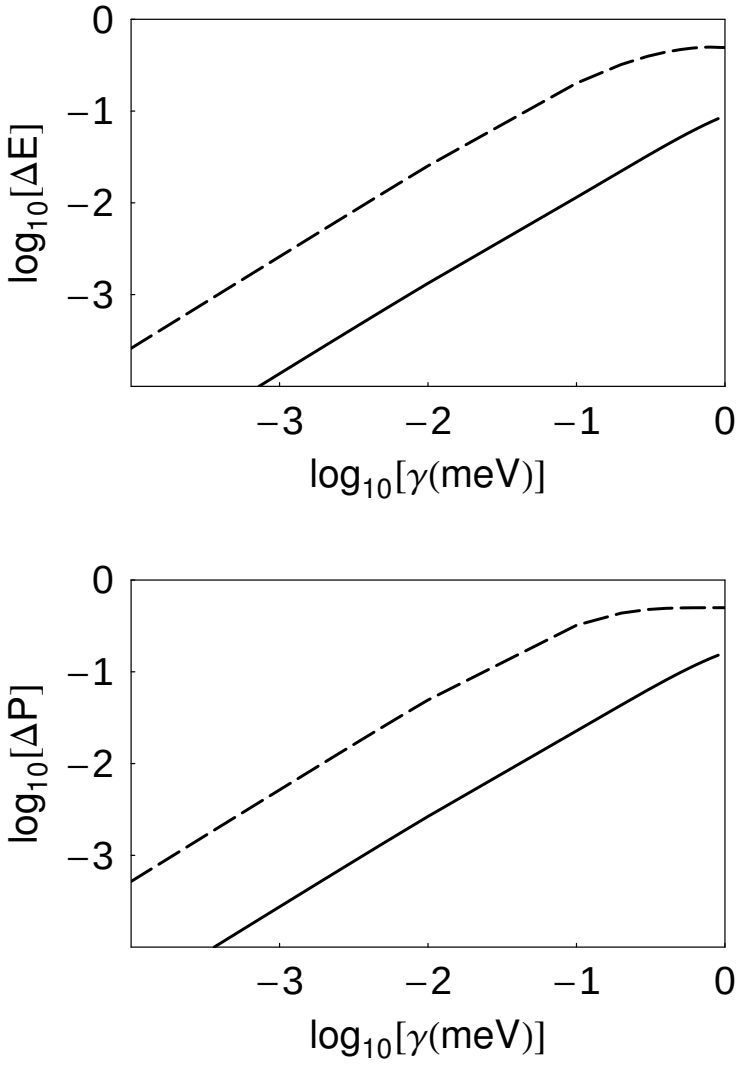

Figure 4.5: Log-Log plot of the deviation from maximal entanglement (upper panel) and maximal purity (lower panel) as a function of the radiative recombination γ (in meV). Solid line: adiabatic evolution. Dashed line: nonadiabatic evolution.

parameters we have investigated. We remark that, due to the incommensurability of the eigenvalues of H_S and H_T, there are not special conditions that would give perfect entanglement with square pulses as in the case of a direct spin-spin coupling. [74] An important figure of merit for the application of this quantum control technique to quantum computation is provided by the *error per gate* parameter. This has to be below a threshold value in order to make scalable quantum computing possible. The estimate for such a threshold depends on assumptions on the error model and device capabilities but the 10^{-4} value [80] is usually used as a benchmark in typical experimental implementations. The error in the entanglement production gives an estimation of the error per gate since the quantum operation done corresponds to a $\sqrt{SWAP}$ modulo some single qubit operations. We see in Figure 4.5 that the 10^{-4} threshold can be achieved for γ smaller than $1\mu eV$. Self assembled QDs have typically a ground state exciton lifetime of the order of one or more nanoseconds and would reasonably be in this region of parameters.

4.2.3 Conclusions

We have analyzed the entanglement production between two spin-impurities induced by an exciton in a neighboring quantum dot. In the case of $\gamma = 0$, the parameters for the quantum control can be analytically determined from the roots of simple integral equations. We showed that the finite lifetime γ^{-1} of the exciton in the dot can affect the purity of the spin states and introduces errors in the entanglement production. In addition we found that such errors increase linearly with γ and can be kept below the 10^{-4} threshold for error correction if parameters typical of self assembled QDs are used in the simulation.

4.3 The indirect interaction mediated by excitons

The optical control of the spin of electrons localized in quantum dots or impurities has several advantages with respect to approaches where electrodes are needed. Ultrafast lasers are available, promising the realization of quantum gates in time scales that are hard to achieve with an electrical control. Lasers are also very flexible for quantum control since pulse shaping can be used to increase accuracy and speed. [50] Finally, metallic electrodes necessarily add a source of noise for the quantum system, and they are not needed in an optical scheme. The possibility of changing the sign of the spin-spin interaction can add flexibility to many control schemes for the qubits, like e.g. in the exchange-only scheme. [77] We have seen that resonances in the spin-spin coupling induced by the binding of the excitons can increase the magnitude of the interaction for distances that are reasonable from a nano-fabrication point of view. This will imply that lasers with lower intensities can be employed in the control. The polarization of the light represents an additional control parameter that can be used to selectively address qubits with an optically induced magnetic field. This is also an advantage from a practical point of view since it could simplify the experimental setup by eliminating the need of an external magnetic field.

Although the feasibility of single impurity spectroscopy in semiconductors has been proven [86, 87], little attention has been paid to optical properties of impurity-bound excitons for information storage and processing. Impurities deserve at least the same attention as quantum dots for such applications. Their homogeneous character and the variety of properties that one can obtain combining different hosts and ions are indeed special advantages. An exciton bound to an impurity has optical properties very similar to an exciton trapped in a shallow quantum dot. Most of the ideas involving excitons in quantum dots as a main ingredient for quantum information and communication can be reformulated for excitons bound to impurities. We have

provided only two examples here, but our phenomenological theory, being based on inputs from the experiments, is very flexible and many other combinations of host and ions can be used to explore a large range of confinement energy and different optical properties. We also have seen that the spin-spin coupling has a resonant behavior at frequencies depending on the separation between the impurities. By organizing the impurities in chains with different separation this can be used to selectively address a single pair of impurities and it allows for scalability.

A very special case is represented by impurities in silicon. This material has obvious technological advantages and many proposals for using impurities in Si for quantum computing have been suggested. [88–90] In particular, the optical control of electronic spins localized by deep donors in Si using a *control* impurity has been proposed. [61] In the scheme we are suggesting here, the exciton bound to the impurity plays the role of the *control* impurity and it takes advantage of the host material for mediating the interaction. Even if Si is an indirect gap material, there is a finite optical coupling to the exciton bound to the impurity due to symmetry breaking. Additional complications in the use of excitons bound to donors for mediating spin-spin coupling arise from the valley degeneracy in Si. [91]

Excitons bound to rare earth magnetic ions can be controlled very rapidly and efficiently due to their strong dipole moment. Their dipole moment is mainly determined by the optical properties of the host material, since it involves the creation of electron hole pairs across the semiconductor gap. At the same time, they interact with the internal degrees of freedom in the core f states. Schemes involving excitons bound to rare earth impurities in III-V materials bring in the advantages of the optical properties of the host and the stability of the internal degrees of freedom of the f orbitals in the rare earth ion where the qubit is stored. This hybrid system is thus extremely powerful, providing both reliable storage and fast processing of information.

Finally, the light controlled spin-spin coupling in a semiconductor matrix is also appealing for the coherent control of macroscopic properties of materials. This was the

idea behind the coherently induced ferromagnetism in Ref. [92]. There, a finite critical temperature for a paramagnetic to ferromagnetic transition in diluted magnetic semiconductors was found when the material is coupled to a strong laser field. The results presented here suggest that the presence of bound states could enhance the effect. Also, the same idea could be used in other systems where the light can induce antiferromagnetic or glassy phases starting from a paramagnetic system. This represents a unique opportunity to study phase transitions in a solid where the coupling is controlled by an external field and may lead to a new class of *controlled* materials to be investigated.

4.4 The indirect interaction mediated by polaritons

Proposals for quantum computers based on spin degrees of freedom require that individual qubits are placed close enough so to have a significant exchange interaction between them. This exchange interaction can be direct (i.e. induced by a controlled overlap of the wavefunctions) or indirect when mediated by spin excitations in a 2D electron gas [78] or by optical excitation across the semiconductor bandgap [6, 7, 79]. In the indirect schemes, the range of the spin coupling is related to the mass of the mediating particles, and the coupling decreases exponentially as a function of the distance between the spins. Here, we showed that the small polariton mass gives an extremely long range for the spin coupling and introduces a non-exponential behavior. This implies that spin-qubits can be located several hundreds of nanometers apart while still retaining control on pair interaction through the use of polaritons. The long range nature of the polariton-mediated interaction presents important technological advantages for quantum information implementations. Using our parameters (see Fig. 2.2), we predict that the strength of the interaction is $|J_{eff}| \simeq 0.005\, Ry^*$ for impurities separated by distances of the order of $R_c = 12\, a_b^* \simeq 150\, nm$. An estimate

for the time needed for an operation can be given as $T = \pi/(2|J_{eff}|) \simeq 40\,ps$, which is much smaller than the typical dephasing time for impurity spin qubits. Recent measurements have reported a spin relaxation time of the order of μs for donors in GaAs [81]. To our knowledge, the spin decoherence time (T_2) of a single donor in GaAs has not been measured, but is also expected to be in the μs range. The decay time for polaritons is reported to be in the range of nanoseconds [82]. Moreover, notice that the time needed for a quantum operation does not change considerably when we further increase the qubit separation. Even with an inter-qubit separation of 1 micron the time needed for one operation increases only by one order of magnitude to about 400 ps, and is still reasonably smaller than the decoherence time. With such a long range interaction, the realization of electric gates to control one-qubit operations and the use of localized magnetic field becomes feasible. The Ising-like interaction at long separation is not a limitation for quantum gate implementations. The polariton mediated coupling could be also used to control the nuclear spin of the donor in a scheme similar to the one in Ref. [78]. In contrast to other cavity QED-based quantum computing implementations [15], the scheme discussed here does not require 0D confined electromagnetic modes, which is much harder to achieve experimentally. In a planar cavity the lateral dimension is not limited by the optical wavelength, which provides a fully scalable geometry for the qubit.

Conclusions

I would like to start these concluding remarks by recalling what we have proposed and done through this dissertation. Our main aim was to achieve a better understanding of the optically-induced spin indirect interaction in semiconductor structures under different conditions. Before turning to the actual physical systems, we developed a formalism that enables us to address a variety of problems in this topic. In Chapter 2 we put this formalism to the test, and learned more about spin indirect interactions of impurities in a bulk semiconductor. Next, in Chapter 3, we sought to determine the effect on the indirect interaction of a micro-cavity. Finally, Chapter 4 presented some possible applications of the theory previously developed.

Outlined in Chapter 1, the formalism we derived is meant to address problems in optically excited semiconductors. More precisely, we found a suitable tool to describe a system of optically generated quasi-particles obeying boson statistics that interact with spins localized in the host lattice. The goal was to derive an expression for the interaction between two localized spins, where the degrees of freedom of the quasi-particle responsible for the indirect interaction are traced out. The formalism is applicable to many situations: bulk semiconductors, quantum wells, quantum dots, micro-cavities, etc. The quasi-particle may be an exciton, polariton, and possibly others. We used the model to study some of them.

In Chapter 2 we employed our model to study the case of a doped bulk semiconductor. We derived an analytical solution to all orders in the interaction between excitons and localized spins. As a consequence, we found that the quasi-particle

binds to pairs of impurities; moreover, the indirect interaction can be made ferro- or antiferro-magnetic. The results are useful to describe doped systems containing impurities with spin 1/2. A question that remains open is if it is possible to generalize the non-perturbative analysis to systems with spin angular momentum $S \neq 1/2$.

In Chapter 3 we focused on the indirect interaction that polaritons mediate between impurities localized in a micro-cavity quantum well. The interesting findings are the existence of two different regimes, and the long-range nature of the polariton interaction. The first one shows that the spin-dependent interaction changes form when the separation between impurities is larger than a certain value. One of the consequences of it is that the critical temperature of a large number of impurities may be made larger than with the use of excitons. Also, the ordering of impurity spins in the ferromagnetic case is different in each regime. The long-range nature of the polariton mediated indirect interaction now opens possibilities for quantum computing two-qubit operations. There are many interesting future lines of investigation. A spin coupling can also be obtained by a real polariton population in a scheme analogue to the RKKY [9] spin coupling mechanism. The spin interaction induced by a 0D cavity and excitons in quantum dots has been recently investigated [83], and also in this 0D case the presence of a strong coupling generates anisotropies in the spin interaction. The use of real carriers is not appealing for quantum computing implementation since it adds decoherence to the spin-qubit. However, it would be interesting to explore the dynamics of spin in the presence of a dense polaritons population that condense in a phase coherent state, as observed recently in II-VI microcavities [84]. High-quality micro-cavities embedding Mn-doped magnetic quantum wells in the strong coupling regime have recently been realized [85]. The polariton mediated spin coupling could be explored in these systems as a method for the ultrafast control of the quantum well magnetization.

Chapter 4 dealt with a more detailed analysis of the applicability of our ideas. We started by modeling a system of impurities and QDs embedded in a QW. The indirect

interaction is here mediated by excitons in the QD. We studied the feasibility of two-qubit operations using this system, including two important realistic assumptions not explicitly considered in Chapters 2-3, namely: *i*) The optical excitation is achieved by a laser pulse, and *ii*) there is decoherence in the form of spontaneous radiation recombination of the exciton. This chapter also discusses some possible applications of the results obtained in Chapters 2-3.

To date, we are not aware of experiments that test our findings. We hope that this work will motivate experimental groups interested in fundamental questions as well as applications to quantum computing to perform experiments following the lines presented here.

Appendix A

Exchange integrals

In this appendix, we show how to calculate an exchange integral in 2D, which appears in the Hamiltonian for the interaction between localized spin and exciton:

$$V = \int d\mathbf{r}_h d\mathbf{r}_e d\mathbf{r}_l \; \psi_{k'}(\mathbf{r}_e, \mathbf{r}_h)\varphi(\mathbf{r}_l)\frac{e^2}{\varepsilon_0|\mathbf{r}_e - \mathbf{r}_l|}\psi_k(\mathbf{r}_l, \mathbf{r}_h)\varphi(\mathbf{r}_e) \tag{A.1}$$

with the functions

$$\begin{aligned} \psi_k(\mathbf{r}_e, \mathbf{r}_h) &= \frac{1}{\sqrt{A}}\, e^{-i\mathbf{k}\cdot(\beta_e \mathbf{r_e} + \beta_h \mathbf{r_h})} \sqrt{\frac{2}{\pi}}\, \frac{1}{\lambda}\, e^{-|\mathbf{r}_e - \mathbf{r}_h|/\lambda} \\ \varphi(\mathbf{r}) &= \frac{1}{\sqrt{a_B^3 \pi}}\, e^{-|\mathbf{r}-\mathbf{R}|/a_B} \end{aligned}$$

for the exciton and localized state respectively, with $\beta_i = m_i/(m_e + m_h)$. Replacing the functions above

$$\begin{aligned} V = C \int d\mathbf{r}_h d\mathbf{r}_e d\mathbf{r}_l \; & e^{i\mathbf{k'}\cdot(\beta_e \mathbf{r}_e + \beta_h \mathbf{r}_h)}\, e^{-|\mathbf{r}_e - \mathbf{r}_h|/\lambda}\, e^{-|\mathbf{r}_l - \mathbf{R}|/a_B} \frac{1}{|\mathbf{r}_e - \mathbf{r}_l|} \times \\ & e^{-i\mathbf{k}\cdot(\beta_e \mathbf{r_l} + \beta_h \mathbf{r_h})}\, e^{-|\mathbf{r}_l - \mathbf{r}_h|/\lambda}\, e^{-|\mathbf{r}_e - \mathbf{R}|/a_B} \end{aligned}$$

with $C = 2\, e^2/(\pi^2 A \lambda^2 a_B^3 \epsilon_0)$. Next we transform to relative coordinates $\mathbf{s} = \mathbf{r}_e - \mathbf{r}_h$ and $\mathbf{t} = \mathbf{r}_l - \mathbf{r}_h$, with Jacobian equal to 1. Our new set of coordinate is $\{\mathbf{r}_e, \mathbf{s}, \mathbf{t}\}$.

Then,

$$
\begin{aligned}
V &= C \int d\mathbf{r}_e \, d\mathbf{s} \, d\mathbf{t} \; e^{i\mathbf{k'}\cdot[\beta_e \mathbf{r_e} + \beta_h(\mathbf{r_e}-\mathbf{s})]} \, e^{-s/\lambda} \, e^{-|(\mathbf{t}-\mathbf{s}+\mathbf{r_e})-\mathbf{R}|/a_B} \frac{1}{|\mathbf{s}-\mathbf{t}|} \times \\
& \quad e^{-i\mathbf{k}\cdot[\beta_e(\mathbf{t}-\mathbf{s}+\mathbf{r_e})+\beta_h(\mathbf{r_e}-\mathbf{s})]} \, e^{-t/\lambda} \, e^{-|\mathbf{r}_e-\mathbf{R}|/a_B} \\
&= C \int d\mathbf{r}_e \, d\mathbf{s} \, d\mathbf{t} \; e^{i\mathbf{k'}\cdot(\mathbf{r_e}-\beta_h \mathbf{s})} \, e^{-s/\lambda} \, e^{-|(\mathbf{t}-\mathbf{s}+\mathbf{r_e})-\mathbf{R}|/a_B} \frac{1}{|\mathbf{s}-\mathbf{t}|} \times \\
& \quad e^{-i\mathbf{k}\cdot(\mathbf{r_e}-\mathbf{s}+\beta_e \mathbf{t})} \, e^{-t/\lambda} \, e^{-|\mathbf{r}_e-\mathbf{R}|/a_B} \; ,
\end{aligned}
$$

where we have used that $\beta_e + \beta_h = 1$. Now we replace exponentials by Gaussians, a common procedure in quantum chemistry: [19]

$$
\begin{aligned}
e^{-|(\mathbf{t}-\mathbf{s}+\mathbf{r_e})-\mathbf{R}|/a_B} &\rightarrow \sqrt{\frac{\alpha_1}{\pi}} \; e^{-\alpha_1[(\mathbf{t}-\mathbf{s}+\mathbf{r_e})-\mathbf{R}]^2} \\
e^{-|\mathbf{r}_e-\mathbf{R}|/a_B} &\rightarrow \sqrt{\frac{\alpha_1}{\pi}} \; e^{-\alpha_1(\mathbf{r}_e-\mathbf{R})^2} \\
e^{-t/\lambda} &\rightarrow \sqrt{\frac{\alpha_2}{\pi}} \; e^{-\alpha_2 \, t^2} \\
e^{-s/\lambda} &\rightarrow \sqrt{\frac{\alpha_2}{\pi}} \; e^{-\alpha_2 \, s^2}
\end{aligned}
$$

with the constants α_i chosen so as to fit the exponentials. The integral reads

$$
\begin{aligned}
V &= C \frac{\alpha_1 \alpha_2}{\pi^2} \int d\mathbf{r}_e \, d\mathbf{s} \, d\mathbf{t} \; e^{i(\mathbf{k'}-\mathbf{k})\cdot\mathbf{r}_e} e^{-i\beta_h \mathbf{k'}\cdot\mathbf{s}} \, e^{-i\mathbf{k}\cdot(\beta_e \mathbf{t}-\mathbf{s})} \frac{1}{|\mathbf{t}-\mathbf{s}|} \times \\
& \quad e^{-\alpha_2 \, s^2} e^{-\alpha_1[(\mathbf{t}-\mathbf{s})+(\mathbf{r_e}-\mathbf{R})]^2} \; e^{-\alpha_2 \, t^2} \, e^{-\alpha_1(\mathbf{r}_e-\mathbf{R})^2} \; ,
\end{aligned}
$$

and multiplying by $exp[i(k'-k)R]$ and c.c., collecting factors of $(\mathbf{r}_e - \mathbf{R})$ and completing squares,

$$
\begin{aligned}
V &= C \frac{\alpha_1 \alpha_2}{\pi^2} \; e^{i(\mathbf{k'}-\mathbf{k})\cdot\mathbf{R}} \int d\mathbf{r}_e \, d\mathbf{s} \, d\mathbf{t} \; e^{-i\beta_h \mathbf{k'}\cdot\mathbf{s}} \, e^{-i\mathbf{k}\cdot(\beta_e \mathbf{t}-\mathbf{s})} \frac{1}{|\mathbf{t}-\mathbf{s}|} \times \\
& \quad e^{-\alpha_2 \, s^2} e^{-2\alpha_1[\mathbf{u}+(\mathbf{r_e}-\mathbf{R})]^2} \, e^{2\alpha_1 \, u^2} \, e^{-\alpha_2 \, t^2}
\end{aligned}
$$

with $u = 1/2[(t-s) - i(k'-k)/(2\alpha_1)]$, and the integration in $\mathbf{r}_e$ can be performed, defining $v = \mathbf{r_e} + (\mathbf{R} + \mathbf{u})$

$$\int dv\, e^{-2\alpha_1 v^2} = \sqrt{\frac{\pi}{2\alpha_1}}\ ,$$

and so

$$\begin{aligned} V &= C\frac{\alpha_1\alpha_2}{\pi^2}\left(\frac{\pi}{2\,\alpha_1}\right)^{3/2}\ e^{i(\mathbf{k'}-\mathbf{k})\cdot\mathbf{R}}\int d\mathbf{s}\, d\mathbf{t}\ e^{-i\beta_h\mathbf{k'}\cdot\mathbf{s}}\, e^{-i\mathbf{k}\cdot(\beta_e\mathbf{t}-\mathbf{s})}\frac{1}{|\mathbf{t}-\mathbf{s}|}\times \\ & e^{-\alpha_2\, s^2}\, e^{-\frac{|\mathbf{k'}-\mathbf{k}|^2}{8\,\alpha_1}}\, e^{-i\,(\mathbf{k'}-\mathbf{k})(\mathbf{t}-\mathbf{s})} e^{\alpha_1|\mathbf{t}-\mathbf{s}|^2/2} e^{-\alpha_2\, t^2} \\ &= C\frac{\alpha_1\alpha_2}{\pi^2}\left(\frac{\pi}{2\,\alpha_1}\right)^{3/2}\ e^{i(\mathbf{k'}-\mathbf{k})\cdot\mathbf{R}} e^{-\frac{|\mathbf{k'}-\mathbf{k}|^2}{8\,\alpha_1}}\int d\mathbf{s}\, d\mathbf{t}\ e^{i(\beta_h\mathbf{k'}+\mathbf{k})\cdot\mathbf{s}}\, e^{-i\beta_e\mathbf{k}\cdot\mathbf{t}}\frac{1}{|\mathbf{t}-\mathbf{s}|}\times \\ & e^{-i\,(\mathbf{k'}-\mathbf{k})(\mathbf{t}-\mathbf{s})} e^{\alpha_1|\mathbf{t}-\mathbf{s}|^2/2}\, e^{-\alpha_2\,(t^2+s^2)}\ . \end{aligned}$$

We define new variables $\mathbf{x} = \mathbf{t} + \mathbf{s}$ and $\mathbf{z} = \mathbf{t} - \mathbf{s}$

$$\begin{aligned} V &= C\frac{\alpha_1\alpha_2}{\pi^2}\left(\frac{\pi}{2\,\alpha_1}\right)^{3/2}\ e^{i(\mathbf{k'}-\mathbf{k})\cdot\mathbf{R}} e^{-\frac{|\mathbf{k'}-\mathbf{k}|^2}{8\,\alpha_1}}\int d\mathbf{x}\, d\mathbf{z}\ e^{i(\beta_h\mathbf{k'}+\mathbf{k})\cdot[(\mathbf{x}-\mathbf{z})/\mathbf{2}]}\times \\ & e^{-i\beta_e\mathbf{k}\cdot[(\mathbf{x}+\mathbf{z})/2]}\frac{1}{|\mathbf{z}|}\, e^{-i\,(\mathbf{k'}-\mathbf{k})\cdot\mathbf{z}} e^{-\alpha_1|\mathbf{z}|^2/2}\, e^{-\alpha_2\,[(\mathbf{x}^2+\mathbf{z}^2)/2]} \end{aligned}$$

We can complete squares in $\mathbf{x}$ and follow the same procedure as before, to obtain

$$\begin{aligned} V &= C\frac{\alpha_1\alpha_2}{\pi^2}\left(\frac{\pi}{2\,\alpha_1}\right)^{3/2}\left(\frac{2\pi}{\alpha_2}\right)^{3/2}\ e^{i(\mathbf{k'}-\mathbf{k})\cdot\mathbf{R}} e^{-|\mathbf{k'}-\mathbf{k}|^2/(8\,\alpha_1)}\ e^{-[\beta_h\mathbf{k'}+(1-\beta_e)\mathbf{k}]^2/(8\alpha_2)}\times \\ & \int d\mathbf{z}\ e^{i(\beta_h\mathbf{k'}+\mathbf{k})\cdot\mathbf{z}/\mathbf{2}} e^{-i\beta_e\mathbf{k}\cdot\mathbf{z}/2}\frac{1}{|\mathbf{z}|}\, e^{-i\,(\mathbf{k'}-\mathbf{k})\cdot\mathbf{z}} e^{-(\alpha_1+\alpha_2)|\mathbf{z}|^2/2}\ , \end{aligned}$$

The use of $\beta_h = 1 - \beta_e$ yields

$$\begin{aligned} V &= C\pi(\alpha_1\alpha_2)^{-1/2}\ e^{i(\mathbf{k'}-\mathbf{k})\cdot\mathbf{R}} e^{-|\mathbf{k'}-\mathbf{k}|^2/(8\,\alpha_1)}\ e^{-\beta_h|\mathbf{k'}+\mathbf{k}|^2/(8\alpha_2)}\times \\ & \int d\mathbf{z}\ e^{i(\beta_h\mathbf{k'}+\mathbf{k})\cdot\mathbf{z}/\mathbf{2}} e^{-i\beta_e\mathbf{k}\cdot\mathbf{z}/2}\frac{1}{|\mathbf{z}|}\, e^{-i\,(\mathbf{k'}-\mathbf{k})\cdot\mathbf{z}} e^{-(\alpha_1+\alpha_2)|\mathbf{z}|^2/2}\ , \end{aligned}$$

and using the definition: $K = 1/2(\mathbf{k}' + \mathbf{k})$ and $q = \mathbf{k}' - \mathbf{k}$

$$\begin{aligned} V &= C\pi(\alpha_1\alpha_2)^{-1/2}\ e^{i\mathbf{q}\cdot\mathbf{R}} e^{-\mathbf{q}^2/(8\,\alpha_1)}\ e^{-\beta_h \mathbf{K}^2/(2\alpha_2)} \times \\ &\int d\mathbf{z}\ e^{i(\beta_h\mathbf{K}-\mathbf{q})\cdot\mathbf{z}} \frac{1}{|\mathbf{z}|}\, e^{-(\alpha_1+\alpha_2)|\mathbf{z}|^2/2}\ . \end{aligned}$$

Evaluating the expression in polar coordinates, we arrive at

$$\begin{aligned} V &= C\pi(\alpha_1\alpha_2)^{-1/2}\ e^{i\mathbf{q}\cdot\mathbf{R}} e^{-\mathbf{q}^2/(8\,\alpha_1)}\ e^{-\beta_h \mathbf{K}^2/(2\alpha_2)} \times \\ &\frac{2\,\sqrt{2}\,\pi^{\frac{5}{2}}}{\sqrt{\alpha_1+\alpha_2}}\, e^{-\frac{|\beta_h\mathbf{K}-\mathbf{q}|^2}{4\,(\alpha_1+\alpha_2)}}\ I\left(0, \frac{|\beta_h\mathbf{K}-\mathbf{q}|^2}{4\ (\alpha_1+\alpha_2)}\right) \\ &= e^{i\mathbf{q}\cdot\mathbf{R}}\ C(\alpha_1\alpha_2)^{-1/2} \frac{2\,\sqrt{2}\,\pi^{\frac{7}{2}}}{\sqrt{\alpha_1+\alpha_2}}\ e^{-\mathbf{q}^2/(8\,\alpha_1)}\ e^{-\beta_h \mathbf{K}^2/(2\alpha_2)} \times \\ &e^{-\frac{|\beta_h\mathbf{K}-\mathbf{q}|^2}{4\,(\alpha_1+\alpha_2)}}\ I\left(0, \frac{|\beta_h\mathbf{K}-\mathbf{q}|^2}{4\ (\alpha_1+\alpha_2)}\right)\ , \end{aligned}$$

where I is the modified Bessel function.

Appendix B

The matrix Representation of the T operator

Using the basis set $|s_z^A, s_z^B, s_z\rangle$ we obtain for the spin products $s^A \cdot s$, $s^B \cdot s$, $s^A \cdot s^B$ the matrices

$$s^A \cdot s = \begin{bmatrix} \frac{1}{4} & 0 & 0 & 0 & 0 & 0 & 0 & 0 \\ 0 & -\frac{1}{4} & 0 & 0 & \frac{1}{2} & 0 & 0 & 0 \\ 0 & 0 & \frac{1}{4} & 0 & 0 & 0 & 0 & 0 \\ 0 & 0 & 0 & -\frac{1}{4} & 0 & 0 & \frac{1}{2} & 0 \\ 0 & \frac{1}{2} & 0 & 0 & -\frac{1}{4} & 0 & 0 & 0 \\ 0 & 0 & 0 & 0 & 0 & \frac{1}{4} & 0 & 0 \\ 0 & 0 & 0 & \frac{1}{2} & 0 & 0 & -\frac{1}{4} & 0 \\ 0 & 0 & 0 & 0 & 0 & 0 & 0 & \frac{1}{4} \end{bmatrix} \tag{B.1a}$$

$$s^B \cdot s = \begin{bmatrix} \frac{1}{4} & 0 & 0 & 0 & 0 & 0 & 0 & 0 \\ 0 & -\frac{1}{4} & \frac{1}{2} & 0 & 0 & 0 & 0 & 0 \\ 0 & \frac{1}{2} & -\frac{1}{4} & 0 & 0 & 0 & 0 & 0 \\ 0 & 0 & 0 & \frac{1}{4} & 0 & 0 & 0 & 0 \\ 0 & 0 & 0 & 0 & \frac{1}{4} & 0 & 0 & 0 \\ 0 & 0 & 0 & 0 & 0 & -\frac{1}{4} & \frac{1}{2} & 0 \\ 0 & 0 & 0 & 0 & 0 & \frac{1}{2} & -\frac{1}{4} & 0 \\ 0 & 0 & 0 & 0 & 0 & 0 & 0 & \frac{1}{4} \end{bmatrix} \tag{B.2a}$$

$$s^A \cdot s^B = \begin{bmatrix} \frac{1}{4} & 0 & 0 & 0 & 0 & 0 & 0 & 0 \\ 0 & \frac{1}{4} & 0 & 0 & 0 & 0 & 0 & 0 \\ 0 & 0 & -\frac{1}{4} & 0 & \frac{1}{2} & 0 & 0 & 0 \\ 0 & 0 & 0 & -\frac{1}{4} & 0 & \frac{1}{2} & 0 & 0 \\ 0 & 0 & \frac{1}{2} & 0 & -\frac{1}{4} & 0 & 0 & 0 \\ 0 & 0 & 0 & \frac{1}{2} & 0 & -\frac{1}{4} & 0 & 0 \\ 0 & 0 & 0 & 0 & 0 & 0 & \frac{1}{4} & 0 \\ 0 & 0 & 0 & 0 & 0 & 0 & 0 & \frac{1}{4} \end{bmatrix} . \tag{B.3a}$$

By substituting these expressions in Υ^A and Υ^B and then in Eq. (2.19), we obtain after matrix inversions and multiplications an expression for

$$T = (1 - F_R^2 \Upsilon^A \Upsilon^B)^{-1} \Upsilon^A [1 + F_R \Upsilon^B] + (A \rightleftharpoons B) \ .$$

The traceless part of this matrix is

$$\begin{bmatrix} \frac{\beta+2\alpha}{4} & 0 & 0 & 0 & 0 & 0 & 0 & 0 \\ 0 & \frac{\beta-2\alpha}{4} & \frac{\alpha}{2} & 0 & \frac{\alpha}{2} & 0 & 0 & 0 \\ 0 & \frac{\alpha}{2} & -\frac{\beta}{4} & 0 & \frac{\beta}{2} & 0 & 0 & 0 \\ 0 & 0 & 0 & -\frac{\beta}{4} & 0 & \frac{\beta}{2} & \frac{\alpha}{2} & 0 \\ 0 & \frac{\alpha}{2} & \frac{\beta}{2} & 0 & -\frac{\beta}{4} & 0 & 0 & 0 \\ 0 & 0 & 0 & \frac{\beta}{2} & 0 & -\frac{\beta}{4} & \frac{\alpha}{2} & 0 \\ 0 & 0 & 0 & \frac{\alpha}{2} & 0 & \frac{\alpha}{2} & \frac{\beta-2\alpha}{4} & 0 \\ 0 & 0 & 0 & 0 & 0 & 0 & 0 & \frac{\beta+2\alpha}{4} \end{bmatrix} , \tag{B.4}$$

where α and β can be conveniently expressed as a function of the single impurity T^T and T^S operators in Eqs. (2.13) or Eqs. (2.31) as

$$\alpha = \frac{2(T^T - T^S)(T^T F_R + 1)}{(T^T F_R - 1)[F_R(T^S - T^T + 2F_R T^T T^S) - 2]} \tag{B.5a}$$

$$\beta = -\alpha \frac{(T^T - T^S)F_R}{(F_R(T^T - T^S + 2F_R T^T T^S) - 2)} , \tag{B.5b}$$

where we have dropped the {A,B} index since we are considering two identical centers. Notice that the matrix in Eq. (B.4) can be rewritten as

$$\alpha(s^A + s^B) \cdot s + \beta s^A \cdot s^B . \tag{B.6}$$

Appendix C

Units and Physical constants

C.1 (Exciton) Rydberg units

In analogy to the *Atomic Rydberg* system of units, $1s$ state of a Wannier exciton units are sought. The starting point consists in choosing $\hbar = 2\,m = e^2/2 = 1$ The energy and wave function of the $1s$ state follows that of the hydrogen atom, with the proper reduced mass and re-scaled by the dielectric constant ε of the medium.

$$\begin{aligned} Ry^* &= \frac{e^4\mu}{2\,\varepsilon^2\hbar^2} \\ a_B^* &= \frac{\varepsilon\hbar^2}{\mu\,e^2}\ , \end{aligned}$$

where μ is the reduced mass of the electron hole system (not to be confused with the mass $m = (m_e + m_h)/2$ related to the center of mass motion appearing in the dispersion law for excitons in Chapters 1, 2, 3). Any other unit may be obtained from the previous relationships. As examples, we show the units of time and speed

$$\begin{aligned} t_0^* &= \frac{\hbar}{Ry^*} \\ a_B^*/t_0^* &= \frac{e^2}{2\,\varepsilon\hbar}\ ; \end{aligned}$$

from here, we obtain the speed of light in a medium of index of refraction n,

$$c[a_B^*/t_0^*] = \frac{c[SI]}{e^2/2\,\varepsilon\hbar}\ .$$

C.1.1 Mn in CdTe

We use the values of the binding energy and Bohr radius of an exciton in bulk CdTe,

$$\begin{aligned} a_B^* &= 65\,\mathring{A} \\ Ry^* &= 11\,meV\ . \end{aligned}$$

Constant		Value
Plank constant	$\hbar$	1
Electric Charge	e	1
Mass of exciton	m	0.36 m_e
Impurity separation	R	(0.4,8) a_B^*
Strength of hole interaction	ζ	-5
Exciton $k=0$ energy	$\hbar\epsilon$	300 Ry^*
Exciton-impurity exchange interaction range	$\hbar\Lambda$	0.01 a_B^*
Exchange coupling exciton-impurity	J	$10^{-4} Ry^* a_B^{*2}$

Table C.1: Approximate values for the physical constants in excitonic Rydberg units for Mn deep impurities in CdTe QW.

C.1.2 Si in GaAs

We use the values of the binding energy and Bohr radius of an exciton in bulk GaAs,

$$\begin{aligned} a_B^* &= 125\,\mathring{A} \\ Ry^* &= 4.4\,meV\ . \end{aligned}$$

Constant		Value
Plank constant	$\hbar$	1
Boltzmann constant	k	0.02 Ry^*/K
Electric Charge	e	1
Speed of light	$\hbar c/n$	1300 $Ry^* a_B^*$
Index of refraction	n	3
Mass of exciton	m	0.28 m_e
Coupling exciton-cavity at $k = 0$	$\hbar g_0$	0.4 Ry^*
Impurity separation	R	$> 0.5 a_B^*$
Strength of hole interaction	ζ	0
Exciton-cavity detunning	$\hbar\Delta$	-0.1 Ry^*
Exciton $k = 0$ energy	$\hbar\epsilon$	300 Ry^*
Extracavity energy	$\hbar\omega_L$	$-Ry^*$
Exciton-impurity exchange interaction range	$\hbar\Lambda$	0.25 a_B^*
Polariton-Extracavity detunning	$\hbar\delta = \omega_L - \Omega_0$	-0.3 Ry^*
Rabi energy	$\hbar\wp$	$-Ry^*$
Exchange coupling exciton-impurity	J	$21 Ry^* a_B^{*2}$

Table C.2: Approximate values for the physical constants in excitonic Rydberg units.

To calculate the factors that appear in the expressions for J_{eff} we use,

$$\begin{aligned} v_0 &= 1 \\ \phi_{1s} &= \sqrt{\frac{2}{\pi}} \frac{1}{a_b^*} \simeq 0.8 \ . \end{aligned}$$

Appendix D

Mean field approximation

First it is worth mentioning that it should always be a mechanism that singles out a direction along which the spins aligns prior to the ordering. This could be the linear term in J that contributes an effective magnetic field (as shown in Chapter 2) or an external magnetic field, etc. For example, the spins become aligned at $T > T_c$ by this "external" agent, the temperature is then lowered below T_c; if the system is irradiated by the laser field, and the external agent is eliminated, the spins will remain aligned as a consequence of ferromagnetic interactions.

To illustrate the procedure, suppose the dynamics is governed by a spin Hamiltonian that contains only one type of interaction, say Heisenberg: $A\sum_{jk} F_{jk} s^j \cdot s^k$. As said before, there is a preferred direction; take this in the z-axis. Single out an impurity k, and assume that its neighbors have mean magnetization (spin) m. The projected Hamiltonian for one impurity k reads

$$A\sum_j F_{jk}\ s^j \cdot s^k \ \ \rightarrow \ \ A\,m\left(\sum_j F_{jk}\right) s_z^k\ .$$

The thermodynamics follows from the partition function

$$\begin{aligned} Z &= Tr[e^{-\alpha\, s_z^k}] \\ \alpha &\doteq \beta\, A\, m \left(\sum_j F_{jk} \right) \ , \end{aligned}$$

using eigenstates of $\{s, s_z\}$ and the fact that the localized states are $s = 1/2$,

$$Z = 2\cosh\left(\frac{\hbar\,\alpha}{2}\right) \ .$$

The magnetization is given by

$$\begin{aligned} m &= \frac{1}{Z} Tr[s_z^k\, e^{-\alpha\, s_z^k}] \\ &= -\frac{\partial}{\partial\alpha}(\ln\, Z_k) \\ &= -\frac{\hbar}{Z}\sinh\left(\frac{\hbar\,\alpha}{2}\right) \ . \end{aligned}$$

For the case $\alpha < 0$ [1], and defining a positive constant $\gamma = \hbar/2\,\beta\, A|\sum_j F_{jk}|$, a transcendental equation for m is found

$$m = \frac{\hbar}{2}\tanh\left(\gamma\, m\right) \ .$$

When this equation has more than the trivial $m = 0$ solution, there is ordering in the system (macroscopic magnetization). The temperature for which these nonzero solutions appear is the Curie T_c temperature; this occurs when the *tanh* has slope equal to $2/\hbar$ at the origin: $1 = \hbar\gamma/2\,\mathrm{sech}^2(0) = \hbar\gamma/2$,

$$kT_c = \frac{A\,\hbar^2}{4}\left|\sum_j F_{jk}\right| \ .$$

[1] The range of physical parameters used for F_{R_P} are such that this functions is negative for all values of its argument. $F_{R_P} > 0$ always.

Appendix E

Separable potentials

Following Mott [36] consider the case of the scattering of two identical particles, one localized and restricted to one orbital ϕ and the other an unbound state M

$$\Psi(r_l, r_u) = \frac{1}{\sqrt{2}}[\phi(r_l)M(r_u) \pm \phi(r_u)M(r_l)] \ . \tag{E.1}$$

The complete time independent schrödinger equation can be reduced to an equation for the wave function $M(r_u)$ describing the unbound state. Applying the total Hamiltonian for the system to the wave function Eq. E.1, multiplying by $\phi(r_l)$ and integrating in r_u reduces the equation to

$$(\bigtriangledown^2 + k^2)M(r_u) = U(r_u)M(r_u) \pm \int K(r_u, r_l)M(r_l)dr_l \tag{E.2}$$

$$K(r_u, r_l) = \phi(r_u)\phi^*(r_l)[k^2 + \lambda^2 + U(r_l, r_u)] \ ,$$

where λ^2 and k^2 are the energies of the localized and unbound state respectively; $U(x, y)$ and $U(x)$ are the complete and integrated Coulomb interactions, respectively.

We are only interested in the exchange part of the interaction, thus we consider the second term on the r.h.s. of Eq. E.2. It is important to notice that this term enters the equation in the form of a non-local potential. Moreover, because it is formed by the

product of well localized state functions ϕ's it is short-range. This last fact allows us to replace $K(r_u, r_l)$ by a separable kernel.[1] On the other hand, the integral of $K(r_u, r_l)$ weighted with the product $M^*(r_u)M(r_l)$ is an exchange integral, say $L(k, k')$. This is in complete analogy with our case of excitons and localized states, where the role of M is played by the exciton wave functions and the exchange integral $J(k, k')$ is calculated exactly as $L(k, k')$. Therefore, if $K(r_u, r_l)$ is separable in (k, k'), so is the corresponding exchange integral.

Following the preceding arguments, we assume that the exchange integral $J_{k,k'}$ can be well approximated by a separable potential, i.e. $J_{k,k'} = Jv_k v_{k'}$, where $v(k)$ is a function only on $k = |\vec{k}|$, and J is a constant.

Finally, we note that a non-local separable potential can support a finite number of bound states. We are particularly interested in the case of a *rank 1 potential*. In this situation, the schrödinger equation reads,

$$-\nabla^2\psi(x) - v(x)\int d^3x'\ v(x')\psi(x') = \varepsilon\psi(x)\ .$$

After some algebra, we arrive to the following condition that ε must satisfy,

$$1 = \frac{1}{(2\pi)^3}\int d^3q \frac{|v(q)|^2}{q^2 - \varepsilon}\ .$$

Given that the r.h.s. is a monotonic function of ε, and that bounds states occur only for negative energies, it is clear that only one bound state can occur. [93]

[1] When the potential is rotationally invariant, it can be written in terms of *partial waves*.

Bibliography

[1] G. Bastard, *Wave Mechanics Applied to Semiconductor Heterostructures*, Haltesd Press (1988).

[2] Y. Alhassid Rev. Mod. Phys., 72, 895 (2000).

[3] S. M. Reimann M. Manninen, Rev. Mod. Phys., 74, 1283 (2002).

[4] G. Khitrova, H. M. Gibbs, F. Jahnke, M. Kira, and S. W. Koch, Rev. Mod. Phys. 71, 1591 (1999).

[5] H. Haug, Stephan W. Koch and S. W. Koch, *Quantum theory of the optical and electronic properties of semiconductors*, World Scientific Publishing Company.

[6] C. Piermarocchi, Pochung Chen, and L. J. Sham, Phys. Rev. Lett. **89**, 167402 (2002).

[7] C. Piermarocchi and G. F. Quinteiro, Phys. Rev. B 70, 235210 (2004).

[8] G. F. Quinteiro and C. Piermarocchi, Phys. Rev. B 72, 045334 (2005).

[9] M. A. Ruderman and C. Kittel Phys. Rev. 96, 99 (1954).

[10] C. Kittel, J. Appl. Phys. 39, 637 (1968).

[11] P. Chen, C. Piermarocchi, and L. J. Sham, Phys. Rev. Lett. 87, 067401 (2001).

[12] R. P. Feynman, Int. J. Theor. Phys. 21 46788 (1982).

[13] A. Steane, Rep. Prog. Phys. 61 (1998) 117173.

[14] A. Galindo* and M. A. Martín-Delgado, Rev. Mod. Phys., Vol. 74, No. 2 (2002).

[15] A. Imamoglu, D. D. Awschalom, G. Burkard, D. P. DiVincenzo, D. Loss, M. Sherwin and A. Small Phys. Rev. Lett. **83** 4204 (1999).

[16] R. de Sousa and S. Das Sarma, Phys. Rev. B 67, 033301 (2003).

[17] L. C. L. Hollenberg, A. S. Dzurak, C. Wellard, A. R. Hamilton, D. J. Reilly, G. J. Milburn and R. G. Clark,Phys. Rev. B 69, 113301 (2004).

[18] N.W. Ashcroft and N. Mermin, *Solid State Physics*, Sanders College Publishing (1976).

[19] A. Szabo and N. S. Ostlund, *Modern Quantum Chemistry: Introduction to advance electronic structure theory*, McMillan Publishing Co., Inc.

[20] J. M. Ziman, *Principles of the Theory of Solids* Cambridge University PRess (1972).

[21] Peter Y. Yu, Manuel Cardona, *Fundamentals of Semiconductors: Physics and Materials Properties* Springer-Verlag (1996).

[22] D. L. Dexter and R. S. Knox, *Excitons*, John Wilew & Sons, Inc (1965) / R. S. Knox, *Theory of excitons*, Academic Press (1963).

[23] G. H. Wannier. Phys. Rev. **52**, 191 (1937)

[24] J. Frenkel. Phys. Rev. **37**, 1276 (1931)

[25] R. S. Knox and N. Inchauspé Phys. Rev. **116**, 1062 (1959)

[26] P. Nozières and D. Pines Phys. Rev. **109**, 1062 (1958)

[27] The quantum theory of light, R. Loudon, Oxford University Press, 1983.

[28] Elements of quantum optics, Pierre Meystre, Murray Sargent III, Springer-Verlag, 1990.

[29] Claude Cohen-Tannoudji, Jacques Dupont-Roc, Gilbert Grynberg,*AtomPhoton Interactions: Basic Processes and Applications* Wiley-Interscience (1992).

[30] C. Ciuti, V. Savona, C. Piermarocchi, and A. Quattropani Phys. Rev. B 58 (1998).

[31] S. D. Drell and L. Verlet, Phys. Rev. **99**, 849 (1955).

[32] M. A. Ruderman and C. Kittel, Phys. Rev. **96**, 99 (1954); T. Kasuya, Prog. Theor. Phys. **16**, 45 (1956); K. Yoshida, Phys. Rev. **106**, 893 (1957).

[33] N. F. Ramsey, Phys. Rev. **91**, 303 (1953).

[34] N. Bloembergen and T. J. Rowland, Phys. Rev. **97** 1679 (1955).

[35] G. Vertogen and W. J. Caspers, Z. Phys. **198** 37 (1967).

[36] N. F. Mott and H. S. W Massey, *The Theory of Atomic Collisions.*, Oxford University Press (1965).

[37] P. W. Anderson, Solid State Physics **14**, 99 (1963).

[38] Y. Yamaguchi, Phys. Rev. **95**, 1628 (1954).

[39] L. H. Schick, Rev. Mod. Phys. **33** 608 (1961).

[40] M. Combescot and O. Betbeder-Matibet, arXiv:cond-mat/0404744 (2004)

[41] A. Taguchi, H. Nakagome and K. Takahei, J. Appl. Phys. **68**, 3390 (1990).

[42] P. J. Dean and D. C. Herbert, *Bound Excitons in Semiconductors* in it Excitons Ed. by K. Cho, Springer-Verlag (1979).

[43] V.F. Masterov and L. F. Zakharenkov, Sov. Phys. Semicond. **24** 383 (1990).

[44] G. Aszodi, J. Weber, Ch. Uihlein, L. Pu-lin, H. Ennen, U. Kaufmann, J. Schneider, and J. Windscheif, Phys. Rev. B **31** 7767 (1985).

[45] P. S. Whitney, K. Uwai, H. Nakagome and K. Takahei, App. Phys. Lett. **53** 2074 (1988).

[46] B. Lambert, A. Le Corre, Y. Toudic, C. Lhomer, G. Grandpierre, and M. Gauneau, J. Phys. Condens. Matter **2** 479 (1990); A. Kozanecki and A. Szcerbakow, App. Phys. Lett. **66** 3630 (1995); M. A. J. Klik, T. Gregorkiewicz, I. V. Bradley, and J-P. R. Wells, Phys. Rev. Lett. **89** 227401 (2002).

[47] A. Baldereschi and J.J. Hopfield, Phys. Rev. Lett **28** 171 (1972).

[48] W. Nolting and A. M. Olés, Phys. Rev. B **22**, 6184 (1980).

[49] J.K. Furdyna, J. Appl. Phys. **64**, R29 (1988).

[50] P. Chen, C. Piermarocchi, and L.J. Sham, Phys. Rev. Lett. **87**, 67401 (2001).

[51] T. V. Shahbazyan, I. E. Perakis, and M. E. Raikh, Phys. Rev. Lett. **84**, 5896 (2000).

[52] G.Cassabois, A. L. C. Triques, F. Bogani, C. Delalande, Ph. Roussignol, and C. Piermarocchi, Phys. Rev. B 61, 1696 (2000).

[53] V. Savona, C. Piermarocchi, A. Quattropani, F. Tassone, P. Schwendimann Phys. Rev. Lett. **78**, 4470 (1997).

[54] V. Savona, C. Piermarocchi, A. Quattropani, P. Schwendimann, F. Tassone Phase Transitions **68**, 169 Part B (1999).

[55] J. J. Hopfield, Phys. Rev. 112, 1555 (1958).

[56] J.M. Bao, A.V. Bragas, J.K. Furdyna, and R. Merlin, Solid State Communications 127 (2003) 771775.

[57] J. J. Hopfield, Phys. Rev. 182, 945 (1969).

[58] J. Fernandez-Rossier, C. Piermarocchi P. Chen, A. H. Mac Donald and L. J. Sham, Phys. Rev. Lett. **70**, Vol. 93 12 (2004).

[59] N. A. Gershenfeld and I. L. Chuang, Science 275, 350 (1997).

[60] A. Steane Rep. Prog. Phys. 61 (1998) 117173.

[61] A. M. Stoneham, A. J. Fisher, and P. T. Greenland, J. Phys. Condens. Matter **15**, L447 (2003).

[62] R. Rodriquez, A. J. Fisher, P. T. Greenland, and A. M. Stoneham, J. Phys. Condens. Matter **16**, 2757 (2004).

[63] G. Ramon, Y. Lyanda-Geller, T. L. Reinecke and L. J. Sham, arXiv:cond-mat/0412003 (2004)

[64] A. Nazir, B. W. Lovett, S. D. Barrett, T. P. Spiller, and G. A. D. Briggs, Phys. Rev. Lett. **93**, 150502 (2004).

[65] E. Pazy, E. Biolatti, T. Calarco, I. D'Amico, P. Zanardi, F. Rossi, and P. Zoller, Europhys. Lett. **62**, 175 (2003).

[66] P. Chen, C. Piermarocchi and L. J. Sham, Phys. Rev. Lett. **87**, 067401 (2001).

[67] J. Bao, A. V. Bragas, J. K. Furdyna, and R. Merlin, Nature Mat. **2**, 175 (2003); J. Bao, A. V. Bragas, J. K. Furdyna, and R. Merlin, Solid State Commun. **127**, 771 (2003); J. Bao, A. V. Bragas, J. K. Furdyna, and R. Merlin, arXiv:cond-mat/0406672 (2004).

[68] L. Besombes, Y. Léger, L. Maingault, D. Ferrand, H. Mariette, and J. Cibert, Phys. Rev. Lett. **93**, 207403 (2004).

[69] D. Bacon, J. Kempe, D. A. Lidar, and K. B. Whaley, Phys. Rev. Lett. **85**, 1758 (2000).

[70] D. P. Di Vincenzo, D. Bacon, J. Kempe, G. Burkard, and K. B. Whaley, Nature **408**, 339 (2000).

[71] Combescot and O. Betbeder-Matibet, Solid State Commun. **132**, 129 (2004).

[72] N. H. Bonadeo, Gang Chen, D. Gammon, D. S. Katzer, D. Park, and D. G. Steel, Phys. Rev. Lett. **81**, 2759 (1998).

[73] X. Hu and S. Das Sarma, Phys. Rev. A **61**, 062301 (2000).

[74] T. A. Kaplan and C. Piermarocchi, Phys. Rev. B **70**, 161311(R) (2004).

[75] A. Peres, Phys. Rev. Lett. **77**, 1413 (1996).

[76] J. J. Sakurai, it Modern Quantum Mechanics Addison-Wesley Piblishing Co. (1994).

[77] D. Bacon, J. Kempe, D. A. Lidar, and K. B. Whaley, Phys. Rev. Lett. **85**, 1758 (2000).

[78] D. Mozyrsky, V. Privman, and M. L. Glasser, Phys. Rev. Lett. 86, 5112 (2001).

[79] G. Ramon, Y. Lyanda-Geller, T. L. Reinecke and L. J. Sham, Phys. Rev. B 71 121305 (2005).

[80] D. Gottesman, *Stabilizer Codes and Quantum Error Correction* PhD thesis, Calif. Inst. Tech. Pasadena, California (1997).

[81] C. Fu, C. Santori, C. Stanley, M. C. Holland, and Yoshihisa Yamamoto,Phys. Rev. Lett. 95, 187405 (2005)

[82] J. P. Reithmaier, G. Se, A. Loffler, C. Hofmann, S. Kuhn1, S. Reitzenstein1, L. V. Keldysh, V. D. Kulakovskii, T. L. Reinecke, and A. Forchel, Nature, VOL 432, 11 (2004).

[83] G. Chiappe, J. Fernandez-Rossier, E. Louis, and E. V. Anda, Phys. Rev. B 72, 245311 (2005).

[84] M. Richard, J. Kasprzak, R. Romestain, R. Andr, and Le Si Dang, Phys. Rev. Lett. 94, 187401 (2005).

[85] S. Bahbah, R. Frey, R. Andre, G. Roosen, C. Flytzanis, Solid State Comm. 136, 147 (2005).

[86] U.Woggon, E.Luthgens, H.Wenisch, and D.Hommel, Phys. Rev. B **63**, 073205 (2001).

[87] S. Strauf, P. Michler, M. Klude, D.Hommel, G. Bacher, and A. Forchel, Phys. Rev. Lett. **89**, 177403 (2002).

[88] B. Golding and M. I. Dykman, arXiv:cond-mat/0309147 (2003).

[89] R. Vrijen, E. Yablonovitch, K. Wang, H. W. Jiang, A. Balandin, V. Roychowdhury, T. Mor, and D. DiVincenzo, Phys. Rev. A **62**, 012306 (2000).

[90] B. E. Kane, Nature **393** 133 (1998).

[91] Y. C. Chang and T.C. McGill, Phys. Rev. B **25** 3945 (1982).

[92] J. Fernández-Rossier, C. Piermarocchi, P. Chen, L. J. Sham, and A. H. MacDonald, Phys. Rev. Lett. **93**, 127201 (2004).

[93] B. W. Knight and G. A. Peterson, Phys. Rev. 132, 1085 (1963).